THE EFFECT OF A CIRCULAR HOLE ON THE BUCKLING OF CYLINDRICAL SHELLS

Thesis by

James Herbert Starnes, Jr.

In Partial Fulfillment of the Requirements

For the Degree of

Doctor of Philosophy

California Institute of Technology

Pasadena, California

1970

(Submitted May 8, 1970)

ACKNOWLEDGMENT

The author wishes to take this opportunity to sincerely thank Dr. E. E. Sechler for the patience and guidance he generously extended during the course of this investigation. The advice and useful comments of Drs. C. D. Babcock and J. Arbocz are also appreciated.

The author also thanks Miss Helen Burrus for patiently typing the manuscript, Mrs. Betty Wood for preparing the graphs and figures, and the employees of GALCIT who cheerfully provided their assistance.

The financial aid provided by the Lockheed Aircraft Corporation, the Northrop Corporation, the Ford Foundation, and the Del Mar Science Foundation is gratefully acknowledged.

ABSTRACT

An experimental and theoretical investigation of the effect of a circular hole on the buckling of thin cylindrical shells under axial compression was carried out. The experimental program consisted of tests performed on seamless electroformed copper shells and Mylar shells with a lap joint seam. The copper shells were tested in a controlled displacement testing machine equipped with a noncontacting surface displacement measuring device. Three-dimensional surface plots obtained in this manner showed the changes in the displacement field over the entire shell, including the hole region, as the applied load was increased. The Mylar shells were tested in a controlled load testing machine and demonstrated the effect of increasing the hole radius on the buckling loads of the cylinder.

The theoretical solution was based on a Rayleigh-Ritz approximation. The solution provided an upper bound for the buckling stresses of the cylinders tested for hole radii less than ten per cent of the shell radii. The theoretical solution also identified the governing parameter of the problem as being related to the hole radius, the shell radius, and the shell thickness.

The theoretical part of the investigation showed that even a small hole should significantly reduce the buckling stresses of circular cylinders. Experimentally, it was found that the effect of a small hole is masked by the effects of initial deformations but, at larger hole radii, the reduction in buckling stress took the form predicted by the theory. The experimental results also showed that

the character of the shell buckling was dependent on the hole size. For very small holes the shell buckled into the general collapse configuration and there was no apparent effect of the hole on the buckling mode of the shell. For slightly larger holes the shell still buckled into the general collapse configuration, but the buckling stresses of the shell were sharply reduced as the hole size increased. For still larger holes the buckling stresses did not decrease as sharply as the hole size increased and the shell buckled into a stable local buckling configuration.

TABLE OF CONTENTS

LIST OF TABLES

LIST OF FIGURES

LIST OF FIGURES (cont'd)

LIST OF FIGURES (cont'd)

LIST OF SYMBOLS

a	Hole radius
A_0, A_2, C_0, C_2	Undetermined coefficients of assumed displacement function
A, I_1, Y_G, α	Geometric properties given in Appendix I
$a_0, a'_2, b'_2, a'_4, b'_4$	Non-zero constants of equation (14) defined in Appendix II
B	Constant decay parameter associated with the assumed displacement function
B_1, B_2	Matrices defined in Appendix II
B_3	Matrix defined by equation (25)
$c_{01}, c_{02}, \ldots, c_{44}$	Constants in equation (17)
D	$Et^3/12(1 - \nu^2)$
E	Young's modulus
F	Stress function
g_0, g_2, g_4	Functions defined in Appendix II
I	Identity matrix
$k_1, k_2, \ldots, k_8$	Functions defined in Appendix II
$N_r, N_\phi, N_{r\phi}$	Stress resultants
$N^o_x, N^o_y, N^o_{xy}, N^o_r, N^o_\phi, N^o_{r\phi}$	Prebuckling stress resultants
P	Axial load applied at shell center
P_{CL}	Classical buckling load

LIST OF SYMBOLS (cont'd)

P_{NH}	Measured buckling load of cylinder without a hole
P_Y	Axial load applied at a distance Y from the shell center
q	Ba
R	Shell radius
r, ϕ	Polar coordinates with origin at hole center
S	Applied compressive stress
S_{CL}	Classical buckling stress
S_{NH}	Stress due to P_{NH}
S_Y	Applied compressive stress due to P_Y
t	Shell thickness
U_b, U_m, U_w	Strain energies defined on pages 26 and 27
w	Radial deflection of shell
x, y	Axial and circumferential coordinates
Y	Distance from shell center to applied load P_Y
ν	Poisson's ratio
μ	$\frac{1}{2}\left[12(1-\nu^2)\right]^{1/4}\left(\frac{a^2}{Rt}\right)^{1/2}$

I. INTRODUCTION

Many authors have investigated the effect of axial compression on the buckling of complete cylindrical shells and several explanations have been offered to try to account for the difference observed between theory and experiment. In recent years, several authors (for example, Refs. 1 and 2) have investigated the effect of initial imperfections as a cause for this discrepancy. Generally, these imperfections were in the form of waves in the surface of the cylinder. It was found that the presence of initial imperfections did significantly reduce the buckling stress of a cylinder to a value below the generally accepted classical value given by:

$$S_{CL} = \frac{1}{\sqrt{3(1 - \nu^2)}} \frac{Et}{R}$$

where E is the modulus of elasticity, ν is Poisson's ratio, t is the shell thickness, and R is the shell radius.

Surface waves are not the only type of imperfection that can be found in a cylindrical shell. In the applications of thin shell structures it is often necessary to design a cylindrical shell with a circular hole in the form of an access port in a missile skin or aircraft fuselage, a ship hatch, or for numerous other reasons. Such a cylindrical structure might be required to carry a static compressive load or, in the case of an aircraft or missile, fluctuating flight loads which have compressive components. Any time a compressive load is applied to a shell structure, it is necessary to investigate the possibility of the

buckling of the structure. Since imperfections in the form of initial surface waves have been shown to reduce the buckling stress of a cylinder, it must be expected that a hole will also have an effect on the buckling stress of the cylinder.

It was the purpose of this investigation to determine the effect of a single circular hole on the buckling of a thin circular cylinder under axially compressive loads. This was done by performing two series of experiments, one on Mylar, and one on copper shells. Sufficient variations of the geometric parameters R/t and a/R, where a is the hole radius, were studied to insure the availability of enough data to be able to draw proper conclusions. The parametric ranges considered were $400 \leq R/t \leq 960$ and $0 \leq a/R \leq 0.5$. The experiments provided measurements of buckling loads, shell displacements, and the distribution of the stresses applied at the ends of the shells. The results of these experiments were correlated on the basis of a theoretical parametric study performed by means of a Rayleigh-Ritz approximation.

During the completion of this thesis, several authors have reported the results of similar investigations. Brogan and Almroth (Ref. 3) carried out a theoretical and experimental investigation of the effect of rectangular holes on the buckling loads of cylinders. Their theoretical results were obtained by a numerical solution of the governing nonlinear equations of the problem. This proved to require large amounts of digital computer time for each buckling load, and therefore placed economic limits on the extent of their parametric study. Tennyson (Ref. 4) has provided experimentally measured

buckling loads of cylinders in the parametric range $162 \leq R/t \leq 331$ with a single circular hole in their sides. Based on the results of his experiments, Tennyson has suggested that the buckling load of a cylinder with a circular hole in its side is related to the parameter a/R. His results were nondimensionalized by dividing each experimental buckling load by the previously measured buckling load of the cylinder without a hole, a form of presentation which is useful for showing how a particular hole will effect a particular shell. For a cylindrical shell under axial compression the above technique is not the most conclusive method for the purpose of making a parametric study. Due to the large scatter in buckling loads experienced for cylinders without holes under axial compression, using such buckling loads as nondimensionalizing parameters has the effect of introducing a variable reference into the parametric study and may provide unreliable conclusions. It is shown in this thesis that the governing parameter is not a/R, but rather a parameter related to a^2/Rt. Jenkins (Ref. 5) has performed buckling experiments on cylinders containing two diametrically opposed circular holes. His results were for cylinders in the parametric range $75 \leq R/t \leq 150$. The combined results of Tennyson (Ref. 4), Jenkins (Ref. 5), and this thesis provide information on the effect of circular holes on the buckling of cylinders over a wide range of the parameter R/t.

II. EXPERIMENT

The experimental portion of this investigation consisted of two series of tests. The first series was performed on DuPont's "Mylar" polyester film, and the second series was performed on electroformed copper shells. The properties and characteristics of these two materials are such that different, but supporting, information was obtained from each series of tests.

A. MYLAR SHELLS

Mylar provided an inexpensive material that, for moderate thicknesses, was easy to handle. Under the loads applied during the experiment, this material remained elastic after the shell had buckled, so long as excessive displacements were prevented. It was this characteristic that made Mylar useful as a test material. A shell could be buckled many times without any noticable degradation of the test specimen. As a result, it was possible to test the same shell for an extensive range of hole radii, and therefore compare the effect of increasing the hole size on the buckling load of a particular shell.

1. Fabrication of the Mylar Shells

The Mylar shells were constructed from material taken from available roll stock with nominal thicknesses of 0.005, 0.0075, and 0.010 inches. Actual measurements showed these values to be accurate to within 2.4 per cent, with the 0.005 inch thickness varying the most. Sheets of the appropriate size were cut from the rolls, and rectangles of the correct dimensions were drawn on these sheets along with hole locating reference marks. Since they were taken from

rolls, these sheets had a tendency to curl. To reduce residual stresses due to fabrication, the rectangles were drawn on the sheets so that the circumference of the resulting cylinder would correspond to the curling of the sheet.

The sheets were cut to the required dimensions on a sheet metal shear. The shear blade was sharpened and adjusted so that it provided uniform cuts. The dimensions of the resulting rectangles were accurate to within 0.01 inches. A lap joint was prepared by slightly roughening the two edges to be joined with fine emory paper. The rectangle was attached to an 8 inch diameter wooden mandrel, and Narmco 7343/7139 cryogenic adhesive was applied to the prepared lap joint. This adhesive was selected as the seam bonding agent because it provides a flexible seam which was demonstrated by buckling one cylinder over 600 times without any apparent damage to the seam. The cylinder was allowed to remain on the mandrel for approximately twenty-four hours with an aluminum bar clamped along the seam. The bar exerted enough pressure on the seam to force out any excess adhesive and to provide a reasonably uniform seam thickness. Waxed paper was used to keep the bar and the mandrel from sticking to the cylinder. It was necessary to allow the seam to cure at room temperature for an additional week.

End plates were fastened to the cylinder by seating the shell in grooves in the end plates which were then filled with Cerrolow, a low melting temperature alloy. Since each cylinder was expected to buckle many times, it was necessary to place a row of staples around the circumference of the cylinder at each end of the shell. These

staples prevented the cylinder from pulling out of the Cerrolow during buckling or when a bending moment was applied to the shell.

The resulting cylinders were 8 inches in diameter and 10 inches long. Each cylinder had a seam that was approximately 0.5 inches wide and had average thicknesses of 0.0115, 0.0168, and 0.0217 inches for nominal cylinder thicknesses of 0.005, 0.0075, and 0.010 inches respectively. Since the seams were made of both Narmco adhesive and Mylar, it was necessary to determine the modulus of elasticity of the seam. This was done by testing seam specimens in a small tension testing machine. The average value of the modulus of elasticity of the seam found in this manner was 6.51×10^5 psi. In a similar fashion it was found that the modulus of elasticity of pure Mylar was 7.25×10^5 psi. Poisson's ratio was assumed to be equal to 0.3 for these experiments. The Cerrolow alloy provided clamped edge conditions for the cylinders.

2. Equipment and Procedure for the Mylar Shell Tests

The Mylar shells were tested in the controlled load testing machine shown in Fig. 1. The load was applied at a point on the top end plate ("top plate") by means of a loading screw, a calibrated load cell, and a ball bearing in a hemispherical cup. The top plate had small holes drilled along one of its diameters ("loading diameter") which were 0.125 inches apart for three inches on either side of the top plate center. There was also a small hole at the top plate center. At the time the top plate was attached to the cylinder, the loading diameter was positioned so that it formed a plane ("loading plane") with the shell seam, the shell axis of revolution, and the center of

the holes to be drilled in the cylinder wall. The loading plane is shown in Fig. 2. The shell was positioned under the loading screw by locating one of the small holes on the loading diameter directly under the center of the loading screw. This was done by means of a carpenter's plumb line which could be attached to the loading screw. The hemispherical cup was then placed in the correct position by inserting a short pin on its undersurface into the proper loading diameter hole, and the load cell was installed between a ball bearing recessed in the end of the loading screw and the ball bearing in the hemispherical cup. The ball bearings were used to reduce torsional loads during the application of the desired axial load.

Since the shells made from 0.005 inch thick Mylar stock were more difficult to handle and test than the thicker shells, it was necessary to use a lighter top plate and more flexible load cell for these shells. The load cells were calibrated in a 3000 pound Riehle Brothers testing machine, and their spring constants were found to be 2.5 and 0.714 pounds per 0.001 inch deflection of the load cell dial gages.

Before any holes were cut in the cylinder wall, the shells were buckled by applying loads along the loading diameter. These buckling loads provided a measure of the quality of the shells. A series of concentric holes with increasing radii was then cut into the wall of the cylinder using previously applied reference marks to locate the hole centers. A high speed hand drill using various cutting tools was employed to cut the holes in the shell walls. The smaller holes were cut using small stone bits of the desired diameter. The larger holes

were cut using a cross-cut dental drill and aluminum hole templates as guides. All hole edges were finished by trimming off any excess material with a sharp knife. For each hole size the value of the buckling load applied at the top plate center (cylinder axis) was always measured. At buckling there was an audible snap and a noticeable decrease in the load indicated by the dial gage. The buckling loads were also measured at various other positions along the loading diameter until a maximum buckling load was found. This procedure continued until the largest desired hole was cut in the shell and tested, or the shell collapsed catastrophically as in the case of some 0.005 inch thick shells. Each buckling load was applied at least three times to check the repeatability of the experiment. As demonstrated by the repeatability of these loads, Mylar is well suited for this type of experiment.

B. COPPER SHELLS

The copper shells were used to provide information about the displacements normal to the shell surface, the presence of other initial imperfections, and a measure of the distribution of the applied load around the circumference of the shell. These shells were more sensitive to handling, more difficult to manufacture, and more expensive than the Mylar shells. However, they provided much useful information that could not be obtained from the Mylar shells.

1. Fabrication of the Copper Shells

The copper shells were manufactured by the electroforming process using the electroplating facilities of GALCIT*. The

* Graduate Aeronautical Laboratories, California Institute of Technology.

manufacturing procedure and electroplating facilities are completely described in reference 1. A layer of wax was applied to a steel mandrel and then turned on a lathe to the desired shell diameter. The wax was then sprayed with a silver suspension to provide an electrically conducting surface, after which it was placed in the GALCIT electroplating facility where the desired amount of copper was deposited on the mandrel. The plating solution used was copper fluoborate. After plating, the shell was rinsed and cut to the desired dimensions on a lathe. A fly cutter was used to cut the hole in the cylinder while the shell was still on the mandrel. Each plated mandrel provided one test shell, one short calibration shell, and four 0.25 inch wide strips of copper. The resulting copper test shells were 8 inches in diameter and 8 inches long. The shell was removed from the mandrel by melting the wax. A benzene bath was used to remove any excess wax or silver from the shell. The shell was weighed and an average thickness was determined by using a specific gravity equal to 8.9 for the resulting copper. Subsequent preloading surface measurements showed no apparent bending of the shell around the hole due to the cutting of the hole.

The four 0.25 inch wide copper strips were mounted in an Instron tension testing machine and were tested to determine the modulus of elasticity of the test specimens. The average value of the modulus of elasticity was 13.98×10^6 psi. A value of 0.3 was assumed for Poisson's ratio of the copper specimens.

2. Equipment and Procedure for the Copper Shell Tests

The copper shells were tested in a controlled displacement testing machine. The testing machine and data acquisition equipment are thoroughly described in reference 2. The testing machine, shown in Fig. 3, consisted of two heavy flat steel plates which were separated by four threaded steel shafts. The shafts were controlled by a gear system that could turn the shafts simultaneously or allow each shaft to be turned independently for purposes of adjustment.

A calibrated load cell was attached to one of the steel plates with Devcon's "Plastic Steel". This load cell was a short 8 inch diameter brass cylindrical shell to which were attached twenty-four foil type strain gages. These strain gages were mounted in pairs every 30 degrees around the circumference of the load cell. One gage of each pair was mounted on the inside surface and one on the outsdie surface of the load cell. Each pair of strain gages was connected in series to the strain gage switching and balancing unit to avoid measuring any bending stresses in the load cell. One end of the copper test shell specimens was mounted on a short 8 inch diameter spacer shell by the use of Cerrolow alloy. The other end of the specimens was similarly bonded to the load cell, and the spacer shell was then bonded to the remaining steel plate by the use of "Plastic Steel".

Attached to the testing machine was a noncontacting measuring device which was capable of scanning the inside of the shell in both the axial and circumferential directions. It consisted of an electric motor drive system, a noncontacting electrical pickup, and a shaft which

passed through the supporting steel plate of the testing machine (see details in reference 2). The drive system was designed to position the end of the shaft holding the pickup in such a manner that it was possible to scan all points on the inside surface of the test shell with the pickup. To make a mapping of the shell surface the shaft and pickup were driven circumferentially through 360 degrees. The shaft was then advanced axially 0.24 inches, and another circumferential scan was made. This continued automatically until the entire test shell length had been traveled.

During the course of the experimental program both inductance and capacitance type pickups were used and both types worked equally well. The distance from the inner surface of the shell to the end of the pickup was represented by an electrical signal which was transmitted to the data acquisition system by means of the pickup signal carrier system. The carrier system for the inductance pickup is described in reference 2, and the modifications necessary for the capacitance pick up are described in reference 6. A voltage corresponding to the distance from the shell to the pickup was measured by a digital voltmeter and recorded on cards by an IBM 526 card punch. The signal was also monitered on an xy-analog plotter. The copper shell data acquisition system is shown in Fig. 4. The short copper calibration shell manufactured with the test shell was used to calibrate the pick up for each test. This was done before mounting the test shell in the testing machine. The voltages corresponding to known distances from pickup to calibration shell were measured and recorded on cards.

Tests were run to determine the effect of the hole in the shell on the pickup signal. Only when the pickup passed over a part of the hole was there noted any influence of the hole on the pickup signal.

After a test specimen was mounted in the testing machine, the strain gage outputs were set to zero and an initial scan was made with no load applied to the shell. This scan gave a measure of the initial imperfections in the shell and provided a reference surface corresponding to the no-load condition. The first loading increment was applied to the shell by turning the threaded shafts of the testing machine. The shafts were adjusted until the load was uniformly distributed around the load cell. At this low initial stress level, it was assumed that the hole in the cylinder was far enough from the load cell not to influence the stress field at the load cell. The distance from the load cell to the edge of the largest hole tested was 4.5 hole diameters. A scan was then made of the shell surface at this load level. The loading procedure was continued until buckling occurred. At buckling there was an audible snap and a decrease in the strain indicated by the strain gage aligned with the hole. To avoid premature buckling of the shell, no adjustment was made in the applied load distribution once half of the expected buckling load had been applied, however the strain gages were monitored at each loading increment which allowed any change in the stress distribution to be recorded.

The data from the surface scans were reduced by the program described in reference 2. In this program the pickup calibration data were represented by a polynomial expression and the voltage output from the pickup, which had been punched on cards, was converted into

the distance from the pickup to the shell surface using the calibration polynomial. A reference "perfect" shell was computed by the method of least squares from the data of the initial surface scan. All distances from pickup to shell surface were then referenced to this "perfect" shell. A three-dimensional plotting routine allowed the results of the scans to be displayed graphically. The initial scan data were subtracted from the scan data of subsequent loading increments, and the difference was also plotted by the same routine.

C. RESULTS OF THE EXPERIMENT

The results of the experimental program indicate that a circular hole in the side of a cylinder can influence the buckling load of the cylinder. Experimentally, it was found that the effect of a small hole is masked by the effects of initial deformations but, at larger hole radii, the reduction in buckling stress took the form predicted by the analysis. The analysis given later and the experimental results presented in this section indicate that the buckling loads of a cylinder with a hole in its side are related to a^2/Rt.

All results are expressed as a function of the nondimensional parameter

$$\mu = \frac{1}{2}\left[12(1 - \nu^2)\right]^{1/4} \left(\frac{a^2}{Rt}\right)^{1/2}$$

Lekkerkerker (Ref. 7) has shown that this parameter governs the solution of the prebuckling stress distribution and displacements and it is reasonable to assume that any attempt to solve the buckling problem as a small perturbation about Lekkerkerker's prebuckling solution would also involve the parameter μ.

Lekkerkerker's solution shows that the increase in the prebuckling stress field due to the hole is restricted to the local area of the hole region. This local area of increased stresses contains both membrane and bending stress increments. These stress increments are maximum at the hole and decay rapidly away from the hole. As μ approaches zero, this local stress field approaches the well known Kirsch solution for a flat plate found in most elasticity texts

(for example, Ref. 8). For a constant applied stress, the magnitude of the maximum membrane stress at the hole will increase significantly above the flat plate value as μ increases. The bending stresses are always much smaller than the membrane stresses.

1. Mylar Shells

The results of the experiments with Mylar cylinders show that the buckling characteristics of a shell with a hole in its side depends on the value of the parameter μ. The measured buckling loads applied at the center of the top plate were nondimensionalized by the classical buckling load of a cylinder without a hole, and a summary of these results for twelve shells is shown in Fig. 5. Similar results for some representative cylinders with various R/t ratios are shown in Figs. 6 through 10 and presented in Table I. The classical buckling load for a cylindrical shell without a hole was used as a nondimensionalizing parameter because it introduces the modulus of elasticity into the experimental results and provides a constant reference when comparing results for different shells with the same dimensions.

From these results it was possible to identify approximate ranges of μ with different buckling characteristics. For values of μ less than 0.4 there was no apparent effect of the hole on the buckling of the cylinder. In this range of μ, the hole was evidently not the predominant imperfection which caused the shell to buckle below the classical buckling load. The shell buckled into the general collapse diamond pattern with the hole randomly located with respect to the diamond ridges. For these values of μ the stress concentration due to the hole is apparently not large enough to cause buckling before the

shell buckles into the general collapse mode due to some other imperfection. There were usually two axial and six circumferential full waves in the buckled shell. For some cases in this range (Figs. 7 and 8), the buckling load rises slightly or appears to be erratic as μ increases. Since the hole is believed to have no effect on the buckling load in this range, this behavior is attributed to slight eccentricities in the shell. Although care was taken to align the loading diameter of the top plate with the intended loading plane, it is probable that slight eccentricities existed. Since the centroid of the shell was assumed to be in the loading plane, such eccentricities would cause a combined loading of pure axial compression and possible bending about two axes. This, of course, would cause unexpected stress levels or erratic behavior.

For values of μ between 0.4 and 1.0 the buckling loads dropped sharply as μ increased. The shell still buckled in to the diamond pattern, but the hole was located on a diamond ridge or the intersection of two of these ridges. This indicates that the hole has initiated or localized the buckling of the shell in some manner. As is well known, when the stress level of a cylindrical shell without a hole approaches its buckling value, the shell becomes sensitive to the slightest disturbance. Apparently the prebuckling stress concentration around the hole is of sufficient magnitude to cause the hole region to snap into a local buckling configuration. This local snap buckling could in turn provide enough of a disturbance at these applied stress levels to instigate the general collapse of the shell. The sensitivity of the shells for this range of μ was verified during the experiments.

The slightest lateral disturbance near the hole would cause the shell to buckle when the applied load was slightly below the known buckling load of the shell.

For values of μ greater than 2.0 the Mylar shells always snapped into the stable local buckling state shown in Fig. 11. The maximum displacement at the hole was on the order of 0.25 inches, which is many times the shell wall thickness. Apparently the stress concentration around a hole in this range of μ is sufficient to cause local buckling to occur before enough load could be applied to make the shell sensitive to disturbances which would cause general collapse. As a result of local buckling the dial gage of the load cell indicated a slight relaxation of the applied load of from one to three pounds. This represents a displacement of the top plate of as much as 0.001 inch. As seen in Fig. 11, the local buckling occurs roughly in the form of an ellipse with semi-major axes parallel to the y-axis of the hole coordinates shown in Fig. 2. The initial length of these semi-major axes seemed to depend on the hole size. After local buckling had occurred it was possible to resume the loading of the cylinder. This continued until the shell finally buckled into the general collapse state shown in Fig. 12. During this additional loading, the lengths of the semi-major axes of the local buckling ellipses increased as the additional load was applied. The applied load required for the general collapse of these shells was equal to or slightly greater than the load required for local buckling. The general collapse load was never more than 17 per cent above the local buckling load. Figures 6 and 10 show examples of shells with differences in local buckling and

general collapse loads. Prior to local buckling the shell was quite sensitive to slight disturbances. When the applied load was just below the local buckling load any lateral disturbance would cause local buckling to occur in the hole region. Once local buckling had occurred the shell did not seem as sensitive to these disturbances as they seldom led to general collapse. Buckling loads continued to decrease as the hole radius increased, but the rate of decline was significantly less than that of the range of μ between 0.4 and 1.0.

For values of μ between 1.0 and 2.0 there is a transition between the sharp decline in buckling load for μ between 0.4 and 1.0 and the milder decline of μ greater than 2.0. In this range of μ the shell would buckle into either the general collapse or the local buckling mode. The differences between local buckling and general collapse loads was usually greater in this range than they were for μ greater than 2.0. This behavior is shown in Figs. 9 and 10. Figure 7 shows the results of a shell for which only general collapse was observed, and Fig. 8 shows the results of a shell for which the general collapse loads were the same as the local buckling loads.

For the purpose of comparison with the analysis and the copper shell experimental results, it was necessary to reduce the Mylar shell results to applied stresses. This was done by replacing the applied loads with a statically equivalent applied membrane stress system acting on the plane ("applied stress plane") which is perpendicular to the cylinder axis and contains the hole center. It was assumed that the hole was far enough from the ends of the cylinder that the clamped edges had no influence on the assumed applied stresses. The assumed

applied stresses and applied stress plane geometry are shown in Fig. 13. Since the applied stresses vary as the cosine of the meridional angle θ, little error is introduced by assuming a constant stress level applied to the cylindrical generators near the hole. Consequently, it is assumed that the membrane stresses applied to points H1 and H2 of the hole edge can be used to represent the applied buckling stress corresponding to local buckling of the shell. This assumption is justified by the local buckling observed in the hole region. Based on the geometry of the applied stress plane shown in Fig. 13, the membrane stresses applied to points H1 and H2 are given by

$$S = \frac{P}{A} + \frac{MY}{I_1} = P\left[\frac{1}{A} + \frac{Y_G}{I_1}(Y_G + R\cos\alpha)\right]$$

where A, I_1, Y_G, and α are given in Appendix I. The resulting applied buckling stresses were nondimensionalized by the classical buckling stress of a cylinder without a hole, and a summary of these results for twelve shells is shown in Fig. 14. Similar results for some representative cylinders are shown in Figs. 15 through 19. Here again any erratic behavior of the results is attributed to eccentricities in the loading plane. Since the larger holes were cut by hand using a template, it is certainly possible that slight misalignment of some holes occurred. This, or any other eccentricity, would cause a higher applied stress on one side of the hole and would cause the shell to buckle at a different applied stress level.

With the establishment of these buckling stress levels, it is possible to extend the results to include loads applied at other points

along the loading diameter. This introduces the possibility of both local buckling at the hole and buckling of the seam. Seam buckling will occur when the applied load at any point on the loading diameter causes the buckling stress of the seam to be achieved before the buckling stress of the hole. The stress at points H1 and H2 due to a load applied at any point on the loading diameter is given by

$$S_Y = P_Y \left[\frac{1}{A} + \frac{1}{I_1} (Y_G - Y)(Y_G + R \cos \alpha) \right]$$

where Y is the distance from the cylinder axis to the applied load. Buckling loads were measured and buckling stresses computed for loads applied along the loading diameter for various values of μ. Results for two representative shells are shown in Figs. 20 and 21 and presented in Table II. These results show that the applied loads have maximum values which are seldom located at the top plate center. Buckling loads to the right of a maximum load in Figs. 20 and 21 correspond to buckling of the seam, while those to the left correspond to buckling at the hole. Since the loading points on the loading diameter were 0.125 inches apart, there was always the possibility of being as much as 0.0675 inches from the location corresponding to the maximum load. As a result, the point of intersection of the two branches of each of the load curves in Figs. 20 and 21 gives the approximate location and magnitude of the maximum load. The buckling stress curves in Figs. 20 and 21 confirm the importance of the locally applied stress to the buckling of the hole region. In all but two of the curves shown, the buckling of the hole is

represented by the nearly constant stress magnitudes to the left of the maximum loads in the figures. The slight negative slope of some of these curves (for example, Fig. 21, $\mu = 5.567$) is attributed to slight misalignment of the hole from the loading plane. The segment of the stress curves to the right of the maximum load with a large negative slope corresponds to buckling of the seam. These curve segments show that the seam buckled before the stress applied at the hole caused buckling at the hole. The two curves (Fig. 20, $\mu = 0$ and $\mu = 0.182$) which have large negative slopes on the left of the maximum load, represent results for values of μ in the range where the hole was not the predominant initial imperfection.

In an attempt to separate the effect of the hole from the effect of other initial imperfections, the results were nondimensionalized by the buckling loads measured at the top plate centers of the cylinders without holes. Summaries of the results of twelve cylinders for buckling loads and buckling stresses are shown in Figs. 22 and 23 respectively. Results for three representative shells are shown in Figs. 24, 25, and 26 for buckling loads and in Figs. 27, 28, and 29 for buckling stresses. These results indicate the approximate reduction in buckling load of a cylinder with a hole in its side after the effect of initial imperfections has been removed.

The results of the Mylar shell experiments did not seem to be particularly sensitive to small irregularities in the hole shape. Some of the larger holes cut with the high speed hand drill were probably slightly elliptic, and some holes had slightly roughened edges. No significant changes in buckling loads were observed. These

irregularities were apparently small enough not to significantly influence the local stress field. There was one noteworthy exception. In order to determine the sensitivity of points of high stress concentration to slight irregularities, a short 0.0625 inch wide slot was cut along the y-axis of Fig. 2. As the slot length increased, the buckling load actually increased. This increase in buckling loads is probably due to the relief of the local bending stress field in the hole region shown to exist by Lekkerkerker (Ref. 7). As the slot length further increased the shell buckled at the ends of the slots instead of at the hole and the buckling loads again decreased. The results of one such investigation are shown in Fig. 30 for a hole corresponding to μ equal to 2.897.

2. Copper Shells

The buckling stress results of the copper shell experiments fell within the scatter band of the Mylar shell results, and are shown in Fig. 14 and presented in Table III. The six shells tested had hole diameters ranging from 0.24 to 0.80 inches, and buckled into a stable local buckling configuration in the hole region in all cases. Although the buckling stress results agreed reasonably well for the copper and Mylar tests, there was a difference in the orientation of the local buckling pattern of the two materials. Instead of being parallel to the y-axis in Fig. 2 as in the Mylar tests, the semi-major axes of the local buckling ellipses of the copper shells made an angle of approximately 45 degrees with this y-axis as shown in Fig. 3. This difference may be attributed to the difference in the two testing machines used in the experimental program. As already mentioned, the

controlled load testing machine used for the Mylar shell tests allowed top plate displacement to occur during local buckling. This type of displacement was prevented by the controlled displacement testing machine used for the copper shell tests. It is entirely possible that the local buckling pattern of the Mylar shells was initially the same as that of the copper shells, and that the top plate displacement and corresponding applied load relaxation was sufficient to cause the Mylar shell local buckling pattern to change its orientation. In the copper shell tests the local buckling pattern maintained its original orientation when additional loading was applied.

The applied stress distribution, recorded by the strain gages on the load cell, showed that only the strain gage directly in line with the hole recorded any significant change due to local buckling. Since the strain gages were only 2.135 inches apart, the effect of the hole on the stress distribution was verified to be a local effect by the fact that the strain gages on either side of the strain gage aligned with the hole indicated little change, if any, due to local buckling. Examples of the stress distribution for various loading increments are shown in Figs. 31 and 32. As seen in Fig. 32, even the large hole in shell C6 influenced the stresses of only three strain gages, and two of these only slightly. Once local buckling had occurred the strain gage aligned with the hole remained at a constant stress level until general collapse occurred.

The results of the surface scans of three copper shells with relatively small, medium, and large holes are shown in Figs. 33 through 35, Figs. 36 through 39, and Figs. 40 through 43 respectively.

The initial surface scans, Figs. 33, 36, and 40, show that initial imperfections of several wall thicknesses in amplitude were present in all of these shells. The displacements of the shell surfaces due to various loading increments were obtained by subtracting the initial scan data from that of the subsequent loading increments. Figure 34 represents the displacements of the surface of shell C5 due to the loading increment ($S/S_{CL} = 0.47$) applied just prior to local buckling ($S/S_{CL} = 0.53$), and shows that very little prebuckling displacement has occurred in the hole region. As shown in Fig. 35, very large displacements of up to four or five wall thicknesses were measured in the hole region after local buckling had occurred in shell C5. The other region of large displacements in Fig. 35 is the result of local buckling occurring in another area of the shell just after the local buckling of the hole region. Figures 37 and 38 show the displacements of the surface of shell C3 for low and near local buckling stress levels respectively, and Figs. 41 and 42 show similar results for shell C6. Comparing Figs. 34, 38, and 42 shows that as the hole gets larger the prebuckling displacement in the hole region also gets larger for stress levels near local buckling. Figures 39 and 43 show that the displacements accompanying the local buckling of these shells were very large. The results of the scans of these three shells show that the effect of a hole on the displacements of a cylinder is a local effect even for the large hole in shell C6.

III. ANALYSIS

A. DEVELOPMENT OF THE ANALYSIS

In order to predict the proper parameter to represent the effect of a circular hole on the buckling stress of a cylinder, a simplified analysis is presented based on the experience gained from the experiments. It is assumed that the critical buckling stress, defined by the local buckling phenomenon, can be obtained by treating the problem as a linear eigenvalue problem. This implies that the general collapse phenomenon observed in the Mylar experiments for values of μ less than 1.0 was caused by local buckling. It also requires that the local bending stresses in the hole region, shown to exist by Lekkerkerker, are assumed to make only a small contribution to the initial buckling of the shell and can be neglected. This assumption is supported by the small prebuckling displacements observed in the copper shell experiments for small values of μ. The analysis can be further simplified by assuming that the stress distribution of a flat plate with a hole closely approximates the membrane stress distribution in the cylinder. This assumption is justified by Lekkerkerker's membrane stress results which approach the flat plate stress concentration values at the hole as the hole becomes small. Since the solution is only intended to represent local buckling in the hole region, it is further assumed that the displacement and membrane stress perturbations at buckling are negligible except in the hole region, and approach zero as the distance from the hole increases.

To solve the problem, within the restrictions of the above assumptions, a coordinate system is adopted which has its origin in the mid-surface of the cylinder at the center of the hole as shown in Fig. 2. The governing equations are transformed into this coordinate system, a displacement function is assumed, and the local buckling stresses are computed by the Rayleigh-Ritz procedure. The displacement function assumed must become zero as the distance from the hole becomes large, and is not required to be zero at the hole. Its derivative with respect to r must approach zero as the hole radius approaches zero in order to provide symmetry at the origin as the hole radius approaches zero.

A displacement function satisfying the above requirements is given by:

$$w(r,\phi) = e^{-Br}\left[(A_o + rC_o) + (A_2 + rC_2)\cos 2\phi\right] \tag{1}$$

where B is a constant which represents the decay of the local buckling displacement, and A_o, A_2, C_o, and C_2 are undetermined coefficients. The trigonometric form of this function was suggested by the local buckling pattern of the Mylar shell experiments.

The change in total potential energy due to buckling is given by:

$$U = U_b + U_w + U_m \tag{2}$$

where U_m is the membrane energy, U_b is the bending energy, and U_w is the energy change due to the prebuckling membrane stresses. These terms are represented by:

$$U_b = \frac{D}{2}\iint \left\{ (w,_{xx} + w,_{yy})^2 - 2(1-\nu)\left[w,_{xx} w,_{yy} - (w,_{xy})^2 \right] \right\} dxdy \qquad (3)$$

$$U_w = \frac{1}{2}\iint \left[N_x^o (w,_x)^2 + N_y^o (w,_y)^2 + 2N_{xy}{}^o\, w,_x\, w,_y \right] dxdy \qquad (4)$$

$$U_m = \frac{1}{2Et}\iint \left[N_r^2 + N_\phi^2 - 2\nu\, N_r N_\phi + 2(1+\nu) N_{r\phi}{}^2 \right] r dr d\phi \qquad (5)$$

where N_x^o, N_y^o, and N_{xy}^o are the prebuckling stress resultants, a subscript following a comma indicates partial differentiation, and

$$D = \frac{Et^3}{12(1-\nu^2)}$$

Also, by introducing a stress function F,

$$\left.\begin{aligned} N_r &= t\sigma_r = \frac{1}{r} F,_r + \frac{1}{r^2} F,_{\phi\phi} \\ N_\phi &= t\sigma_\phi = F,_{rr} \\ N_{r\phi} &= t\tau_{r\phi} = -\left(\frac{1}{r} F,_\phi\right),_r \end{aligned}\right\} \qquad (6)$$

and the coordinate transformation

$$\left.\begin{aligned} \frac{\partial}{\partial x} &= \sin\phi \frac{\partial}{\partial r} + \frac{1}{r}\cos\phi \frac{\partial}{\partial \phi} \\ \frac{\partial}{\partial y} &= \cos\phi \frac{\partial}{\partial r} - \frac{1}{r}\sin\phi \frac{\partial}{\partial \phi} \end{aligned}\right\} \qquad (7)$$

(3) can be written as

$$U_b = \frac{D}{2}\iint\left\{\left[(w,_{rr})^2 + \frac{2}{r^3} w,_r w,_{\phi\phi} + \frac{1}{r^2}(w,_r)^2 + \frac{1}{r^4}(w,_{\phi\phi})^2\right]\right.$$

$$+ 2(1-\nu)\left[\frac{1}{r^2}(w,_{r\phi})^2 - \frac{2}{r^3} w,_{r\phi}\, w,_{\phi} + \frac{1}{r^4}(w,_{\phi})^2\right] \qquad (8)$$

$$\left. + 2\nu\left[\frac{1}{r} w,_{rr}\, w,_r + \frac{1}{r^2} w,_{rr}\, w,_{\phi\phi}\right]\right\} r\,dr\,d\phi$$

For the coordinate system shown in Fig. 2, the stress distribution in a flat plate with a circular hole given in reference 8 can be written as:

$$N_r^o = -\frac{1}{2} St\left(1 - \frac{a^2}{r^2}\right) + \frac{1}{2} St\left(1 + 3\frac{a^4}{r^4} - 4\frac{a^2}{r^2}\right)\cos 2\phi$$

$$N_\phi^o = -\frac{1}{2} St\left(1 + \frac{a^2}{r^2}\right) - \frac{1}{2} St\left(1 + 3\frac{a^4}{r^4}\right)\cos 2\phi \qquad (9)$$

$$N_{r\phi}^o = -\frac{1}{2} St\left(1 - 3\frac{a^4}{r^4} + 2\frac{a^2}{r^2}\right)\sin 2\phi$$

where S is the magnitude of the applied compressive stress. By using (7), (9), and the transformation

$$N_x^o = N_r^o \sin^2\phi + N_\phi^o \cos^2\phi + N_{r\phi}^o \sin 2\phi$$

$$N_y^o = N_r^o \cos^2\phi + N_\phi^o \sin^2\phi - N_{r\phi}^o \sin 2\phi \qquad (10)$$

$$N_{xy}^o = \frac{1}{2}(N_r^o - N_\phi^o)\sin 2\phi + N_{r\phi}^o \cos 2\phi$$

(4) can be written as

$$U_w = -\frac{1}{4} St \iint \left\{ \left[2 \sin^2\phi - 3 \frac{a^4}{r^4} \cos 2\phi + \frac{a^2}{r^2}(4 \cos 2\phi - 1) \right] (w,_r)^2 \right.$$

$$+ \left[\left(\frac{2}{r} - 6 \frac{a^4}{r^5} + 4 \frac{a^2}{r^3} \right) \sin 2\phi \right] w,_r w,_\phi \qquad (11)$$

$$\left. + \left[\frac{2}{r^2} \cos^2\phi + 3 \frac{a^4}{r^6} \cos 2\phi + \frac{a^2}{r^4} \right] (w,_\phi)^2 \right\} r dr d\phi$$

Before expressing the final form of the membrane energy, it is necessary to determine the stress function F. This is done by solving the linear shallow shell compatibility equation

$$\nabla^4 F = -\frac{Et}{R} w,_{xx} \qquad (12)$$

which is consistent with the assumptions made for this simplified analysis. By using (1) and (7), equation (12) can be written as

$$\nabla^4 F = g_o(r) + g_2(r) \cos 2\phi + g_4(r) \cos 4\phi \qquad (13)$$

where $g_o(r)$, $g_2(r)$, and $g_4(r)$ are given by (A1) of Appendix II. The homogeneous solution of (13) is given in reference 9 as

$$F_c = a_o \ell nr + b_o r^2 + c_o r^2 \ell nr + d_o r^2 \phi + a'_o \phi$$

$$+ \frac{1}{2} a''_1 \, r\phi \sin\phi + (a_1 r + b_1 r^3 + a'_1 r^{-1} + b'_1 \, r \ell nr) \cos \phi$$

$$+ \frac{1}{2} \, c''_1 \, r\phi\cos\phi + (c_1 r + d_1 r^3 + c'_1 \, r^{-1} + d'_1 \, r\ell nr) \sin \phi \qquad (14)$$

$$+ \sum_{n=2}^{\infty} (a_n r^n + b_n r^{n+2} + a'_n r^{-n} + b'_n r^{-n+2}) \cos n \phi$$

$$+ \sum_{n=2}^{\infty} (c_n r^n + d_n r^{n+2} + c'_n r^{-n} + d'_n r^{-n+2}) \sin n \phi$$

A particular solution of (13) will be determined by the method of variation of parameters. This is done by assuming that (13) is satisfied by

$$F_p = h_o(r) + h_2(r) \cos 2 \phi + h_4(r) \cos 4 \phi \qquad (15)$$

where $h_o(r)$, $h_2(r)$, and $h_4(r)$ are to be determined. Substituting (15) into (13) and using the linear independence of $\cos m\phi$ gives three ordinary differential equations of the form:

$$\frac{d^4 h_m}{dr^4} + \frac{2}{r} \frac{d^3 h_m}{dr^3} - \frac{(2m^2+1)}{r^2} \frac{d^2 h_m}{dr^2} + \frac{(1+2m^2)}{r^3} \frac{dh_m}{dr}$$

$$+ \frac{m^4 - 4m^2}{r^4} h_m = g_m(r) \qquad (16)$$

where m = 0, 2, 4. The homogeneous forms of each of (16) have four independent solutions and are of the form:

$$
\begin{aligned}
h_{0c} &= C_{01}\,\ell nr + C_{02}r^2 + C_{03}r^2\,\ell nr + C_{04} \\
h_{2c} &= C_{21}r^2 + C_{22}r^4 + C_{23}r^{-2} + C_{24} \\
h_{4c} &= C_{41}r^4 + C_{42}r^6 + C_{43}r^{-4} + C_{44}r^{-2}
\end{aligned}
\tag{17}
$$

Using (17) and applying the method of variation of parameters to (16) gives:

$$
\begin{aligned}
h_0(r) = \frac{Et}{8R}\Bigg\{ & A_0\left[\frac{4}{B^2}e^{-Br} - \frac{4}{B^2}\int\frac{e^{-Br}}{r}\,dr\right] \\
& - A_2\left[e^{-Br}\left(\frac{r}{B} + \frac{1}{B^2}\right) + r^2\int\frac{e^{-Br}}{r}\,dr\right] \\
& + C_0\left[e^{-Br}\left(\frac{4r}{B^2} + \frac{12}{B^3}\right) - \frac{8}{B^3}\int\frac{e^{-Br}}{r}\,dr\right] \\
& - C_2\left[e^{-Br}\left(\frac{2r}{B^2} + \frac{2}{B^3}\right)\right]\Bigg\}
\end{aligned}
\tag{18a}
$$

$$h_2(r) = \frac{Et}{8R}\left\{ A_0 e^{-Br}\left[\frac{4}{B^2} + \frac{12}{B^3 r} + \frac{12}{B^4 r^2}\right] \right.$$

$$- A_2 e^{-Br}\left[\frac{r}{B} + \frac{3}{B^2} + \frac{6}{B^3 r} + \frac{6}{B^4 r^2}\right] - A_2 r^2 \int \frac{e^{-Br}}{r}\, dr$$

$$+ C_0 e^{-Br}\left[4\frac{r}{B^2} + \frac{20}{B^3} + \frac{48}{B^4 r} + \frac{48}{B^5 r^2}\right] \tag{18b}$$

$$\left. - C_2 e^{-Br}\left[\frac{4r}{B^2} + \frac{12}{B^3} + \frac{24}{B^4 r} + \frac{24}{B^5 r^2}\right]\right\}$$

$$h_4(r) = \frac{Et}{4R}\left\{ A_2 e^{-Br}\left[\frac{1}{B^2} + \frac{7}{B^3 r} + \frac{27}{B^4 r^2} + \frac{60}{B^5 r^3} + \frac{60}{B^6 r^4}\right] \right.$$

$$\left. + C_2 e^{-Br}\left[\frac{r}{B^2} + \frac{9}{B^3} + \frac{48}{B^4 r} + \frac{168}{B^5 r^2} + \frac{360}{B^6 r^3} + \frac{360}{B^7 r^4}\right]\right\} \tag{18c}$$

The integral in (18) is the exponential integral (Ref. 10) and, for convenience, will be replaced by

$$-\int_{Br}^{\infty} \frac{e^{-z}}{z}\, dz = -E_1(Br) \tag{19}$$

where it is understood that $E_1(\infty) = 0$. Equations (15), (18), and (19) complete the particular solution of (13), and it is possible to write

$$F = F_c + F_p \tag{20}$$

The constants in (14) are determined from the boundary conditions:

$$N_r = 0 \quad \text{at} \quad r = a \tag{21a}$$

$$N_{r\phi} = 0 \quad \text{at} \quad r = a \tag{21b}$$

and the requirement that

$$N_r = N_\phi = N_{r\phi} \longrightarrow 0 \quad \text{as} \quad r \text{ becomes large} \tag{21c}$$

It is also required that N_r, N_ϕ, and $N_{r\phi}$ are periodic with respect to ϕ and that the strain energy be bounded as r becomes large. Since the problem is treated as a local phenomenon with w, N_r, N_ϕ, and $N_{r\phi}$ equal to zero and the strain energy being bounded as r becomes large, there is no loss of generality if r is allowed to go to infinity. Therefore, integration over r will be taken to range from a to infinity in the energy exppressions, and (21c) will be taken to mean

$$N_r = N_\phi = N_{r\phi} = 0 \quad \text{as} \quad r \longrightarrow \infty \tag{21c'}$$

Applying these conditions and the linear independence of $\sin m\phi$ and $\cos m\phi$ give:

1. $d_0 = 0$ from the periodicity of N_r
2. $b_0 = c_0 = a_2 = c_2 = a_n = b_n = c_n = d_n = 0$ for $n \geq 3$ from $N_r = 0$ as $r \longrightarrow \infty$
3. $b_1 = d_1 = b_2 = d_2 = 0$ from $N_\phi = 0$ as $r \longrightarrow \infty$

4. $a'_0 = a''_1 = c''_1 = c'_2 = d'_2 = a'_3 = b'_3 = c'_3 = d'_3 = c'_4 = d'_4 = 0$

$a'_n = b'_n = c'_n = d'_n = 0 \quad \text{for } n \geq 5$

and

$$a'_1 = \frac{1}{2} a^2 b'_1$$

$$c'_1 = \frac{1}{2} a^2 d'_1 \tag{i}$$

from (21a, b)

5. (5), (6), and (20) give

$$U_m = \frac{4\pi}{Et} \int_a^\infty \left[(b'_1)^2 + (d'_1)^2 \right] \frac{1}{r} \, dr + M_1 \tag{ii}$$

where M_1 is the result of the other terms in (20) and is bounded.

Completion of the integration in (ii) gives

$$U_m = \frac{4\pi}{Et} \left\{ \left[(b'_1)^2 + (d'_1)^2 \right] \ell nr \right\} \Big|_a^\infty + M_1$$

which becomes unbounded as $r \longrightarrow \infty$, unless

$$(b'_1)^2 + (d'_1)^2 = 0 \tag{iii}$$

Since $(b'_1)^2 > 0$ and $(d'_1)^2 > 0$, (iii) can be satisfied only if

$$b'_1 = d'_1 = 0 \tag{iv}$$

Then (i), (iv) give

$$a'_1 = c'_1 = 0$$

Of the seven remaining constants, a_1 and c_1 are not required to determine N_r, N_ϕ, or $N_{r\phi}$, and therefore can be assumed to be equal to zero without any loss of generality. The remaining constants a_0, a'_2, b'_2, a'_4, and b'_4 are determined by applying (21a, b) and are given in (A2) of Appendix II.

Since the constants in (14) have been determined, it is now possible to use the stress function to compute the stress resultants. Therefore, using (6) and (20) gives

$$\begin{aligned} N_r &= k_1(r) + k_2(r) \cos 2\phi + k_3(r) \cos 4\phi \\ N_\phi &= k_4(r) + k_5(r) \cos 2\phi + k_6(r) \cos 4\phi \\ N_{r\phi} &= k_7(r) \sin 2\phi + k_8(r) \sin 4\phi \end{aligned} \tag{22}$$

where $k_i(r)$, $i = 1, 8$ are given by (A3) of Appendix II.

By using equations (1), (5), (8), (11), and (22), it is now possible to express the change in total potential energy due to buckling, (2), in terms of the undetermined coefficients A_0, A_2, C_0, and C_2. Applying the Rayleigh-Ritz procedure gives the four equations

$$\frac{\partial U}{\partial A_0} = 0; \quad \frac{\partial U}{\partial A_2} = 0; \quad \frac{\partial U}{\partial C_0} = 0; \quad \frac{\partial U}{\partial C_2} = 0 \tag{23}$$

After collecting like terms of the undetermined coefficients, equations (23) can be written in matrix form as

$$\left[B_1 - SB_2\right] \begin{Bmatrix} A_0 \\ A_2 \\ C_0 \\ C_2 \end{Bmatrix} = 0 \tag{24}$$

where B_1 and B_2 are two 4 x 4 symmetric matrices given by (A4) and (A5) of Appendix II. Pre-multiplying (24) by B_2^{-1} and defining

$$B_3 = B_2^{-1} B_1 \tag{25}$$

gives

$$\left[B_3 - SI\right] \begin{Bmatrix} A_0 \\ A_2 \\ C_0 \\ C_2 \end{Bmatrix} = 0 \tag{26}$$

where I is the identity matrix. The eigenvalues, S, are then obtained from the determinant

$$\left|B_3 - SI\right| = 0 \tag{27}$$

B. RESULTS OF THE ANALYSIS

The elements of the matrix B_3 are functions of a, B, E, R, t, and ν and contain several integrals which must be evaluated numerically. Consequently the expansion of (27) and the determination of the eigenvalues were done numerically on an IBM 360/75 digital computer. The results were minimized with respect to the decay parameter B for each value of the hole radius. A range of R/t ratios was considered, and it was found that all results fell on a single curve when

plotted with respect to a^2/Rt. These results are presented in Table IV and shown in Fig. 44 plotted with respect to the square root of a^2/Rt for convenience.

The results of this analysis identify the parameter of the problem as being related to a^2/Rt, rather than just a/R. Following Lekkerkerker's results (Ref. 7), the parameter was assumed to be a function of the square root of a^2/Rt, namely,

$$\mu = \frac{1}{2}\left[12(1-\nu^2)\right]^{1/4}\left(\frac{a^2}{Rt}\right)^{1/2}$$

The dependence on Poisson's ratio was not confirmed by either the experimental or analytical results. The analytical results are compared with the experimental results in Fig. 14. As can be seen in Fig. 14, the analysis provides an upper bound for the local buckling stress of a cylinder with a circular hole up to a value of μ equal to approximately 2.5. For values of μ greater than 2.5 some of the assumptions required for the analysis are no longer valid. It is possible that the shallow shell approximation associated with equation (12) is no longer applicable for μ greater than 2.5. Also, as shown by the results of cylinder C6, larger values of μ have large prebuckling deformation in the region of the hole and require that the problem should be treated as a nonlinear response problem.

IV. CONCLUSIONS

As a result of this investigation, it is possible to conclude that a circular hole in a cylinder can greatly reduce the buckling stresses of the cylinder. The amount of reduction in buckling stress depends on a parameter which is related to the ratio a^2/Rt. Based on a perturbation about Lekkerkerker's prebuckling stress solution, it is expected that this parameter should be

$$\mu = \frac{1}{2}\left[12(1-\nu^2)\right]^{1/4}\left(\frac{a^2}{Rt}\right)^{1/2}$$

The character of the buckling of the shell can be described as a local buckling phenomenon which leads to the general collapse of the shell. If the hole is small enough, the stress concentration at the hole is not sufficient to cause buckling due to the hole before the shell buckles due to some other initial imperfection. The stability of the local buckling mode for larger holes depends on whether or not the stress level in the shell is high enough to make the shell sensitive to small disturbances. For moderate values of μ, local buckling in the hole region provides enough of a disturbance to cause general collapse of the shell to occur without any increase in applied load. For larger values of μ, local buckling in the hole region is stable, and general collapse occurs only after increasing the applied load. Since the general collapse loads were only slightly higher than the local buckling loads in this case, a conservatively designed structure should be designed on the basis of the local buckling stresses.

The results can be extended to include both applied axial loads and bending moments about an axis perpendicular to the cylinder diameter which passes through the hole center. This would be done by interpreting the combined stresses applied to the cylinder generators tangent to the hole as being the applied stress.

The simplified analytical approximation presented in this thesis provides a reasonable solution for values of μ less than approximately 2.5. For larger values of μ it is necessary to treat the problem as a nonlinear response problem. A nonlinear approach would also be required to compute the general collapse stresses occurring after stable local buckling has occurred.

The discrepancy between the experimental and analytical results for values of μ less than 2.5 is possibly due to several factors. First, it is well known that the Rayleigh-Ritz procedure provides nonconservative buckling results if the assumed displacement function is incorrect. The orientation of the local buckling pattern of the copper shell experiments indicate that the assumed displacement function used in the analysis may not have been sufficiently general. Secondly, no consideration of coupling between the effect of the hole and other initial imperfections was made. The larger discrepancy observed in Fig. 14 for lower values of μ is attributed to the additional effect of these initial imperfections. The higher stress levels associated with these lower values of μ correspond to greater sensitivity of the shell to initial imperfections. A third contributor to this discrepancy could be the neglected bending stresses in the hole

region. While the magnitude of these bending stresses is always smaller than the membrane stresses in the hole region, it is very probable that they do play some role in local buckling.

REFERENCES

1. Babcock, C. D.: The Buckling of Cylindrical Shells with an Initial Imperfection under Axial Compression Loading. Ph. D. Thesis, California Institute of Technology, 1962.

2. Arbocz, J.: The effect of General Imperfections on the Buckling of Cylindrical Shells. Ph. D. Thesis, California Institute of Technology, 1968.

3. Brogan, F. and Almroth, B.: Buckling of Cylinders with Cutouts. AIAA J., Vol. 8, Feb. 1970, pp. 236-240.

4. Tennyson, R. C.: The Effects of Unreinforced Circular Cutouts on the Buckling of Circular Cylindrical Shells under Axial Compression. J. of Engineering for Industry, Trans. of the American Soc. of Mech. Eng., Vol. 90, Nov. 1968, pp. 541-546.

5. Jenkins, W. C.: Buckling of Cylinders with Cutouts under Combined Loading. MDAC Paper WD 1390, McDonnell-Douglas Astronautics Co., Western Division, 1970.

6. Singer, J.; Arbocz, J. and Babcock, C. D.: Buckling of Imperfect Stiffened Cylindrical Shells under Axial Compression. Proceedings AIAA/ASME 11th Structures Conference, Denver, Colorado, April 22-24, 1970.

7. Lekkerkerker, J. G.: On the Stress Distribution in Cylindrical Shells Weakened by a Circular Hole. Ph. D. Thesis, Technological University, Delft, 1965.

8. Sechler, E. E.: Elasticity in Engineering. John Wiley and Sons, Inc., New York, 1952.

9. Fung, Y. C.: Foundations of Solid Mechanics. Prentice-Hall, Inc., Englewood Cliffs, New Jersey, 1965.

10. Abramowitz, M. and Stegun, I. A.: Handbook of Mathematical Functions, Dover Publications, Inc., New York, 1965.

Other references applicable to this study

Effect of Initial Imperfections

11. Donnell, L. M.: A New Theory for the Buckling of Thin Cylinders under Axial Compression and Bending. Trans. of the American Soc. of Mech. Eng., Vol. 56, 1935, pp. 795-806.

12. Donnell, L. M. and Wan, C. C.: Effects of Imperfections on Buckling of Thin Cylinders and Columns under Axial Compression. J. Appl. Mech., Vol. 17, 1950, pp. 73-83.

Prebuckling Stress Distribution

13. Lur'e, A. I.: Statics of Thin-Walled Elastic Shells. State Publishing House of Technical and Theoretical Literature, Moscow, 1947. Translation, Atomic Energy Commission, AEC-tr-3798, 1959.

14. Van Dyke, P.: Stresses about a Circular Hole in a Cylindrical Shell. AIAA J., Vol. 3, Sept. 1965, pp. 1733-1742.

APPENDIX I

GEOMETRIC PROPERTIES OF THE ASSUMED APPLIED STRESS PLANE

Let

a = hole radius

E = modulus of elasticity of Mylar

E_s = modulus of elasticity of seam

R = shell radius

t = shell thickness

t_s = seam thickness

w_s = seam width

Then

$$\alpha = \arcsin\left(\frac{a}{R}\right)$$

The effective area of the cross section is given by

$$A = 2\pi Rt + w_s\left(t_s \frac{E_s}{E} - t\right) - 2Rt\alpha$$

The distance from the cylinder axis to the cross section centroid is given by

$$Y_G = \frac{R}{A}\left[w_s\left(t_s \frac{E_s}{E} - t\right) + 2at\right]$$

The moment of inertia about the axis through the cross section centroid perpendicular to the loading diameter is given by

$$I_1 = \pi R^3 t + 2\pi R t\, Y_G^2 + \frac{1}{12}\, w_s\left(t_s \frac{E_s}{E} - t\right)^3$$

$$+ w_s(R - Y_G)^2\left(t_s \frac{E_s}{E} - t\right) - R^3 t\left(\alpha + \frac{1}{2} \sin 2\alpha\right)$$

$$+ 2a^2 R \frac{t}{\alpha} - 2Rt\alpha\left(Y_G + \frac{a}{\alpha}\right)^2$$

APPENDIX II

DETAILS OF THE ANALYTICAL SECTION

In equation (13)

$$g_0(r) = -\frac{Et}{2R} e^{-Br}\left[A_0(B^2 - \frac{B}{r}) + A_2(-\frac{1}{2}B^2 + \frac{3}{2}\frac{B}{r}) + C_0(-3B + B^2r + \frac{1}{r}) + C_2(\frac{5}{2}B - \frac{1}{2}B^2r - \frac{3}{2}\frac{1}{r})\right]$$

$$g_2(r) = -\frac{Et}{2R} e^{-Br}\left[A_0(-B^2 - \frac{B}{r}) + A_2(B^2 - \frac{B}{r} - \frac{4}{r^2}) + C_0(B - B^2r + \frac{1}{r}) + C_2(-3B + B^2r - \frac{3}{r})\right] \qquad (A1)$$

$$g_4(r) = \frac{Et}{2R} e^{-Br}\left[A_2(\frac{1}{2}B^2 + \frac{5}{2}\frac{B}{r} + \frac{4}{r^2}) + C_2(\frac{3}{2}B + \frac{1}{2}B^2r + \frac{3}{2}\frac{1}{r})\right]$$

Let

$$q = Ba$$

then, the non-zero coefficients of (14) are

$$a_0 = \frac{Et}{4R}\left\{2A_0a^2e^{-q}\left[\frac{1}{q^2} + \frac{1}{q}\right] - A_2a^2E_1(q) + 2C_0a^3e^{-q}\left[\frac{1}{q} + \frac{2}{q^2} + \frac{2}{q^3}\right] - C_2a^3e^{-q}\left[\frac{1}{q}\right]\right\} \qquad (A2a)$$

$$a_2' = \frac{Et}{4R}\left\{ - A_0 a^4 e^{-q}\left[\frac{1}{q} + \frac{3}{q^2} + \frac{6}{q^3} + \frac{6}{q^4}\right] + \frac{1}{2}A_2 a^4 E_1(q)\right.$$

$$+ \frac{1}{2}A_2 a^4 e^{-q}\left[\frac{1}{q} + \frac{3}{q^2} + \frac{6}{q^3} + \frac{6}{q^4}\right]$$

$$- C_0 a^5 e^{-q}\left[\frac{1}{q} + \frac{4}{q^2} + \frac{12}{q^3} + \frac{24}{q^4} + \frac{24}{q^5}\right] \qquad \text{(A2b)}$$

$$\left. + C_2 a^5 e^{-q}\left[\frac{1}{q} + \frac{2}{q^2} + \frac{6}{q^3} + \frac{12}{q^4} + \frac{12}{q^5}\right]\right\}$$

$$b_2' = \frac{Et}{4R}\left\{ A_0 a^2 e^{-q}\left[\frac{1}{q} + \frac{1}{q^2}\right] - A_2 a^2 E_1(q)\right.$$

$$\left. + C_0 a^3 e^{-q}\left[\frac{1}{q} + \frac{2}{q^2} + \frac{2}{q^3}\right] - C_2 a^3 e^{-q}\left[\frac{1}{q} + \frac{1}{q^2}\right]\right\} \qquad \text{(A2c)}$$

$$a_4' = -\frac{Et}{8R}\left\{ A_2 a^6 e^{-q}\left[\frac{1}{q} + \frac{5}{q^2} + \frac{20}{q^3} + \frac{60}{q^4} + \frac{120}{q^5} + \frac{120}{q^6}\right]\right.$$

$$\left. + C_2 a^7 e^{-q}\left[\frac{1}{q} + \frac{6}{q^2} + \frac{30}{q^3} + \frac{120}{q^4} + \frac{360}{q^5} + \frac{720}{q^6} + \frac{720}{q^7}\right]\right\} \qquad \text{(A2d)}$$

$$b_4' = \frac{Et}{8R}\left\{A_2 a^4 e^{-q}\left[\frac{1}{q} + \frac{3}{q^2} + \frac{6}{q^3} + \frac{6}{q^4}\right]\right.$$

$$\left. + C_2 a^5 e^{-q}\left[\frac{1}{q} + \frac{4}{q^2} + \frac{12}{q^4} + \frac{24}{q^4} + \frac{24}{q^5}\right]\right\} \qquad \text{(A2e)}$$

where $E_1(q)$ is the exponential integral.

In equation (22)

$$k_1(r) = \frac{a_0}{r} + \frac{Et}{4R}\left\{-2A_0 e^{-Br}\left[\frac{1}{Br} + \frac{1}{B^2r^2}\right] + A_2 E_1(Br)\right.$$

$$\left. - 2C_0 e^{-Br}\left[\frac{1}{B} + \frac{2}{B^2 r} + \frac{2}{B^3 r^2}\right] + C_2 e^{-Br}\left[\frac{1}{B}\right]\right\} \qquad \text{(A3a)}$$

$$k_2(r) = -6\frac{a_2'}{r^4} - 4\frac{b_2'}{r^2} + \frac{Et}{4R}\left\{-2A_0 e^{-Br}\left[\frac{1}{Br} + \frac{7}{B^2r^2} + \frac{18}{B^3r^3} + \frac{18}{B^4r^4}\right]\right.$$

$$+ A_2 e^{-Br}\left[\frac{3}{Br} + \frac{9}{B^2r^2} + \frac{18}{B^3r^3} + \frac{18}{B^4r^4}\right] - A_2 E_1(Br)$$

$$- 2C_0 e^{-Br}\left[\frac{1}{B} + \frac{8}{B^2 r} + \frac{32}{B^3 r^2} + \frac{72}{B^4 r^3} + \frac{72}{B^5 r^4}\right] \qquad \text{(A3b)}$$

$$\left. + 2C_2 e^{-Br}\left[\frac{1}{B} + \frac{6}{B^2 r} + \frac{18}{B^3 r^2} + \frac{36}{B^4 r^3} + \frac{36}{B^5 r^4}\right]\right\}$$

$$k_3(r) = -20\frac{a'_4}{r^6} - 18\frac{b'_4}{r^4} - \frac{Et}{4R}\left\{A_2 e^{-Br}\left[\frac{1}{Br}+\frac{23}{B^2r^2}+\frac{146}{B^3r^3}+\frac{546}{B^4r^4}+\frac{1200}{B^5r^5}+\frac{1200}{B^6r^6}\right]\right.$$

$$\left. + C_2 e^{-Br}\left[\frac{1}{B}+\frac{24}{B^2r}+\frac{192}{B^3r^2}+\frac{984}{B^4r^3}+\frac{3384}{B^5r^4}+\frac{7200}{B^6r^5}+\frac{7200}{B^7r^6}\right]\right\} \tag{A3c}$$

$$k_4(r) = -\frac{a_0}{r^2} + \frac{Et}{4R}\left\{2A_0 e^{-Br}\left[1+\frac{1}{Br}+\frac{1}{B^2r^2}\right] + A_2\left[E_1(Br) - e^{-Br}\right]\right.$$

$$\left. + 2C_0 e^{-Br}\left[r+\frac{1}{B}+\frac{2}{B^2r}+\frac{2}{B^3r^2}\right] - C_2 e^{-Br}\left[r-\frac{1}{B}\right]\right\} \tag{A3d}$$

$$k_5(r) = 6\frac{a'_2}{r^4} + \frac{Et}{4R}\left\{2A_0 e^{-Br}\left[1+\frac{3}{Br}+\frac{9}{B^2r^2}+\frac{18}{B^3r^3}+\frac{18}{B^4r^4}\right]\right.$$

$$- A_2 e^{-Br}\left[2+\frac{3}{Br}+\frac{9}{B^2r^2}+\frac{18}{B^3r^3}+\frac{18}{B^4r^4}\right] + A_2 E_1(Br)$$

$$+ 2C_0 e^{-Br}\left[r+\frac{3}{B}+\frac{12}{B^2r}+\frac{36}{B^3r^2}+\frac{72}{B^4r^3}+\frac{72}{B^5r^4}\right] \tag{A3e}$$

$$\left. - 2C_2 e^{-Br}\left[r+\frac{1}{B}+\frac{6}{B^2r}+\frac{18}{B^3r^2}+\frac{36}{B^4r^3}+\frac{36}{B^5r^4}\right]\right\}$$

$$k_6(r) = 20\frac{a_4'}{r^6} + 6\frac{b_4'}{r^4} + \frac{Et}{4R}\left\{A_2 e^{-Br}\left[1 + \frac{7}{Br} + \frac{41}{B^2r^2} + \frac{182}{B^3r^3} + \frac{582}{B^4r^4} + \frac{1200}{B^5r^5} + \frac{1200}{B^6a^6}\right]\right.$$

$$\left. + C_2 e^{-Br}\left[r + \frac{7}{B} + \frac{48}{B^2r} + \frac{264}{B^3r^2} + \frac{1128}{B^4r^3} + \frac{3528}{B^5r^4} + \frac{7200}{B^6r^5} + \frac{7200}{B^7r^6}\right]\right\} \qquad \text{(A3f)}$$

$$k_7(r) = -6\frac{a_2'}{r^4} - 2\frac{b_2'}{r^2} - \frac{Et}{4R}\left\{4A_0 e^{-Br}\left[\frac{1}{Br} + \frac{4}{B^2r^2} + \frac{9}{B^3r^3} + \frac{9}{B^4r^4}\right]\right.$$

$$+ A_2 e^{-Br}\left[\frac{3}{Br} + \frac{9}{B^2r^2} + \frac{18}{B^3r^3} + \frac{18}{B^4r^4}\right] + A_2 E_1(Br) \qquad \text{(A3g)}$$

$$- 4C_0 e^{-Br}\left[\frac{1}{B} + \frac{5}{B^2r} + \frac{17}{B^3r^2} + \frac{36}{B^4r^3} + \frac{36}{B^5r^4}\right]$$

$$\left. + 4C_2 e^{-Br}\left[\frac{1}{B} + \frac{3}{B^2r} + \frac{9}{B^3r^2} + \frac{18}{B^4r^3} + \frac{18}{B^5r^4}\right]\right\}$$

$$k_8(r) = -20\frac{a_4'}{r^6} - 12\frac{b_4'}{r^4} - \frac{Et}{R}\left\{A_2 e^{-Br}\left[\frac{1}{Br} + \frac{8}{B^2r^2} + \frac{41}{B^3r^3} + \frac{141}{B^4r^4} + \frac{300}{B^5r^5} + \frac{300}{B^6r^6}\right]\right.$$

$$\left. - C_2 e^{-Br}\left[\frac{1}{B} + \frac{9}{B^2r} + \frac{57}{B^3r^2} + \frac{264}{B^4r^3} + \frac{864}{B^5r^4} + \frac{1800}{B^6r^5} + \frac{1800}{B^7r^6}\right]\right\} \qquad \text{(A3h)}$$

The matrices in (24) are

$$B_1 = \begin{bmatrix} G_1 & G_3 & G_5 & G_7 \\ G_3 & G_{11} & G_{13} & G_{15} \\ G_5 & G_{13} & G_{21} & G_{23} \\ G_7 & G_{15} & G_{23} & G_{31} \end{bmatrix} \tag{A4}$$

and

$$B_2 = \begin{bmatrix} G_2 & G_4 & G_6 & G_8 \\ G_4 & G_{12} & G_{14} & G_{16} \\ G_6 & G_{14} & G_{22} & G_{24} \\ G_8 & G_{16} & G_{24} & G_{32} \end{bmatrix} \tag{A5}$$

where

$$G_1 = \frac{Ea^2}{R^2} e^{-2q}\left[\frac{3}{8}\,\frac{1}{q} + \frac{3}{16}\,\frac{1}{q^2}\right] + \frac{Et^2}{6(1-\nu^2)}\,\frac{1}{a^2}\left\{ e^{-2q}\left[\frac{1}{2}\,q^3 + \frac{1}{4}\,q^2 - \nu q^2\right] + q^2 E_1(2q)\right\}$$

$$G_2 = e^{-2q}\left[\frac{1}{2}\,q + \frac{1}{4}\right] - q^2 E_1(2q)$$

$$G_3 = -\frac{Ea^2}{R^2} e^{-2q}\left[\frac{1}{4}\,\frac{1}{q} + \frac{7}{16}\,\frac{1}{q^2} + \frac{\nu}{16}\,\frac{1}{q^2}\right] + \frac{Ea^2}{R^2} e^{-q} E_1(q)\left[\frac{5}{8} + \frac{\nu}{8}\right]\left[\frac{1}{q} + \frac{1}{q^2}\right]$$

$$- \frac{Ea^2}{R^2}\,\frac{1}{q^2}\,E_1(2q)\left[\frac{5}{8} + \frac{\nu}{8}\right] + \frac{E}{R^2}\,\frac{a^2}{q^2}\left[\frac{3}{8} - \frac{\nu}{8}\right]\int_q^\infty \left[z e^{-z} E_1(z)\right] dz$$

$$G_4 = e^{-2q}\left[\frac{3}{8} + \frac{3}{4}q + \frac{1}{4}q^2 - \frac{1}{2}q^3\right] + E_1(2q)\left[q^4 - 2q^2\right]$$

$$G_5 = \frac{Ea^3}{R^2} e^{-2q}\left[\frac{3}{8}\frac{1}{q} + \frac{3}{8}\frac{1}{q^2} + \frac{3}{16}\frac{1}{q^3}\right]$$

$$+ \frac{Et^2}{6(1-\nu^2)}\frac{1}{a}\left\{e^{-2q}\left[\frac{1}{2}q^3 - \frac{1}{2}q^2 + \frac{1}{4}q - \nu(q^2-q)\right] - qE_1(2q)\right\}$$

$$G_6 = aq\,E_1(2q)$$

$$G_7 = \frac{Ea^3}{R^2} e^{-2q}\left[-\frac{1}{4}\frac{1}{q} + \frac{1}{4}\frac{1}{q^2} + \frac{1}{8}\frac{1}{q^3}\right]$$

$$G_8 = ae^{-2q}\left[\frac{1}{2} + \frac{1}{4}\frac{1}{q}\right]$$

$$G_{11} = \frac{Ea^2}{R^2} e^{-2q}\left[\frac{7}{32}\frac{1}{q} + \frac{7}{64}\frac{1}{q^2}\right] - \frac{1}{2}\frac{Ea^2}{R^2}\left[E_1(q)\right]^2$$

$$- \frac{1}{2}\frac{Ea^2}{R^2q^2}\int_q^\infty \left[ze^{-z}E_1(z)\right]dz + \frac{1}{2}\frac{Ea^2}{R^2q^2}\int_q^\infty \left[zE_1(z)E_1(z)\right]dz$$

$$+ \frac{Et^2}{24(1-\nu^2)a^2}\left\{e^{-2q}\left[q^3 + \frac{1}{2}q^2 + 24\right] + 18q^2E_1(2q)\right.$$

$$\left. - 2\nu e^{-2q}\left[q^2 + 8q + 4\right]\right\}$$

$$G_{12} = e^{-2q}\left[\frac{9}{8} - \frac{7}{4}q\right] + \left[\frac{7}{2}q^2 + 2\right] E_1(2q)$$

$$G_{13} = -\frac{Ea^3}{R^2} e^{-2q}\left[\frac{1}{4}\frac{1}{q} + \frac{9}{16}\frac{1}{q^2} + \frac{29}{32}\frac{1}{q^3} + \nu\left(\frac{1}{16}\frac{1}{q^2} + \frac{5}{32}\frac{1}{q^3}\right)\right]$$

$$+ \frac{Ea^3}{R^2} e^{-q} E_1(q)\left[\frac{5}{8}\frac{1}{q} + \frac{5}{4}\frac{1}{q^2} + \frac{5}{4}\frac{1}{q^3} + \nu\left(\frac{1}{8}\frac{1}{q} + \frac{1}{4}\frac{1}{q^2} + \frac{1}{4}\frac{1}{q^3}\right)\right]$$

$$- \frac{Ea^3}{R^2 q^3} E_1(2q)\left[\frac{5}{4} + \frac{\nu}{4}\right] + \frac{Ea^3}{R^2 q^3}\left[\frac{3}{8} - \frac{\nu}{8}\right]\int_q^\infty \left[z^2 e^{-z} E_1(z)\right] dz$$

$$G_{14} = ae^{-2q}\left[2q^2 - q - \frac{1}{2} - \frac{1}{4}\frac{1}{q}\right] + 4a\left[q - q^3\right] E_1(2q)$$

$$G_{15} = \frac{Ea^3}{R^2} e^{-2q}\left[\frac{7}{32}\frac{1}{q} + \frac{3}{32}\frac{1}{q^2} + \frac{3}{64}\frac{1}{q^3} - \frac{3}{16}\frac{\nu}{q^3}\right] - \frac{1}{2}\frac{Ea^3}{R^2 q} e^{-q} E_1(q)$$

$$- \frac{1}{4}\frac{Ea^3}{R^2 q^3}\int_q^\infty \left[z^2 e^{-z} E_1(z)\right] dz + \frac{1}{2}\frac{Ea^3}{R^2 q^3}\int_q^\infty \left[z e^{-z} E_1(z)\right] dz$$

$$+ \frac{1}{a}\frac{Et^3}{12(1-\nu^2)}\left\{e^{-2q}\left[\frac{1}{2}q^3 - \frac{1}{2}q^2 + \frac{17}{4}q + 12 - \nu(q^2 + 7q)\right] - 9qE_1(2q)\right\}$$

$$G_{16} = ae^{-2q}\left[2 + \frac{1}{q}\right] - \frac{7}{2} aqE_1(2q)$$

$$G_{21} = \frac{Ea^4}{R^2} e^{-2q}\left[\frac{3}{8}\frac{1}{q} + \frac{9}{16}\frac{1}{q^2} + \frac{9}{32}\frac{1}{q^4}\right]$$

$$+\frac{Et^2}{6(1-\nu^2)}\left\{e^{-2q}\left[\frac{1}{2}q^3 - \frac{5}{4}q^2 + \frac{5}{4}q - \frac{3}{8} + \nu(-q^2+2q-1)\right] + E_1(2q)\right\}$$

$$G_{22} = a^2e^{-2q}\left[\frac{1}{2} + \frac{1}{4}\frac{1}{q} + \frac{1}{8}\frac{1}{q^2}\right] - a^2 E_1(2q)$$

$$G_{23} = \frac{Ea^4}{R^2} e^{-2q}\left[-\frac{1}{4}\frac{1}{q} + \frac{1}{8}\frac{1}{q^2} + \frac{1}{8}\frac{1}{q^3} + \frac{1}{16}\frac{1}{q^4}\right]$$

$$G_{24} = a^2e^{-2q}\left[-\frac{3}{4}q + \frac{7}{8} - \frac{1}{8}\frac{1}{q} - \frac{1}{16}\frac{1}{q^2}\right] + \frac{3}{2}a^2q^2 E_1(2q)$$

$$G_{31} = \frac{Ea^4}{R^2} e^{-2q}\left[\frac{7}{32}\frac{1}{q} - \frac{27}{64}\frac{1}{q^2} + \frac{21}{64}\frac{1}{B^3a^3} + \frac{117}{128}\frac{1}{q^4} + \frac{\nu}{4}\frac{1}{q^4}\right]$$

$$+ \frac{Et^2}{12(1-\nu^2)}\left\{e^{-2q}\left[\frac{1}{2}q^3 - \frac{5}{4}q^2 + \frac{21}{4}q + \frac{45}{8} + \nu(q^2+6q-3)\right] + 9E_1(2q)\right\}$$

$$G_{32} = a^2e^{-2q}\left[\frac{1}{4} + \frac{9}{8}\frac{1}{q} + \frac{9}{16}\frac{1}{q^2}\right] + 3a^2E_1(2q)$$

TABLE I

RESULTS OF MYLAR SHELL EXPERIMENTS WITH

LOADS APPLIED AT TOP PLATE CENTER

Shell 6 R = 4.0 inches t = 0.010 inches

a inches	a/R	μ	P pounds	P/P_{CL}	S/S_{CL}
0.0	0.0	0.0	223.5	0.810	0.824
0.025	0.00625	0.114	223.5	0.810	0.829
0.05	0.0125	0.227	223.5	0.810	0.834
0.075	0.01875	0.341	223.5	0.810	0.839
0.10	0.0250	0.454	221.0	0.801	0.835
0.125	0.03125	0.568	201.0	0.728	0.764
0.16	0.040	0.727	158.5	0.574	0.608
0.20	0.050	0.909	131.0	0.475	0.507
0.25	0.0625	1.136	113.5	0.411	0.445
0.30	0.075	1.363	98.5*	0.357	0.391
			116.0	0.420	0.460
0.325	0.08125	1.477	93.5*	0.339	0.374
			101.0	0.366	0.403
0.35	0.0875	1.591	91.0*	0.330	0.366
			99.75	0.361	0.401

* Local buckling - all other values are general collapse.

TABLE I (cont'd)

RESULTS OF MYLAR SHELL EXPERIMENTS WITH

LOADS APPLIED AT TOP PLATE CENTER

Shell 6 R = 4.0 inches t = 0.010 inches

a inches	a/R	μ	P pounds	P/P_{CL}	S/S_{CL}
0.4	0.10	1.818	86.0*	0.312	0.350
			98.5	0.357	0.401
0.625	0.1563	2.840	83.5*	0.303	0.361
			93.5	0.339	0.404
0.84	0.210	3.818	81.0*	0.293	0.372
			88.5	0.321	0.406
1.025	0.2563	4.658	73.5*	0.226	0.356
			82.25	0.298	0.399
1.225	0.3063	5.567	72.25*	0.262	0.372
			76.0	0.275	0.391
1.6	0.40	7.272	61.0*	0.221	0.355
			63.5	0.230	0.370
2.025	0.5063	9.203	51.0*	0.185	0.346
			54.5	0.197	0.370

* Local buckling - all other values are general collapse.

TABLE I (cont'd)

RESULTS OF MYLAR SHELL EXPERIMENTS WITH

LOADS APPLIED AT TOP PLATE CENTER

Shell 7 R = 4.0 inches t = 0.010 inches

a inches	a/R	μ	P pounds	P/P_{CL}	S/S_{CL}
0.0	0.0	0.0	191.0	0.692	0.703
0.04	0.010	0.182	189.75	0.687	0.706
0.08	0.020	0.364	191.0	0.692	0.718
0.12	0.030	0.545	193.5	0.701	0.734
0.16	0.040	0.727	178.5	0.647	0.684
0.20	0.050	0.909	161.0	0.583	0.623
0.24	0.060	1.091	137.25	0.497	0.537
0.28	0.070	1.273	123.5	0.447	0.488
0.32	0.080	1.454	116.0	0.420	0.463
0.39	0.0975	1.772	109.75	0.398	0.446
0.43	0.1075	1.954	101.0	0.366	0.415
0.48	0.120	2.181	96.0	0.348	0.399
0.60	0.150	2.727	91.0	0.330	0.391
0.6375	0.1594	2.897	89.75	0.325	0.389

TABLE I (cont'd)

RESULTS OF MYLAR SHALL EXPERIMENTS WITH

LOADS APPLIED AT TOP PLATE CENTER

Shell 14 R = 4.0 inches t = 0.010 inches

a inches	a/R	μ	P pounds	P/P_{CL}	S/S_{CL}
0.0	0.0	0.0	208.5	0.755	0.769
0.04	0.010	0.182	206.5	0.748	0.769
0.08	0.020	0.364	208.5	0.755	0.784
0.12	0.030	0.545	203.5	0.737	0.772
0.1425	0.3563	0.648	173.5	0.629	0.662
0.20	0.050	0.909	143.5	0.520	0.555
0.2275	0.05688	1.034	131.0	0.475	0.511
0.25	0.0625	1.136	126.0	0.456	0.494
0.285	0.07125	1.295	113.5	0.411	0.449
0.325	0.08125	1.477	106.0	0.384	0.423
0.37	0.925	1.682	98.5	0.357	0.398
0.44	0.110	2.0	96.0	0.348	0.395
0.52	0.130	2.363	91.4	0.331	0.384
0.60	0.150	2.727	91.0	0.330	0.391
2.0	0.50	9.089	51.2	0.186	0.344

TABLE I (cont'd)

RESULTS OF MYLAR SHELL EXPERIMENTS WITH

LOADS APPLIED AT TOP PLATE CENTER

Shell 17 R = 4.0 inches t = 0.0075 inches

a inches	a/R	μ	P pounds	P/P_{CL}	S/S_{CL}
0.0	0.0	0.0	98.5	0.634	0.646
0.05	0.0125	0.262	98.5	0.634	0.654
0.08	0.020	0.420	93.5	0.602	0.625
0.12	0.030	0.630	78.5	0.506	0.530
0.175	0.04375	0.918	76.0	0.489	0.520
0.22	0.055	1.155	63.5*	0.409	0.440
			76.0	0.489	0.526
0.31	0.0775	1.627	53.5*	0.345	0.379
			66.0	0.425	0.467
0.40	0.10	2.099	51.0*	0.328	0.370
			53.5	0.345	0.388
0.49	0.1225	2.571	48.5*	0.312	0.362
			49.75	0.320	0.369

* Local buckling - all other values are general collapse.

TABLE I (cont'd)

RESULTS OF MYLAR SHELL EXPERIMENTS WITH

LOADS APPLIED AT TOP PLATE CENTER

Shell 20 R = 4.0 inches t = 0.005 inches

a inches	a/R	μ	P pounds	P/P_{CL}	S/S_{CL}
0.0	0.0	0.0	42.15	0.611	0.623
0.04	0.010	0.257	42.29	0.613	0.631
0.08	0.020	0.514	35.01	0.507	0.527
0.12	0.030	0.771	30.72	0.445	0.467
0.16	0.040	1.028	30.72	0.445	0.472
0.235	0.05875	1.510	23.94*	0.347	0.375
			29.29	0.424	0.458
0.275	0.06875	1.767	23.23*	0.337	0.367
			27.15	0.393	0.429
0.325	0.08125	2.089	22.87*	0.331	0.366
			25.72	0.373	0.412

* Local buckling - all other values are general collapse.

TABLE I (cont'd)

RESULTS OF MYLAR SHELL EXPERIMENTS WITH

LOADS APPLIED AT TOP PLATE CENTER

Shell 20 R = 4.0 inches t = 0.005 inches

a inches	a/R	μ	P pounds	P/P_{CL}	S/S_{CL}
0.40	0.10	2.571	20.37*	0.295	0.332
			23.58	0.342	0.385
0.495	0.1237	3.181	19.66*	0.285	0.329
			22.87	0.331	0.383
0.60	0.150	3.856	18.94*	0.274	0.326
			22.15	0.321	0.381
1.98	0.495	12.726	10.73*	0.156	0.287
			12.52	0.181	0.334

* Local buckling - all other values are general collapse.

TABLE II

LOCAL BUCKLING RESULTS OF MYLAR SHELL EXPERIMENTS

WITH LOADS APPLIED ALONG LOADING DIAMETER

Shell 7 R = 4.0 inches t = 0.010 inches

a inches	μ	P_Y pounds	Y inches	P_Y/P_{CL}	S_Y/S_{CL}
0.0	0.0	183.5	-0.75	0.665	0.921
		188.5	-0.625	0.683	0.905
		196.0	-0.50	0.710	0.897
		201.0	-0.375	0.728	0.875
		213.5	-0.25	0.773	0.882
		203.5	-0.125	0.737	0.796
		191.0	0.0	0.692	0.704
		181.0	0.125	0.656	0.627
0.04	0.182	202.25	-0.50	0.733	0.935
		206.0	-0.375	0.746	0.906
		213.5	-0.25	0.773	0.891
		203.5	-0.125	0.737	0.803
		189.75	0.0	0.687	0.706
		178.5	0.125	0.647	0.624

TABLE II (cont'd)

LOCAL BUCKLING RESULTS OF MYLAR SHELL EXPERIMENTS

WITH LOADS APPLIED ALONG LOADING DIAMETER

Shell 7 R = 4.0 inches t = 0.010 inches

a inches	μ	P_Y pounds	Y inches	P_Y/P_{CL}	S_Y/S_{CL}
0.08	0.364	186.0	-0.50	0.674	0.868
		196.0	-0.375	0.710	0.870
		207.25	-0.25	0.751	0.873
		203.5	-0.125	0.737	0.811
		191.0	0.0	0.692	0.718
		178.5	0.125	0.647	0.630
		168.5	0.25	0.610	0.557
0.12	0.545	172.25	-0.375	0.624	0.772
		183.5	-0.25	0.665	0.780
		193.5	-0.125	0.701	0.779
		193.5	0.0	0.701	0.734
		181.0	0.125	0.656	0.646
		172.25	0.25	0.624	0.575

TABLE II (cont'd)

LOCAL BUCKLING RESULTS OF MYLAR SHELL EXPERIMENTS

WITH LOADS APPLIED ALONG LOADING DIAMETER

Shell 7 R = 4.0 inches t = 0.010 inches

a inches	μ	P_Y pounds	Y inches	P_Y/P_{CL}	S_Y/S_{CL}
0.16	0.727	156.0	-0.25	0.565	0.670
		168.5	-0.125	0.610	0.685
		178.5	0.0	0.647	0.684
		186.0	0.125	0.674	0.670
		176.0	0.25	0.638	0.593
		166.0	0.375	0.601	0.521
0.20	0.909	148.5	-0.125	0.538	0.609
		161.0	0.0	0.583	0.623
		168.5	0.125	0.610	0.613
		176.0	0.25	0.638	0.599
		166.0	0.375	0.601	0.526
		143.5	0.50	0.520	0.422

TABLE II (cont'd)

LOCAL BUCKLING RESULTS OF MYLAR SHELL EXPERIMENTS

WITH LOADS APPLIED ALONG LOADING DIAMETER

Shell 7 R = 4.0 inches t = 0.010 inches					
a inches	μ	P_Y pounds	Y inches	P_Y/P_{CL}	S_Y/S_{CL}
0.24	1.091	128.5	-0.125	0.466	0.533
		137.25	0.0	0.497	0.537
		141.0	0.125	0.511	0.518
		154.75	0.25	0.561	0.532
		168.5	0.375	0.610	0.540
		156.0	0.50	0.565	0.463
		148.5	0.625	0.538	0.406
		141.0	0.75	0.511	0.352
		134.75	0.875	0.488	0.305
0.28	1.273	123.5	0.0	0.447	0.488
		133.5	0.125	0.484	0.496
		142.25	0.25	0.513	0.494
		153.5	0.375	0.556	0.497
		156.0	0.50	0.565	0.468
		149.75	0.625	0.543	0.413
		142.25	0.75	0.515	0.359
		136.0	0.875	0.493	0.311

TABLE II (cont'd)

LOCAL BUCKLING RESULTS OF MYLAR SHELL EXPERIMENTS

WITH LOADS APPLIED ALONG LOADING DIAMETER

Shell 7 R = 4.0 inches t = 0.010 inches

a inches	μ	P_Y pounds	Y inches	P_Y/P_{CL}	S_Y/S_{CL}
0.32	1.454	116.0	0.0	0.420	0.463
		121.0	0.125	0.438	0.454
		131.0	0.25	0.475	0.460
		141.0	0.375	0.511	0.461
		151.0	0.50	0.547	0.458
		148.5	0.625	0.538	0.414
		141.0	0.75	0.511	0.360
		136.0	0.875	0.493	0.314
		128.5	1.0	0.466	0.266
0.39	1.772	109.75	0.0	0.398	0.446
		116.0	0.125	0.420	0.443
		126.0	0.25	0.456	0.450
		134.75	0.375	0.488	0.449
		146.0	0.50	0.529	0.451
		146.75	0.625	0.543	0.426
		142.25	0.75	0.515	0.370
		136.0	0.875	0.493	0.320
		129.75	1.0	0.470	0.274

TABLE II (cont'd)

LOCAL BUCKLING RESULTS OF MYLAR SHELL EXPERIMENTS

WITH LOADS APPLIED ALONG LOADING DIAMETER

Shell 7 R = 4.0 inches t = 0.010 inches

a inches	μ	P_Y pounds	Y inches	P_Y/P_{CL}	S_Y/S_{CL}
0.43	1.954	101.0	0.0	0.366	0.415
		113.5	0.25	0.411	0.410
		121.0	0.375	0.438	0.407
		129.75	0.50	0.470	0.405
		139.75	0.625	0.506	0.402
		142.25	0.75	0.515	0.374
		136.0	0.875	0.493	0.324
		131.0	1.4	0.475	0.280
		126.0	1.125	0.456	0.238
0.48	2.181	93.5	0.0	0.339	0.389
		113.5	0.375	0.411	0.387
		123.5	0.50	0.447	0.391
		133.5	0.625	0.484	0.389
		143.5	0.75	0.520	0.382
		138.5	0.875	0.502	0.334
		131.0	1.0	0.475	0.284
		126.0	1.125	0.456	0.241
		121.0	1.25	0.438	0.202

TABLE II (cont'd)

LOCAL BUCKLING RESULTS OF MYLAR SHELL EXPERIMENTS

WITH LOADS APPLIED ALONG LOADING DIAMETER

Shell 7 R = 4.0 inches t = 0.010 inches

a inches	μ	P_Y pounds	Y inches	P_Y/P_{CL}	S_Y/S_{CL}
0.60	2.727	91.0	0.0	0.330	0.391
		116.0	0.50	0.420	0.379
		126.0	0.625	0.456	0.380
		136.0	0.75	0.493	0.375
		137.25	0.875	0.497	0.343
		131.0	1.0	0.475	0.294
		126.0	1.125	0.456	0.250
		118.5	1.25	0.429	0.205
0.6375	2.897	71.0	-0.75	0.257	0.418
		76.0	-0.50	0.273	0.408
		83.5	-0.25	0.303	0.405
		89.75	0.0	0.325	0.389
		101.0	0.25	0.366	0.386
		117.25	0.50	0.425	0.387
		124.75	0.625	0.452	0.380
		139.75	0.75	0.506	0.389
		138.5	0.875	0.502	0.350
		132.25	1.0	0.479	0.300
		127.25	1.125	0.461	0.256
		121.0	1.25	0.438	0.212

TABLE II (cont'd)

LOCAL BUCKLING RESULTS OF MYLAR SHELL EXPERIMENTS

WITH LOADS APPLIED ALONG LOADING DIAMETER

Shell 6 R = 4.0 inches t = 0.010 inches

a inches	μ	P_Y pounds	Y inches	P_Y/P_{CL}	S_Y/S_{CL}
0.84	3.818	61.0	-0.75	0.221	0.380
		63.5	-0.50	0.230	0.361
		73.5	-0.25	0.266	0.377
		81.0	0.0	0.293	0.372
		88.5	0.25	0.321	0.358
		103.5	0.50	0.375	0.363
		118.5	0.75	0.429	0.351
		145.0	1.0	0.525	0.350
		137.25	1.25	0.497	0.257
		128.5	1.50	0.466	0.171
1.025	4.658	57.25	-0.75	0.207	0.375
		61.0	-0.50	0.221	0.365
		68.5	-0.25	0.248	0.371
		73.5	0.0	0.266	0.356
		83.5	0.25	0.303	0.357
		96.0	0.50	0.348	0.356
		112.25	0.75	0.407	0.352
		137.25	1.0	0.497	0.353
		138.5	1.25	0.502	0.277

TABLE II (cont'd)

LOCAL BUCKLING RESULTS OF MYLAR SHELL EXPERIMENTS

WITH LOADS APPLIED ALONG LOADING DIAMETER

Shell 6	R = 4.0 inches	t = 0.010 inches			
a inches	μ	P_Y pounds	Y inches	P_Y/P_{CL}	S_Y/S_{CL}
1.225	5.567	59.75	-0.50	0.216	0.379
		72.75	0.0	0.262	0.372
		81.0	0.25	0.293	0.369
		92.25	0.50	0.334	0.365
		106.0	0.75	0.384	0.356
		128.5	1.0	0.466	0.354
		141.0	1.25	0.511	0.304
		129.75	1.50	0.470	0.202
1.60	7.272	51.0	-0.50	0.185	0.364
		61.0	0.0	0.221	0.355
		68.0	0.25	0.246	0.351
		76.0	0.50	0.275	0.342
		88.5	0.75	0.321	0.340
		104.75	1.0	0.380	0.333
		127.25	1.25	0.461	0.321
		133.5	1.50	0.484	0.248

TABLE III

COPPER SHELL RESULTS

Shell	$t \times 10^3$ inches	R inches	$E \times 10^6$ psi	a inches	μ	S_L/S_{CL}	S_G/S_{CL}
C 1	3.59	4.001	13.32	0.16	1.21	0.433	
C 2	4.57	4.001	13.90	0.198	1.33	0.395	0.520
C 3	4.64	4.001	13.75	0.24	1.60	0.391	0.620
C 4	4.62	4.001	14.57	0.16	1.07	0.507	0.512
C 5	4.40	4.003	13.98	0.12	0.82	0.531	0.551
C 6	4.17	4.003	14.35	0.40	2.82	0.398	

All Shells were 8 inches long.

S_L = Local Buckling

S_G = General Collapse

TABLE IV

RESULTS OF THE ANALYSIS

R/t = 100		R/t = 200		R/t = 400		R/t = 533		R/t = 800	
μ	S/S_{CL}	μ	S/S_{CL}	μ	S/S_{CL}	μ	S/S_{CL}	μ	S/S_{CL}
0.091	1.95	0.128	1.87	0.182	1.76	0.21	1.71	0.257	1.64
0.182	1.76	0.257	1.64	0.364	1.50	0.42	1.42	0.515	1.30
0.273	1.63	0.386	1.47	0.728	1.05	0.63	1.16	0.772	1.01
0.364	1.50	0.515	1.30	1.09	0.76	0.84	0.94	1.03	0.80
0.546	1.26	0.772	1.01	1.45	0.60	1.26	0.67	1.54	0.57
0.728	1.05	1.03	0.80	1.82	0.52	1.68	0.54	2.06	0.49
0.91	0.88	1.28	0.66	2.55	0.48	2.10	0.49	2.58	0.48
1.09	0.76	1.54	0.57	2.91	0.49	2.52	0.48	3.08	0.50
1.27	0.67	1.80	0.52	3.27	0.51	2.94	0.49	3.60	0.54
1.45	0.60	2.06	0.49	3.64	0.54	3.34	0.52		
1.64	0.55	2.31	0.48			3.78	0.54		
1.82	0.52	2.58	0.48						

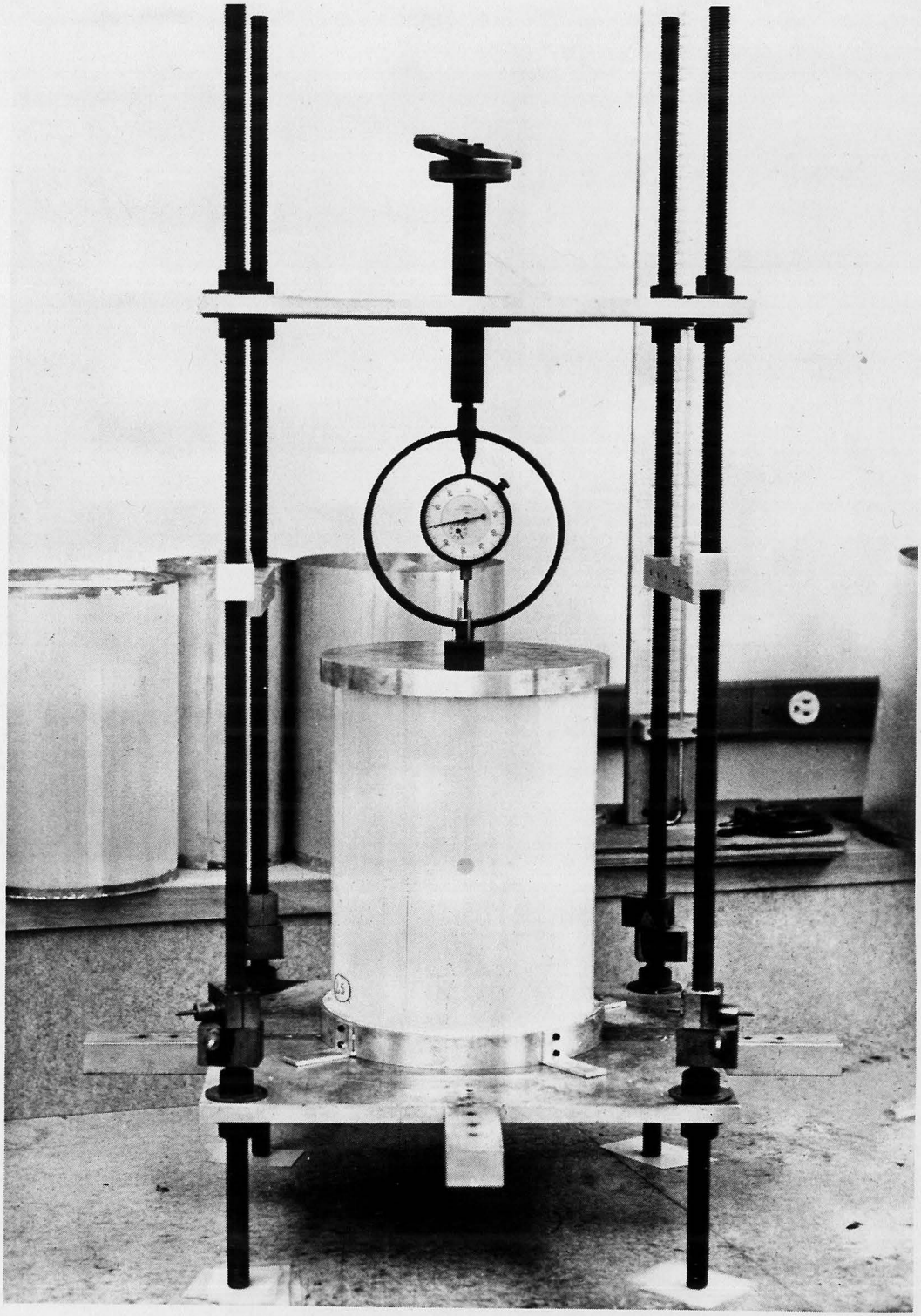

FIG. 1 MYLAR SHELL AND TEST APPARATUS

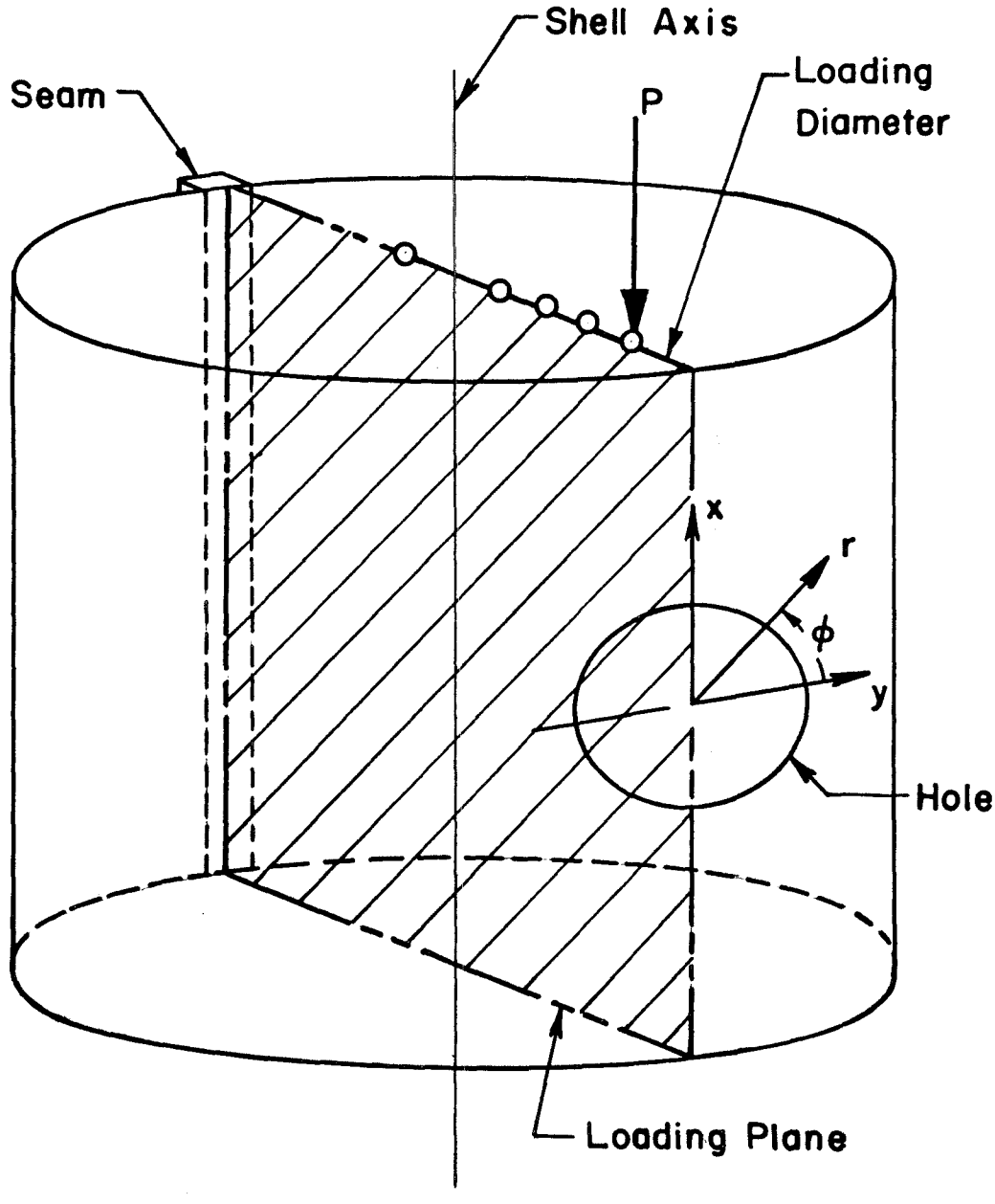

FIG. 2 MYLAR SHELL LOADING PLANE AND HOLE COORDINATES

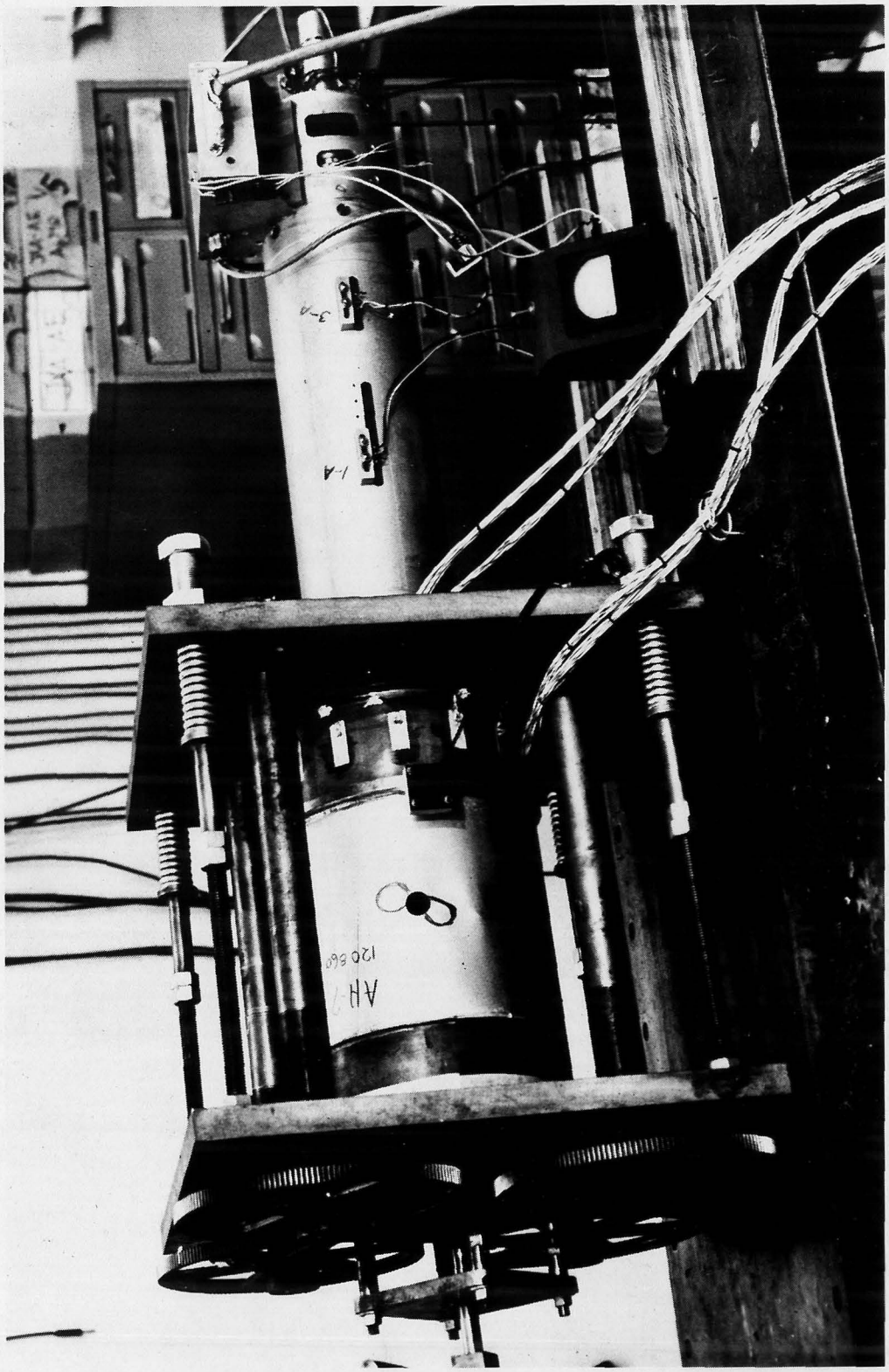

FIG. 3 COPPER SHELL AND TEST APPARATUS

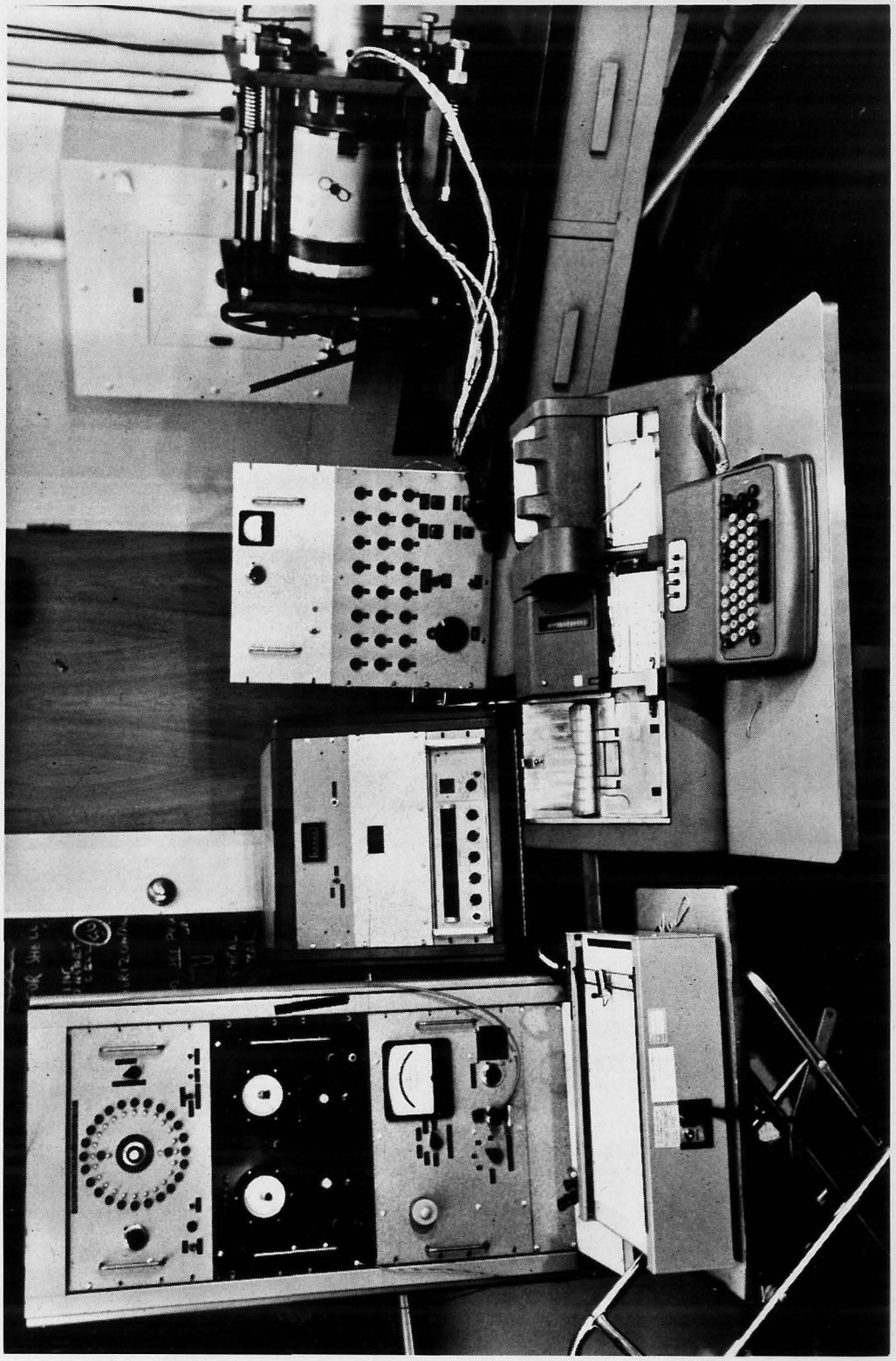

FIG. 4 COPPER SHELL DATA ACQUISITION SYSTEM

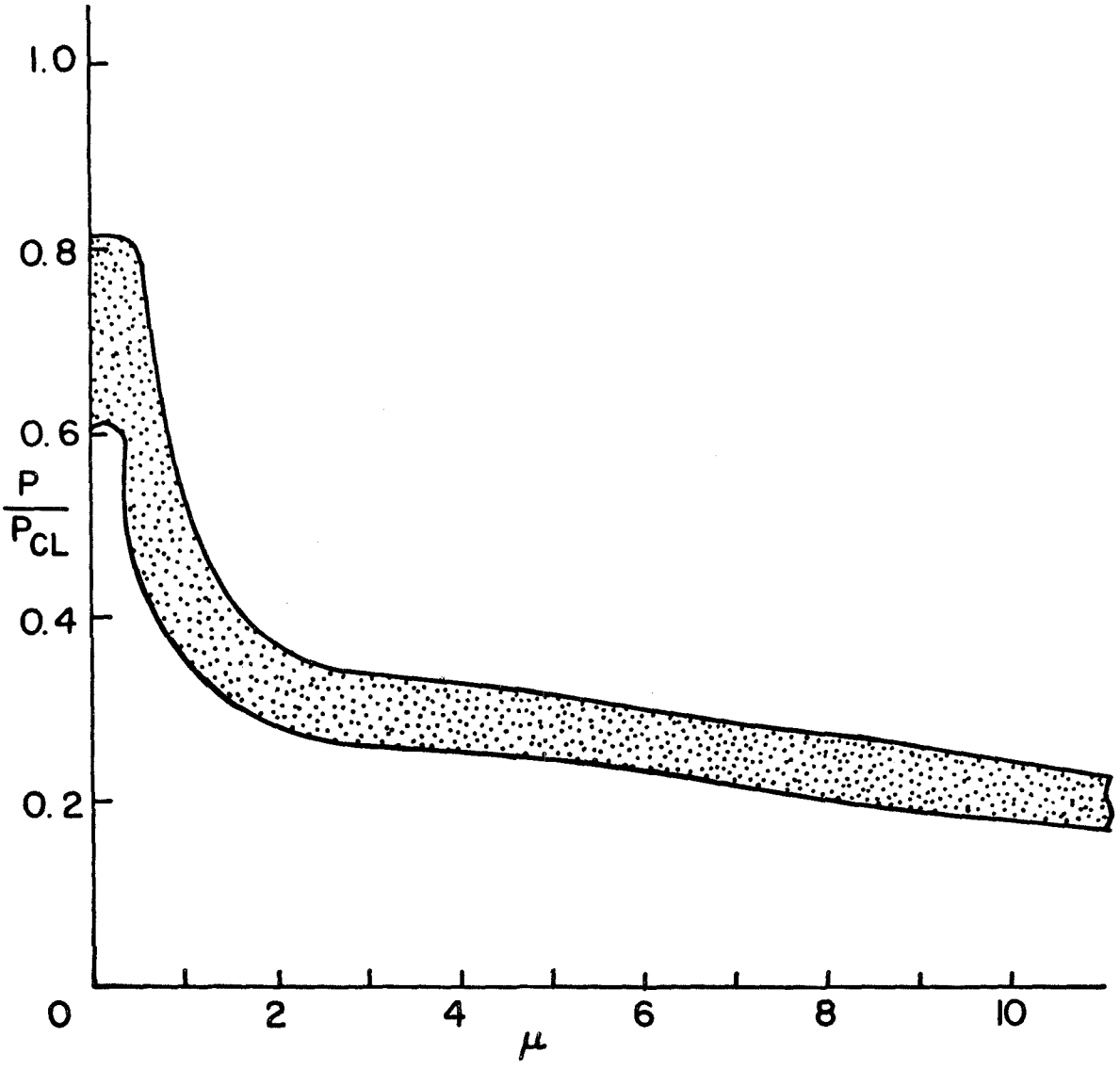

FIG. 5 SUMMARY OF BUCKLING LOADS FOR MYLAR SHELLS

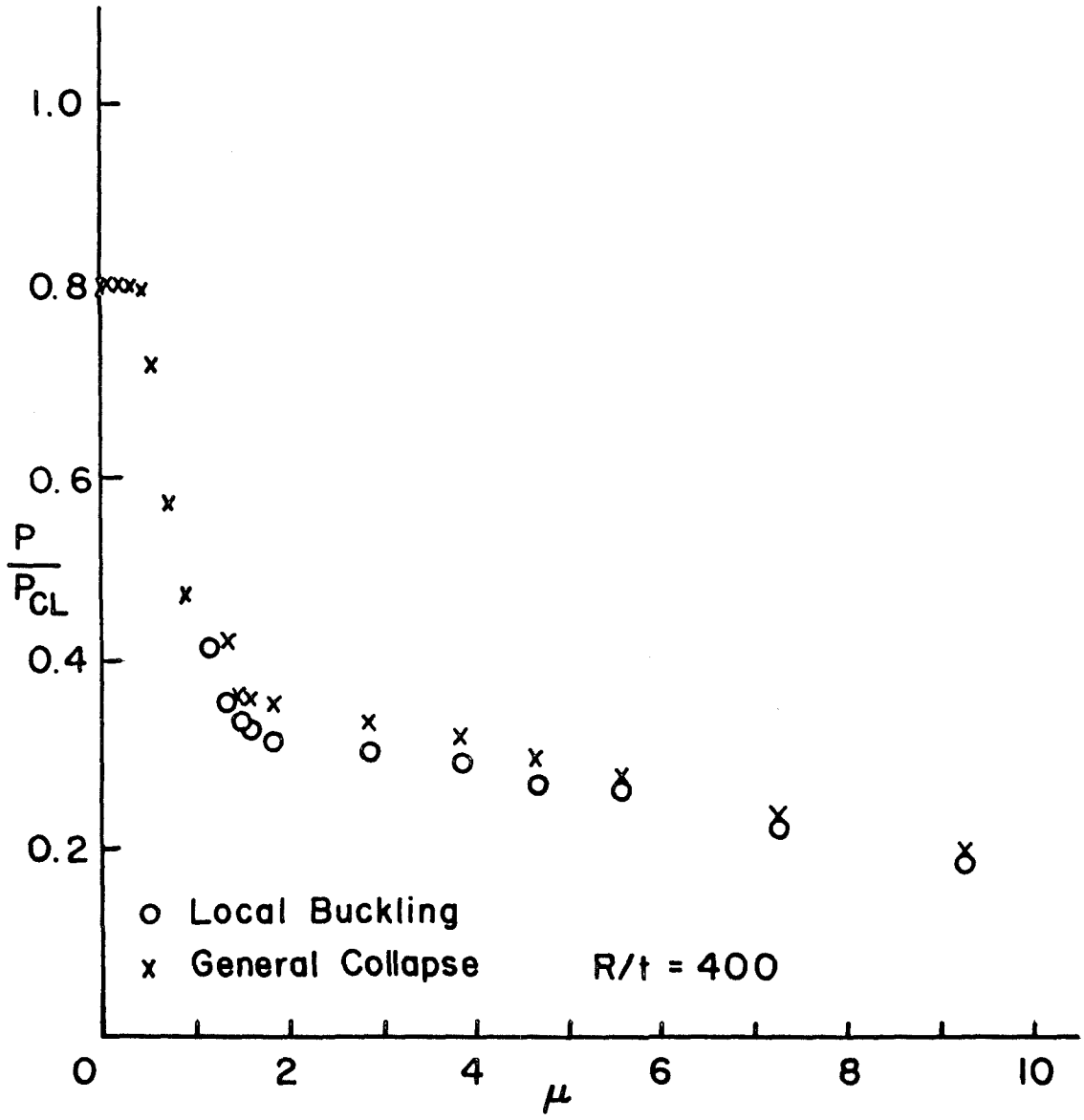

FIG. 6 BUCKLING LOADS OF SHELL 6

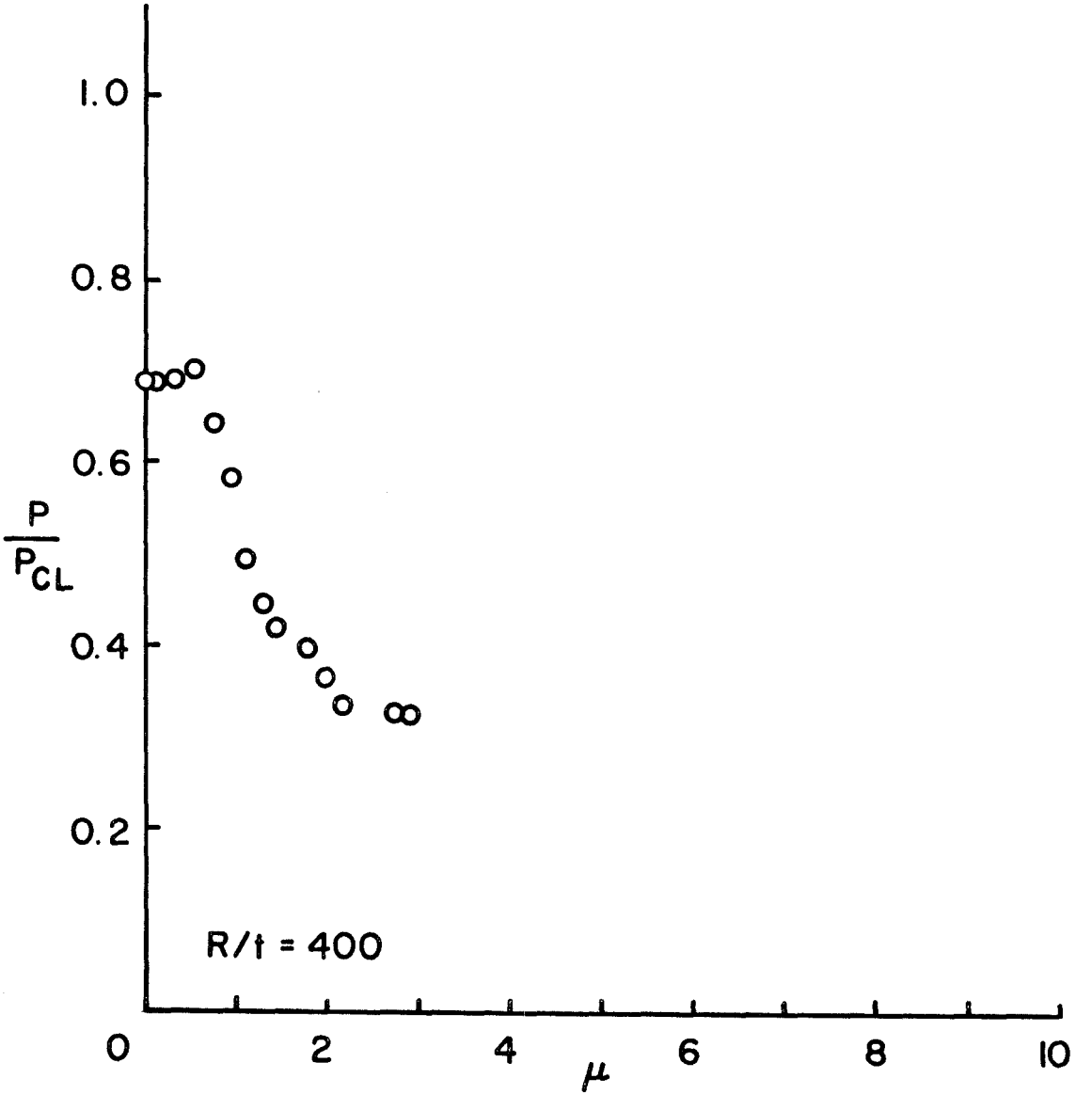

FIG. 7 BUCKLING LOADS OF SHELL 7

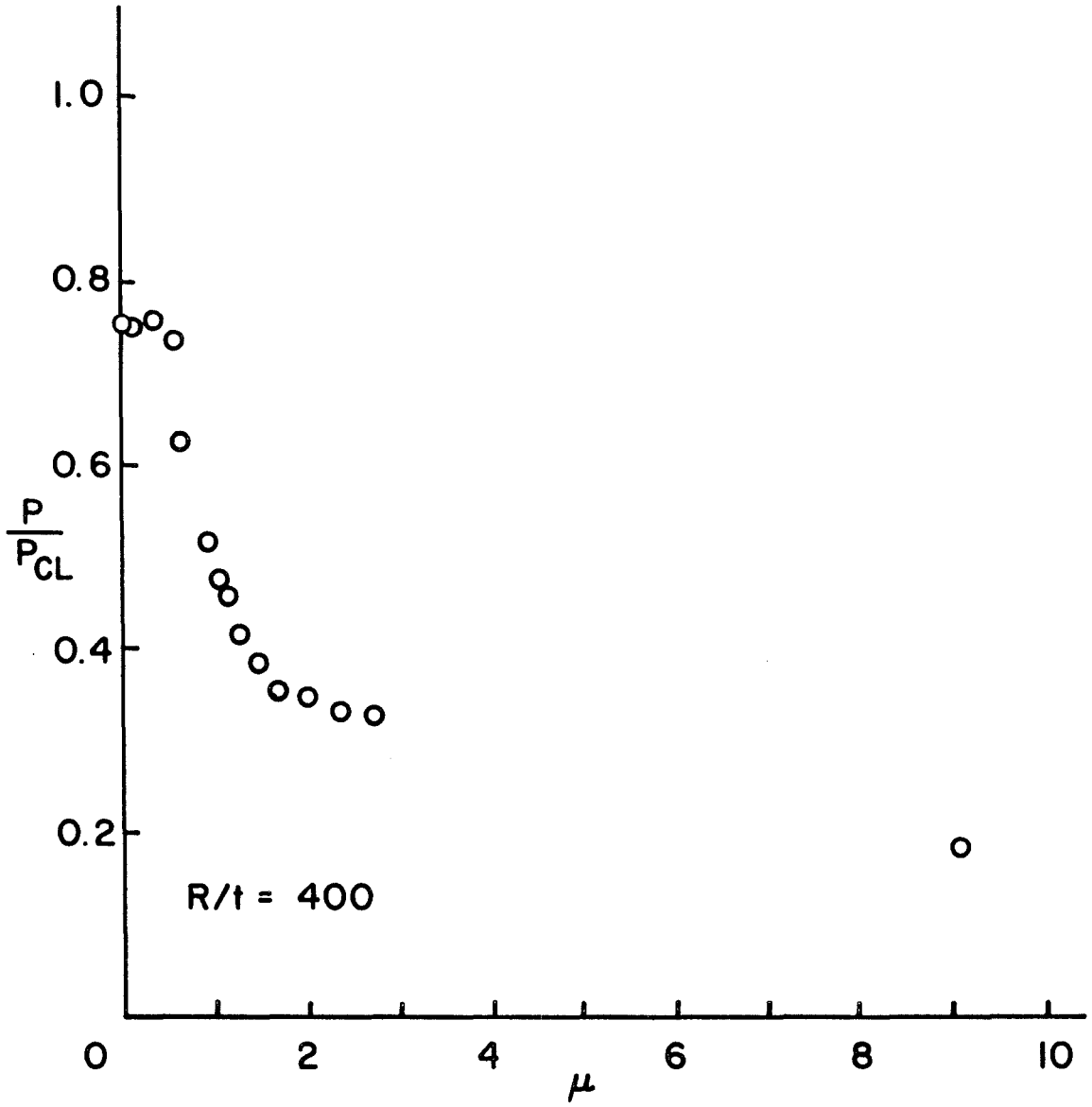

FIG. 8 BUCKLING LOADS OF SHELL 14

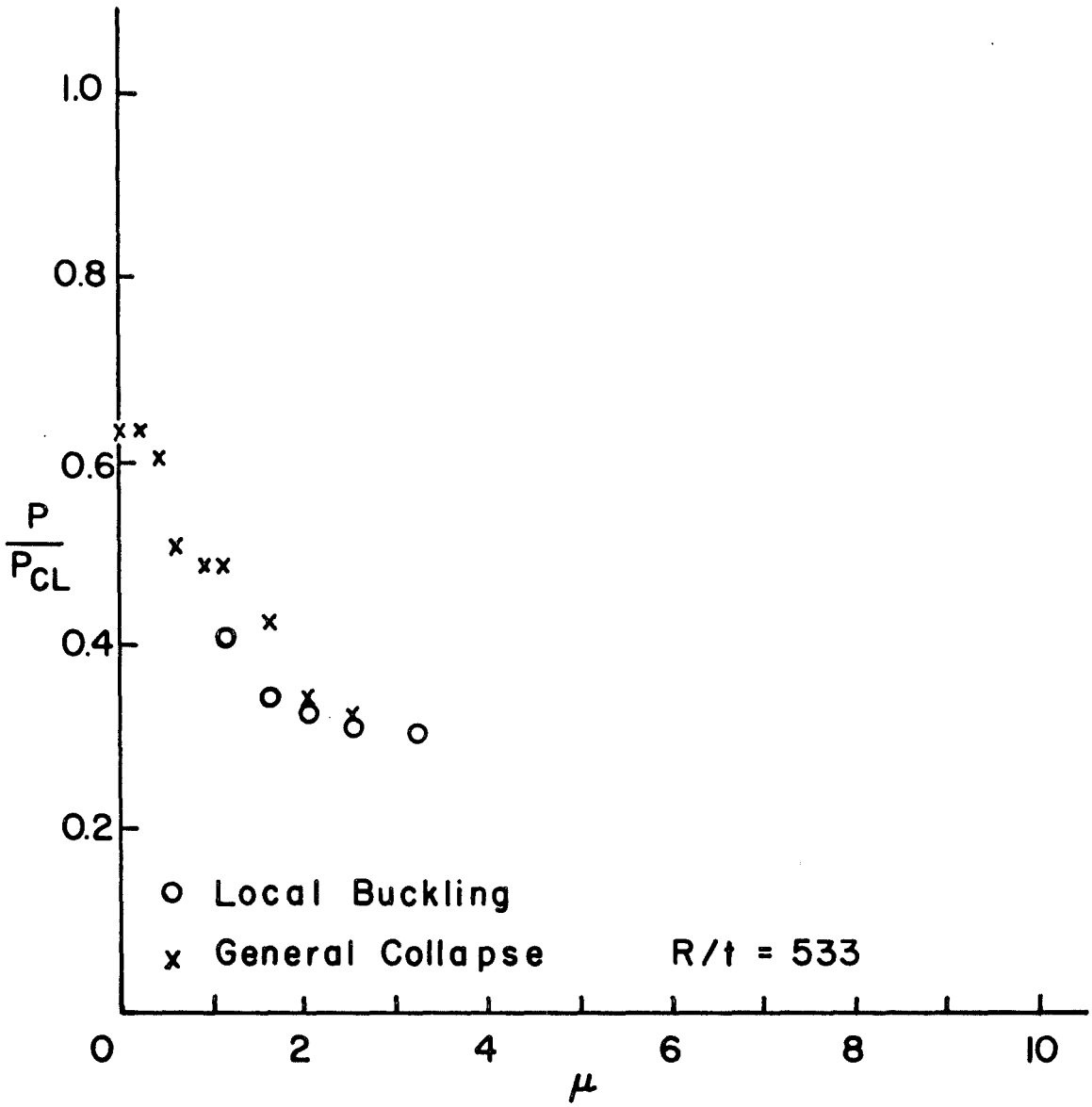

FIG. 9 BUCKLING LOADS OF SHELL 17

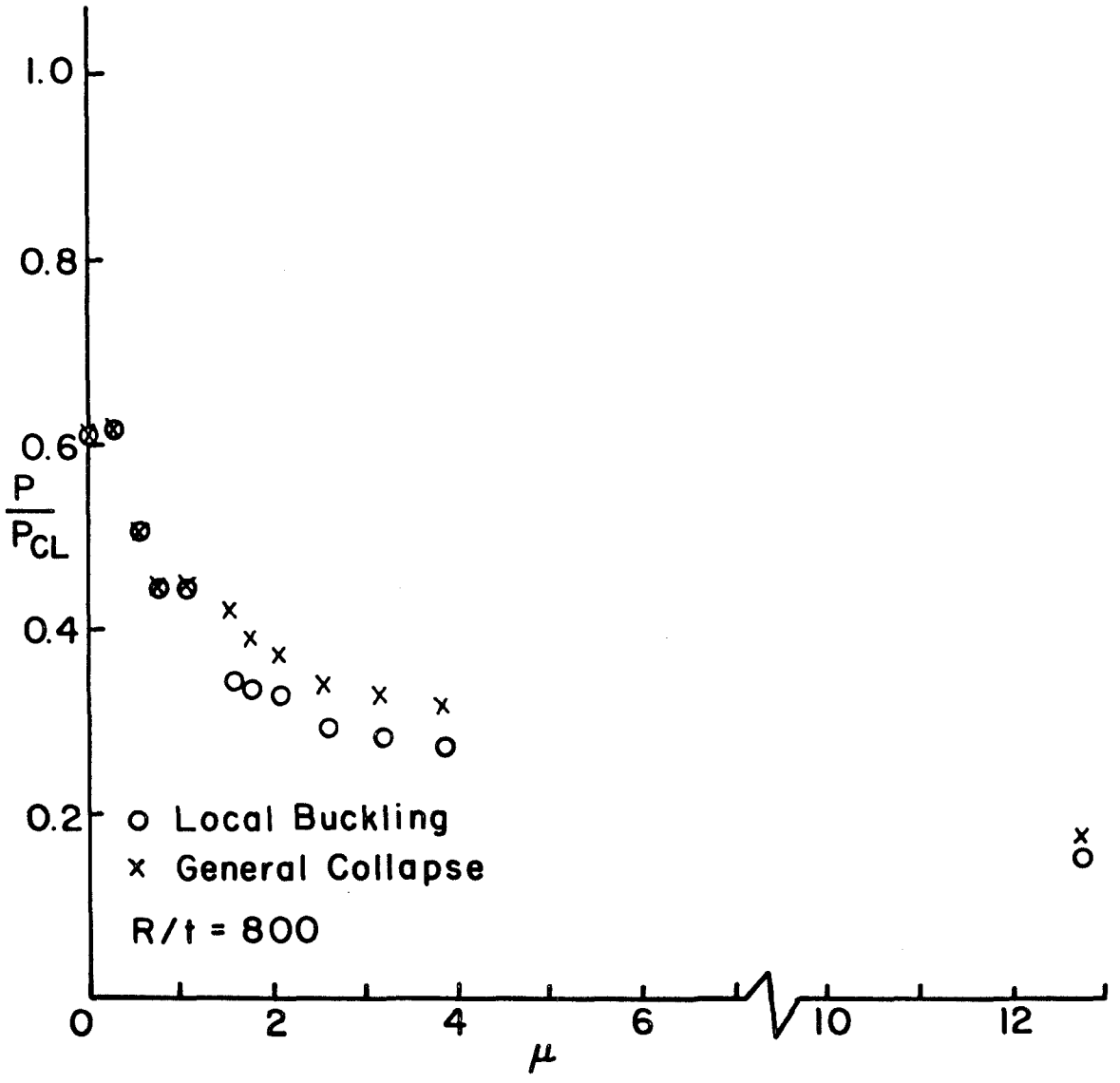

FIG.10 BUCKLING LOADS OF SHELL 20

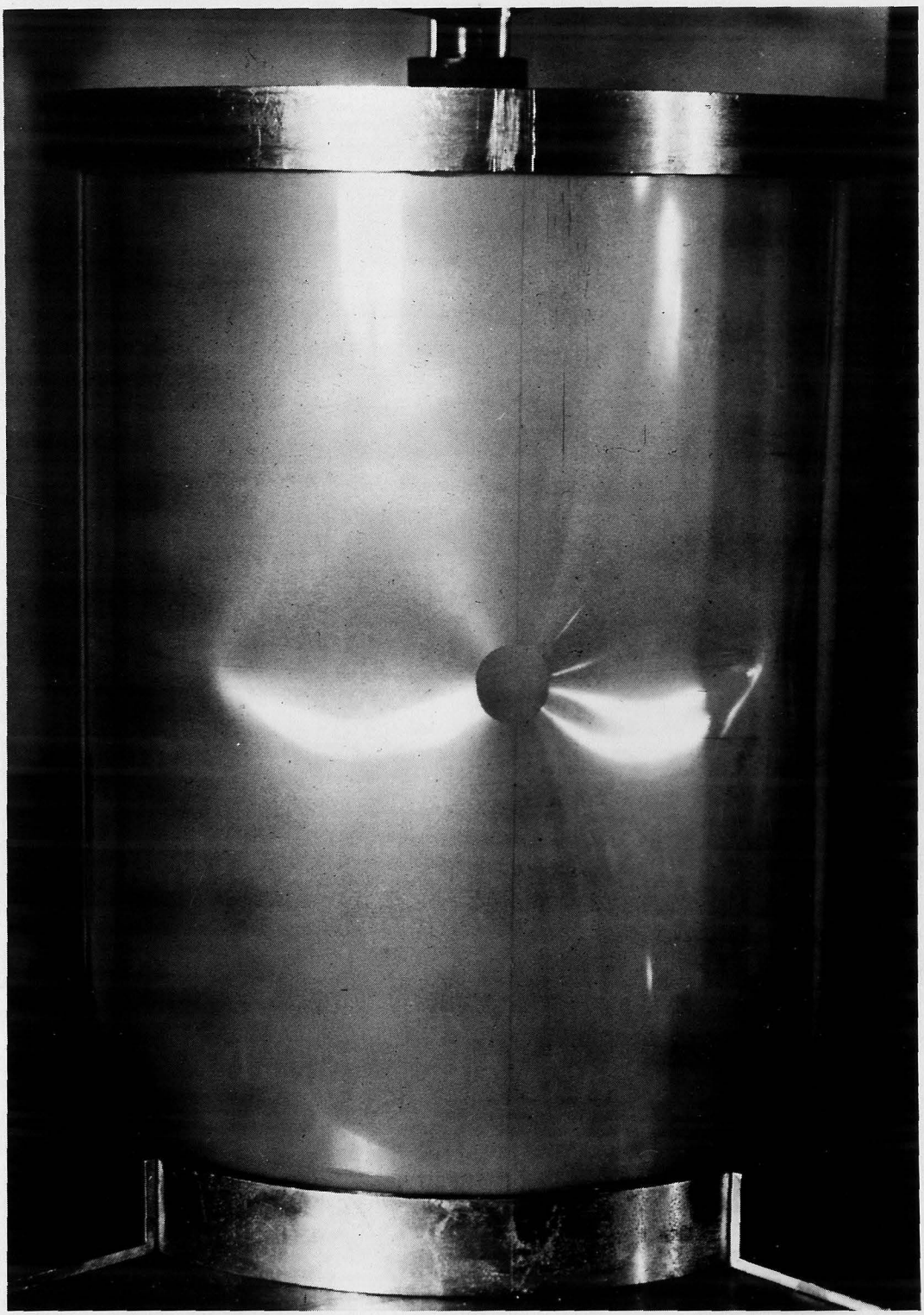

FIG. 11 LOCAL BUCKLING OF A MYLAR SHELL FOR $\mu > 2$

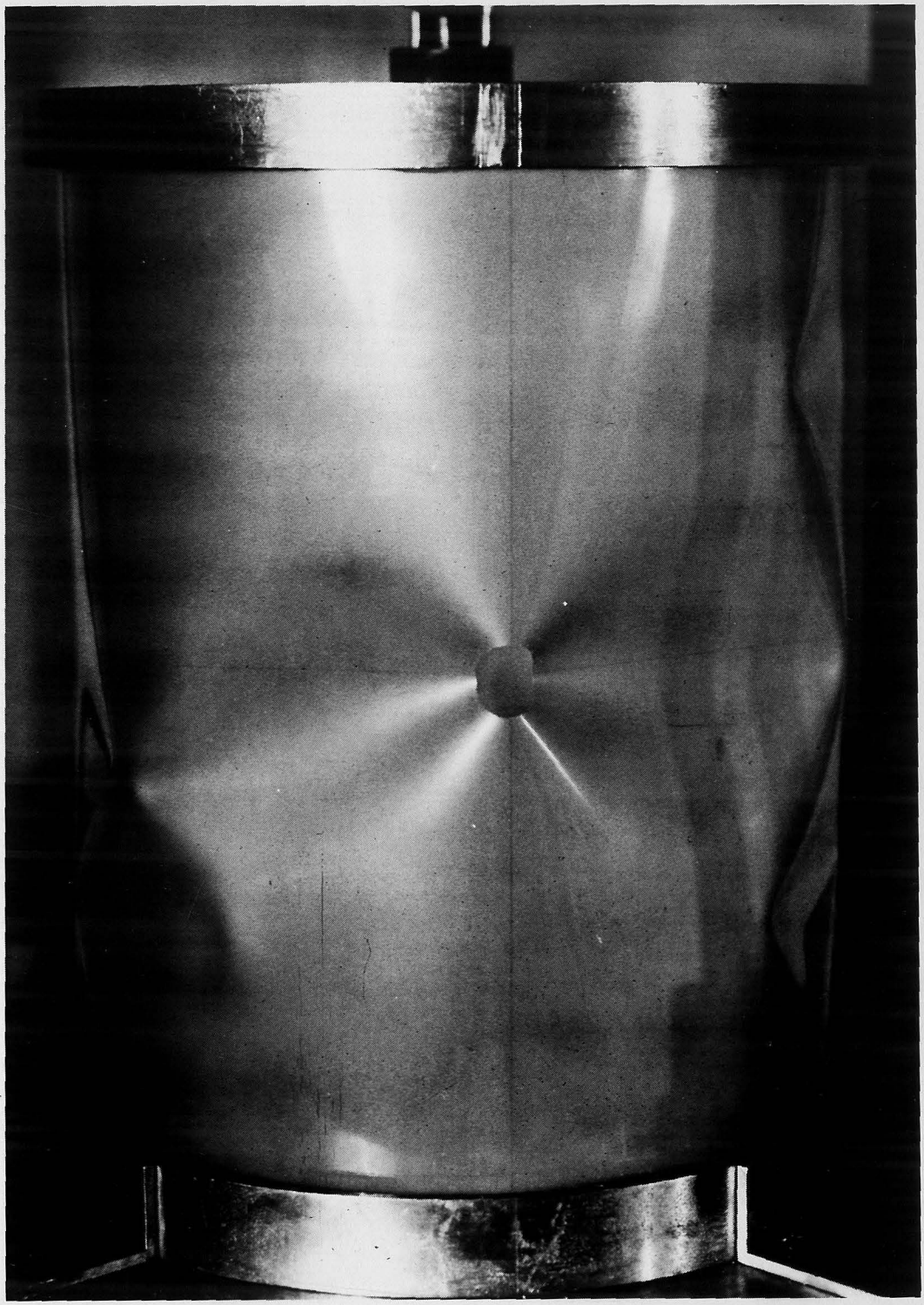

FIG. 12 GENERAL COLLAPSE OF A MYLAR SHELL FOR $\mu > 2$

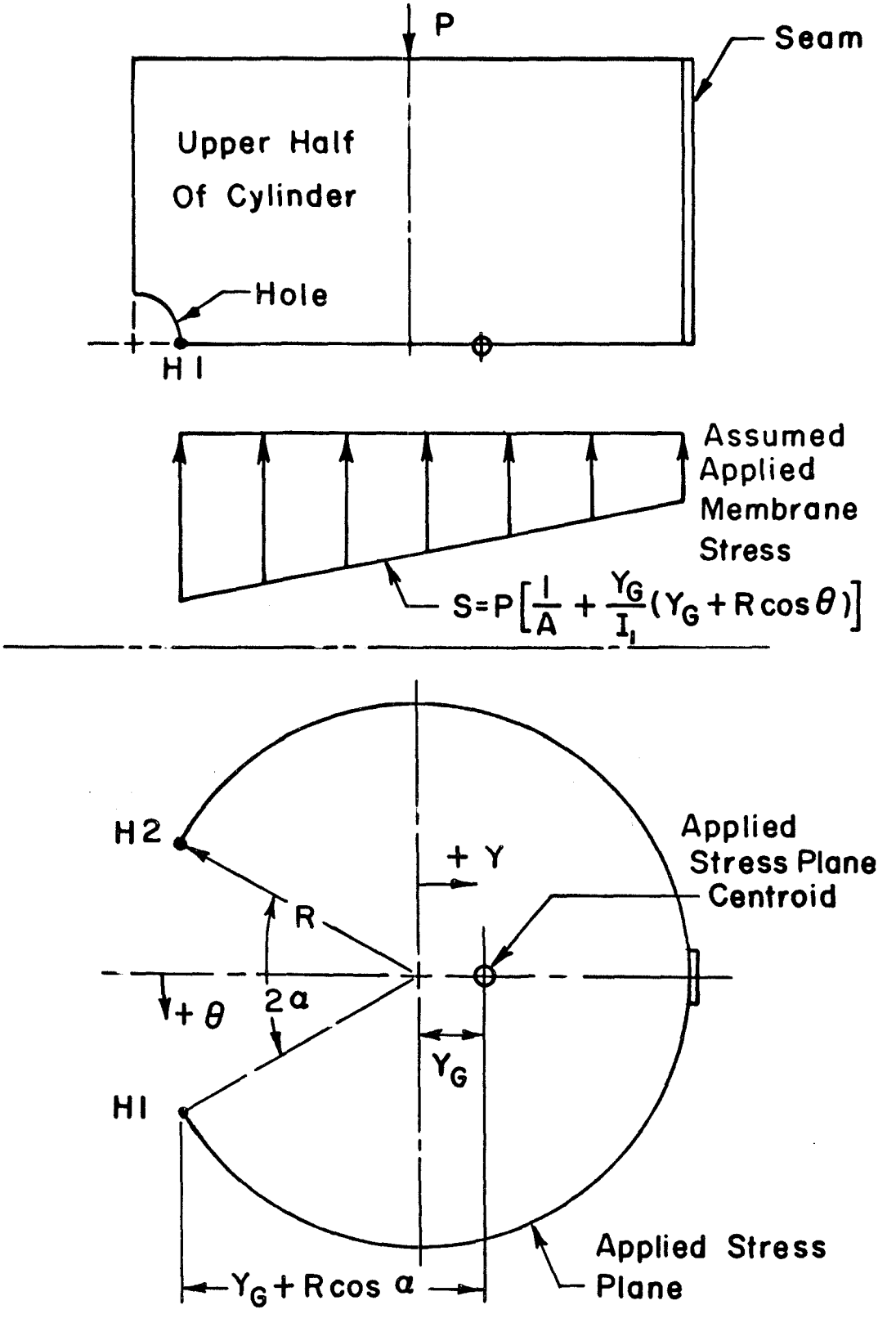

FIG. 13 ASSUMED APPLIED STRESSES AND APPLIED STRESS PLANE GEOMETRY

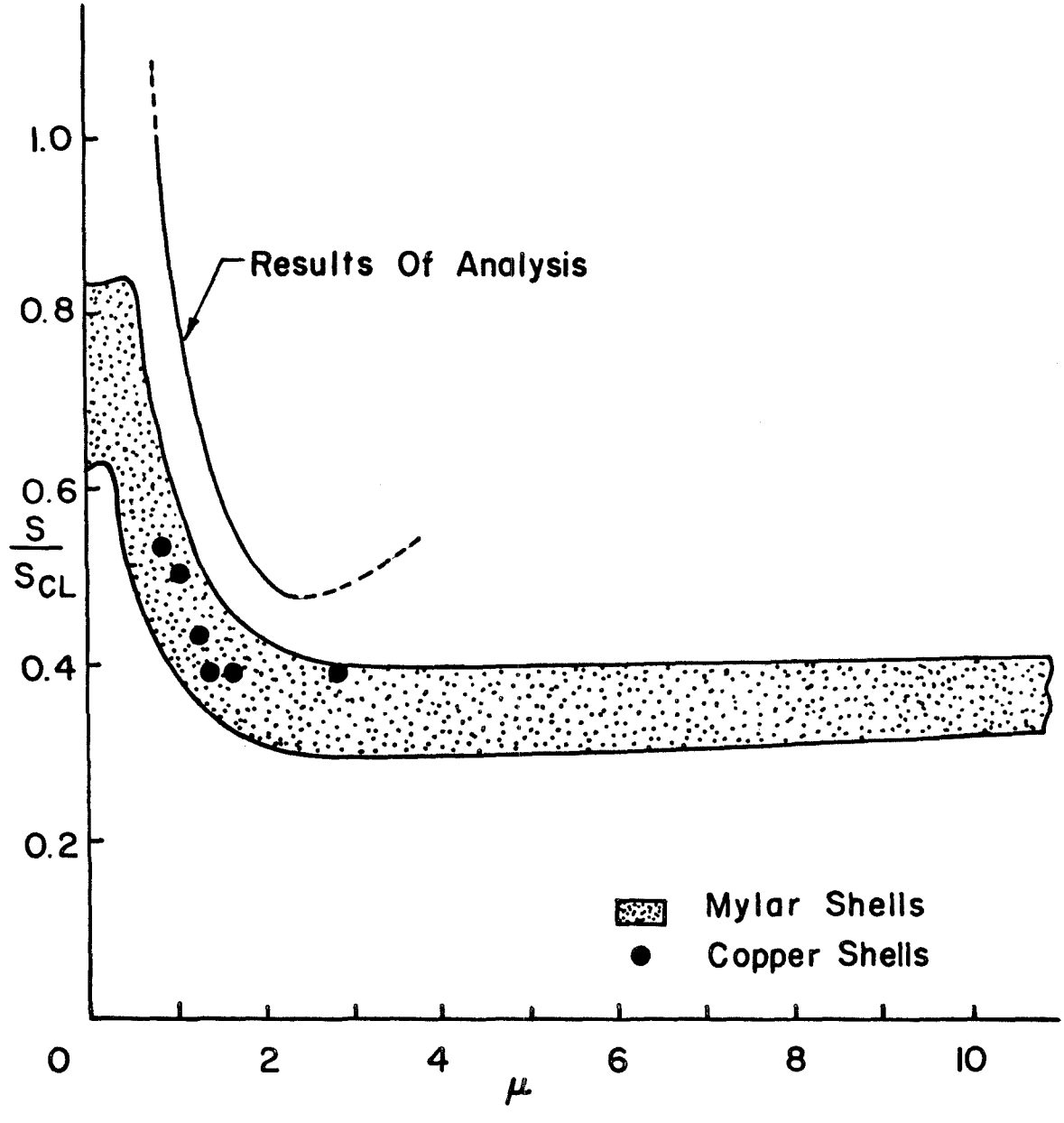

FIG. 14 SUMMARY OF THE BUCKLING STRESSES AND ANALYSIS FOR ALL SHELLS

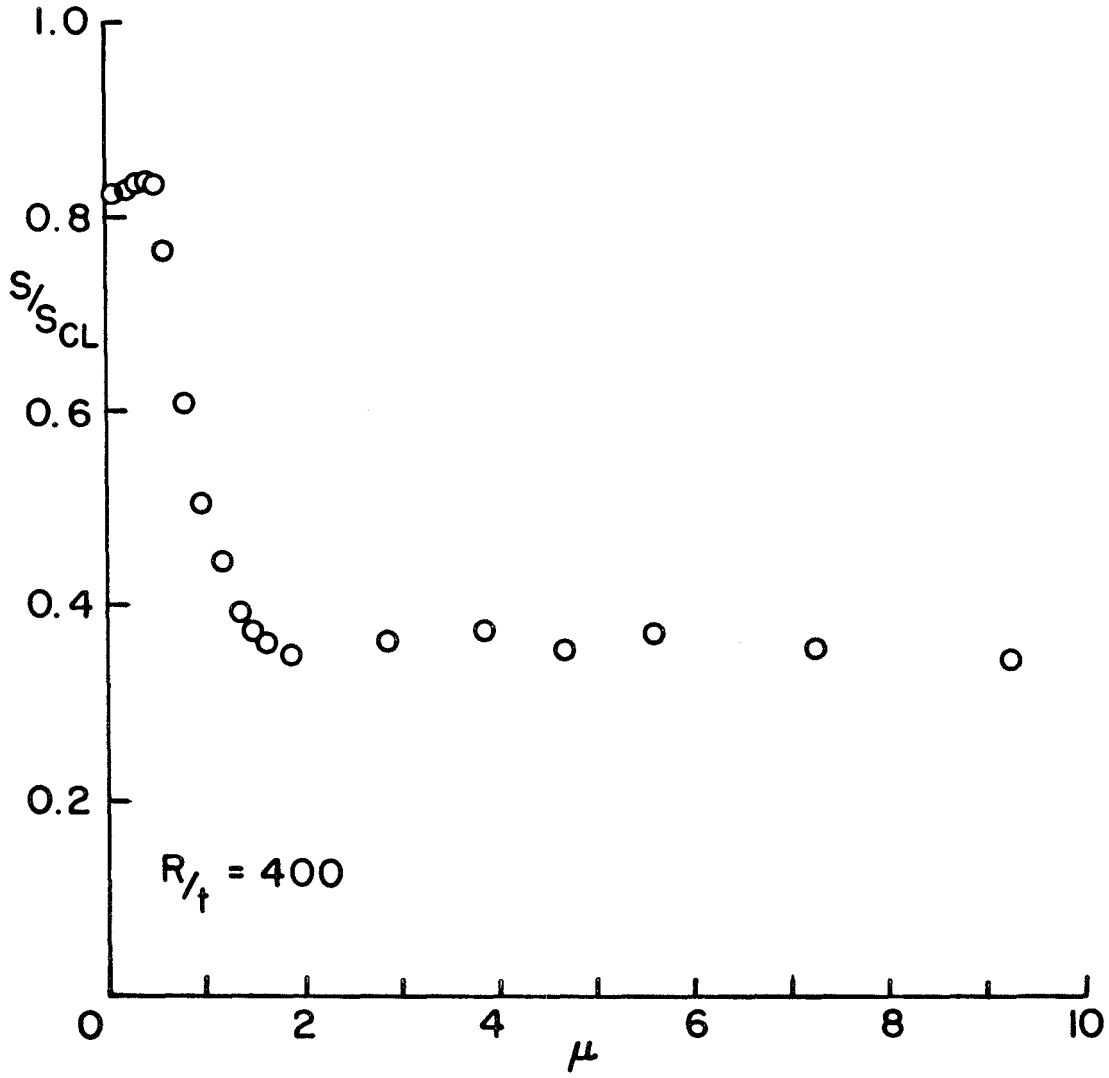

FIG. 15 BUCKLING STRESSES OF SHELL 6

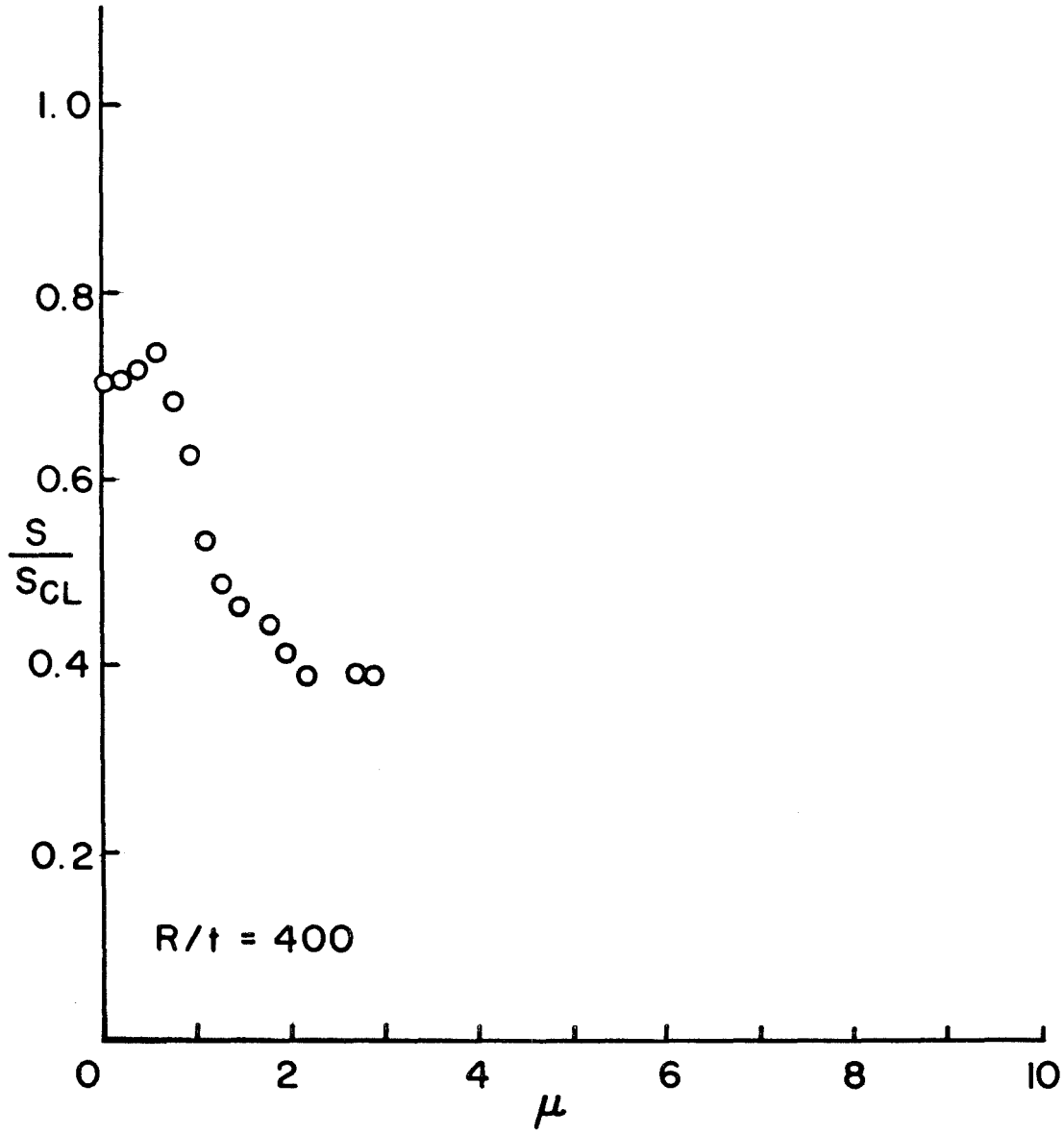

FIG. 16 BUCKLING STRESSES OF SHELL 7

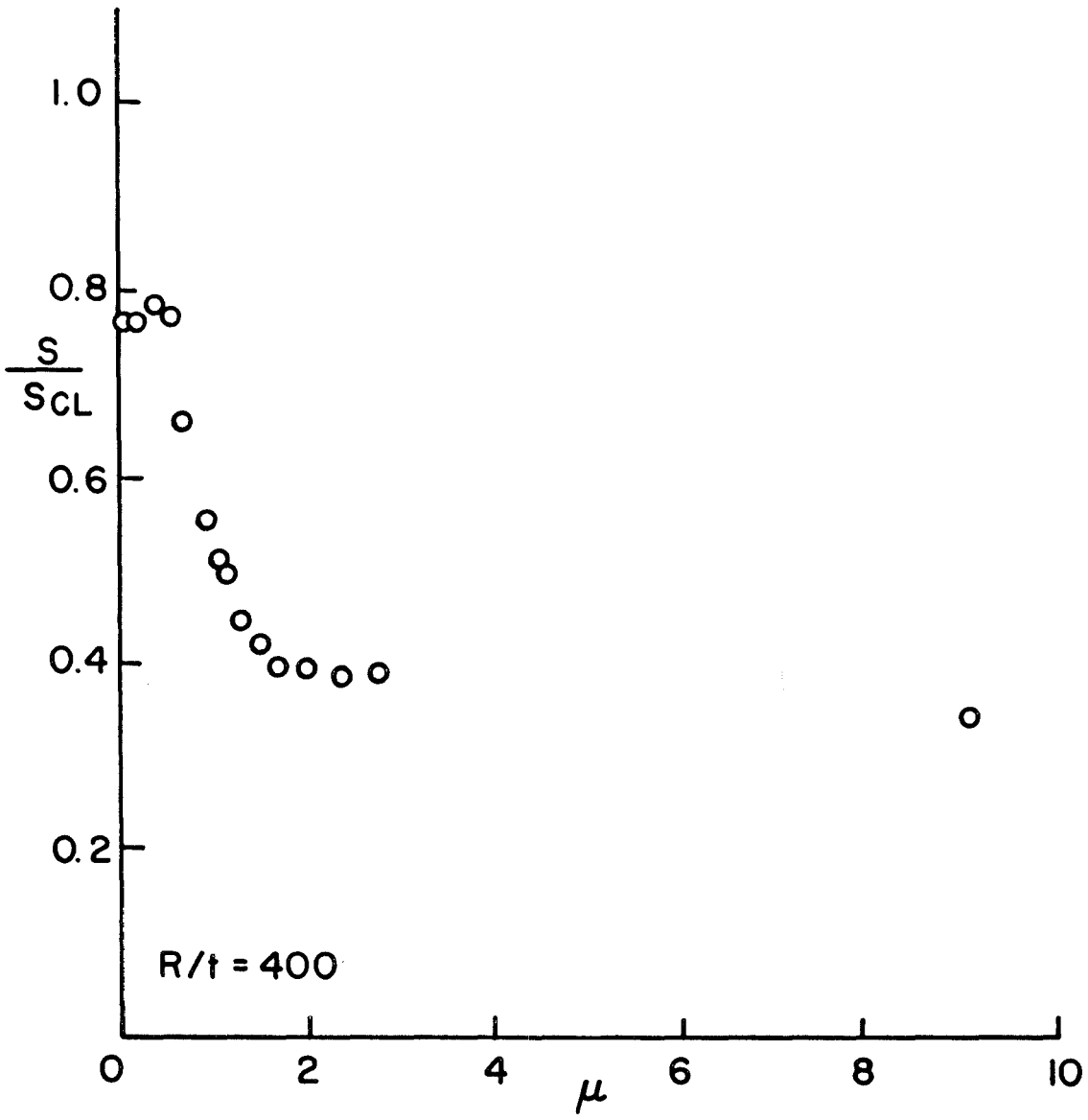

FIG. 17 BUCKLING STRESSES OF SHELL 14

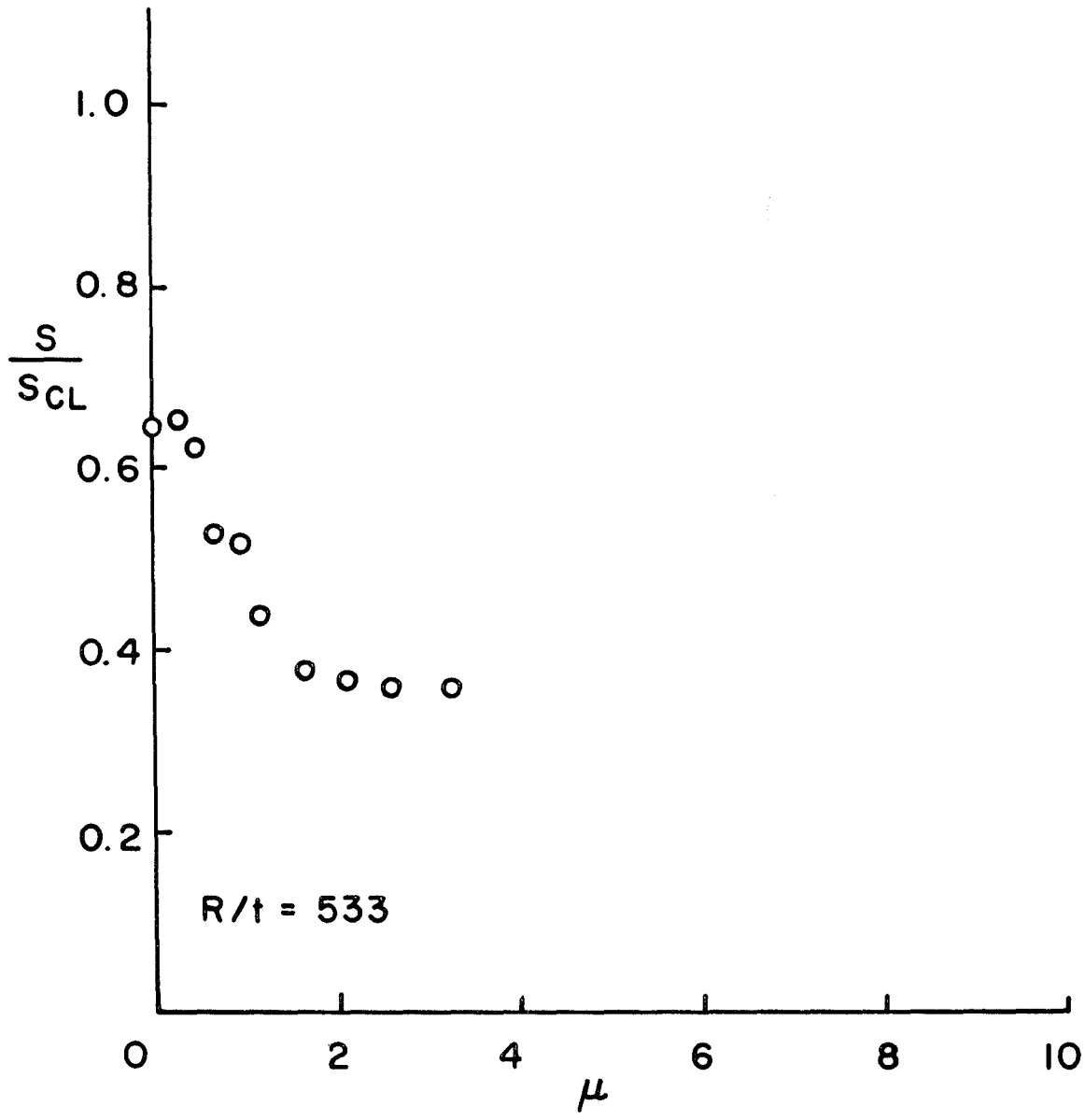

FIG. 18 BUCKLING STRESSES OF SHELL 17

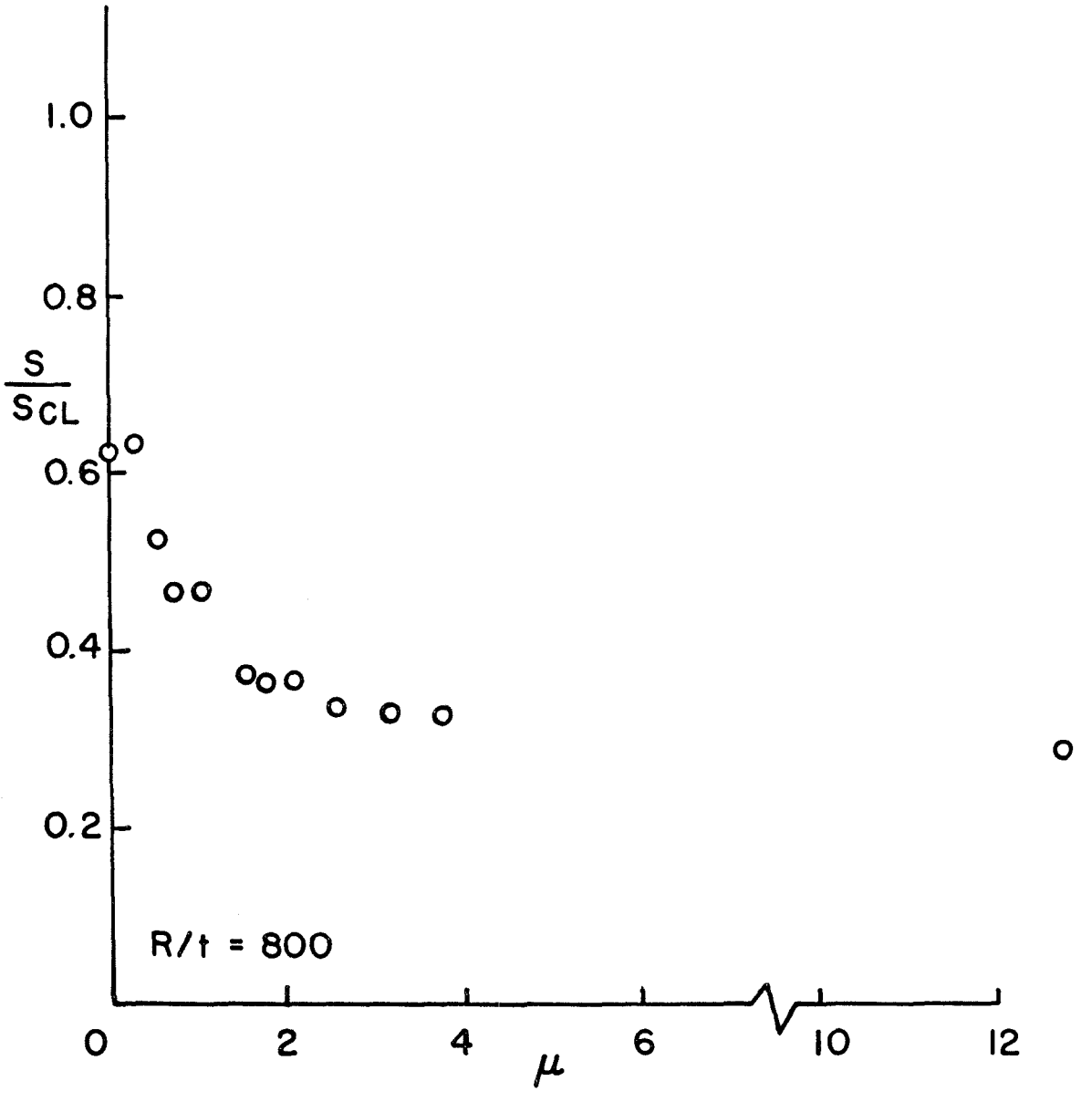

FIG. 19 BUCKLING STRESSES OF SHELL 20

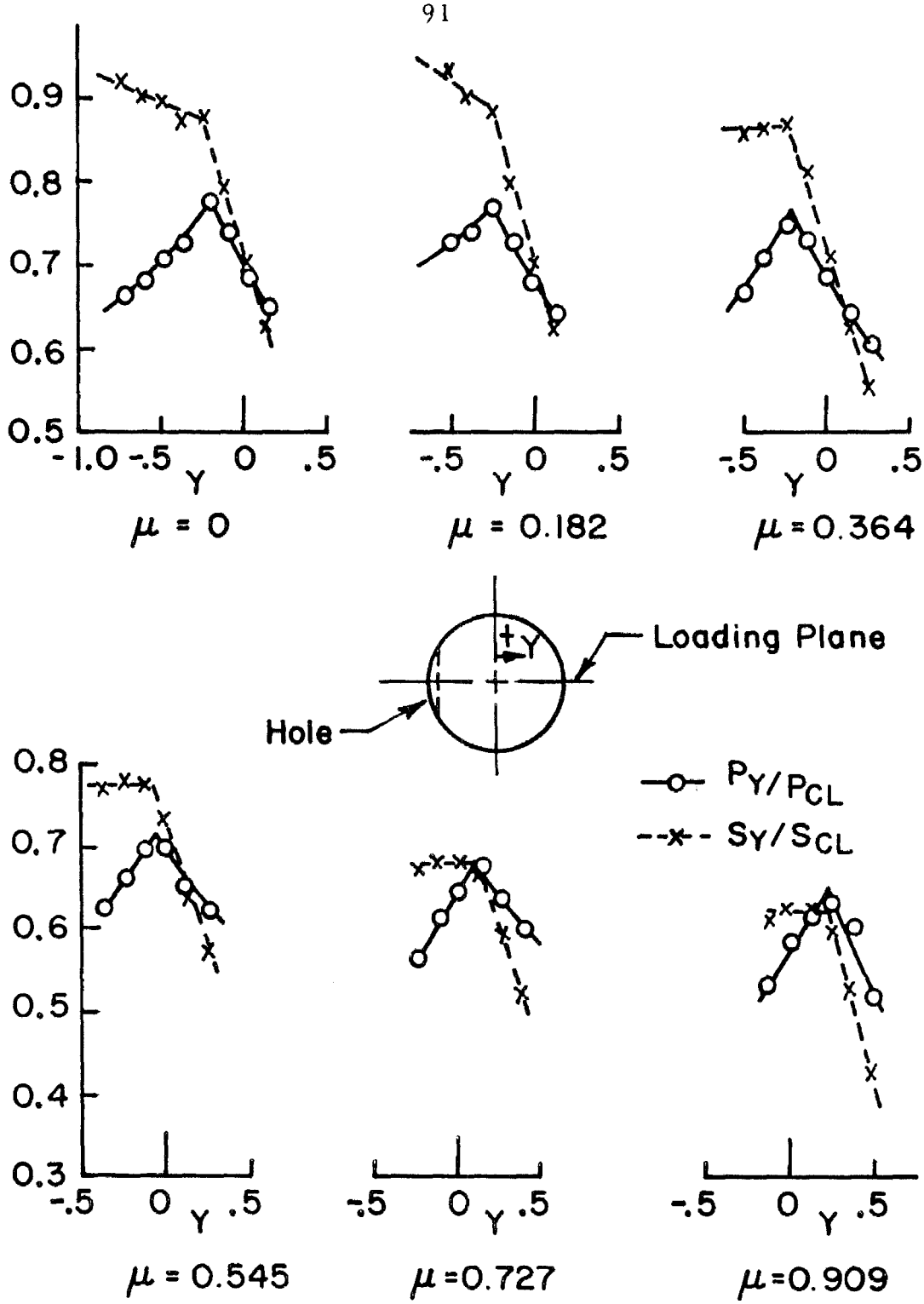

FIG. 20 EFFECT OF LOAD LOCATION ON THE BUCKLING LOADS AND STRESSES OF SHELL 7

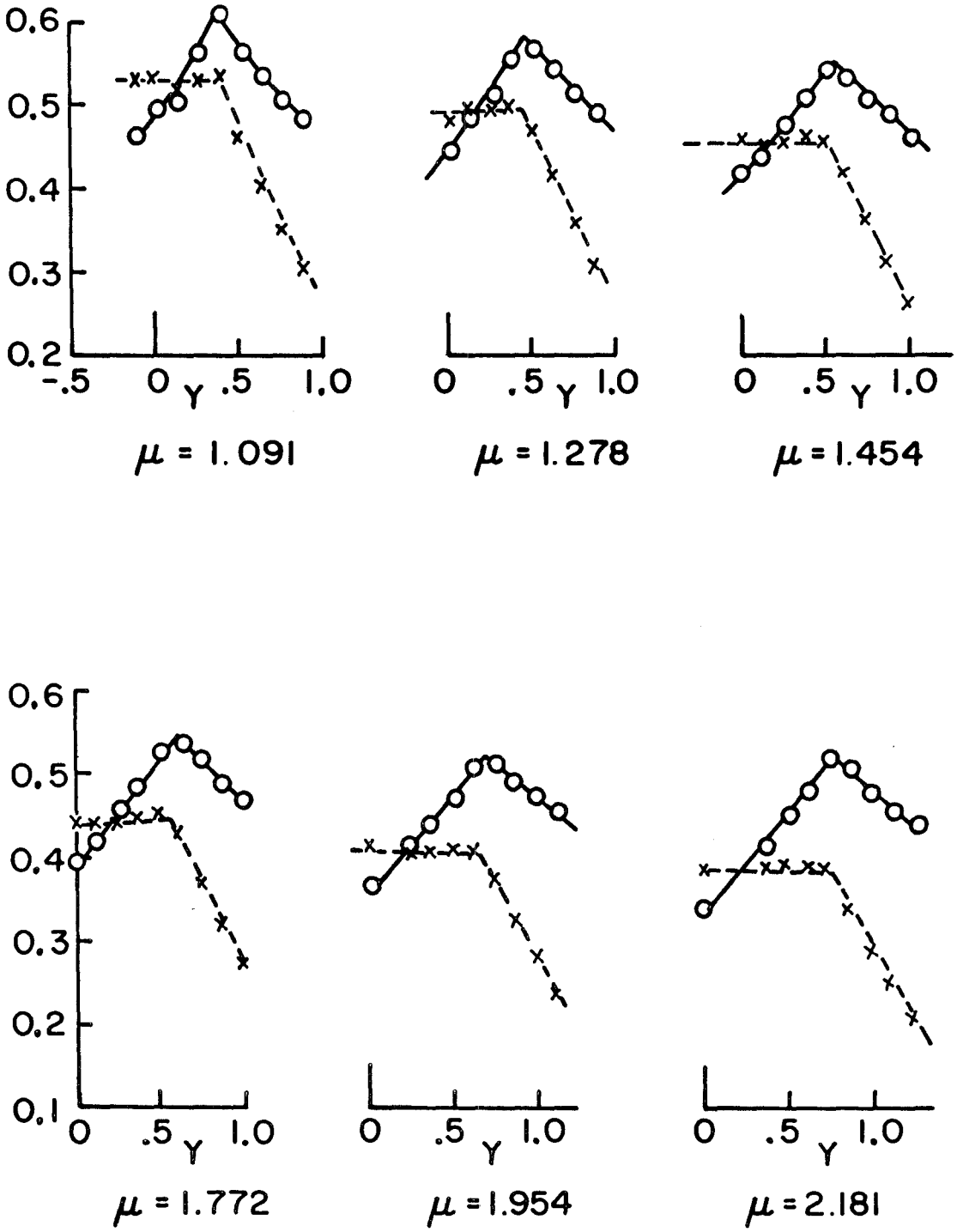

FIG.20 (CONT.) EFFECT OF LOAD LOCATION ON THE BUCKLING LOADS AND STRESSES OF SHELL 7

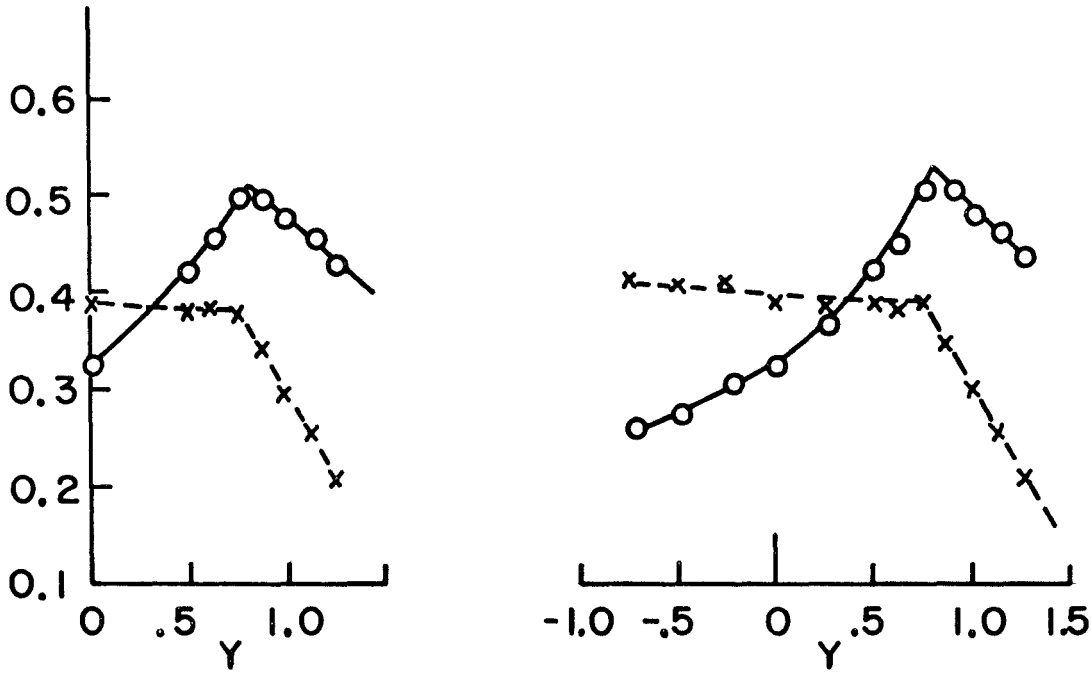

$\mu = 2.727$ $\mu = 2.897$

FIG.20 (CONT.) EFFECT OF LOAD LOCATION ON THE BUCKLING LOADS AND STRESSES OF SHELL 7

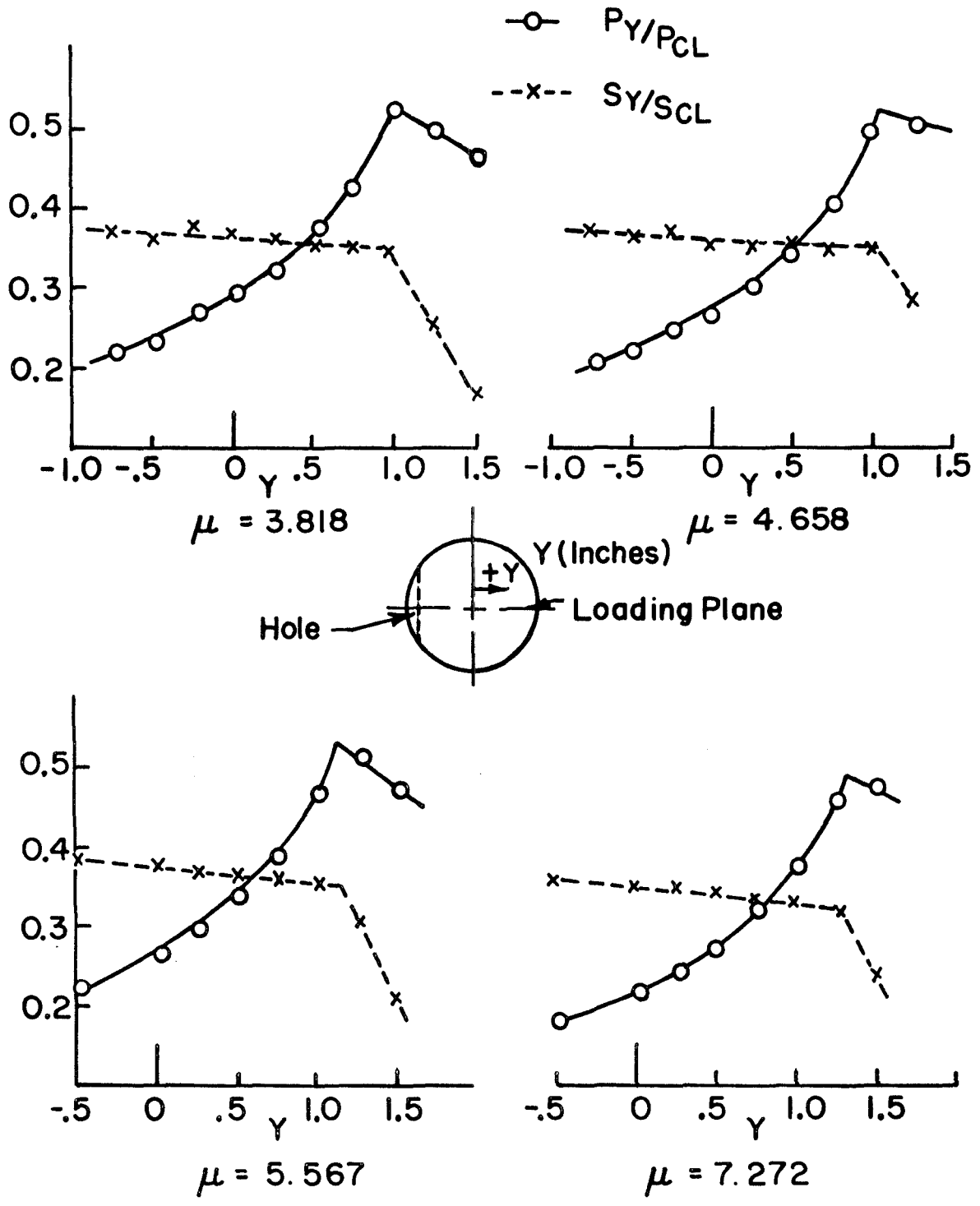

FIG.21 EFFECT OF LOAD LOCATION ON THE BUCKLING LOADS AND STRESSES OF SHELL 6

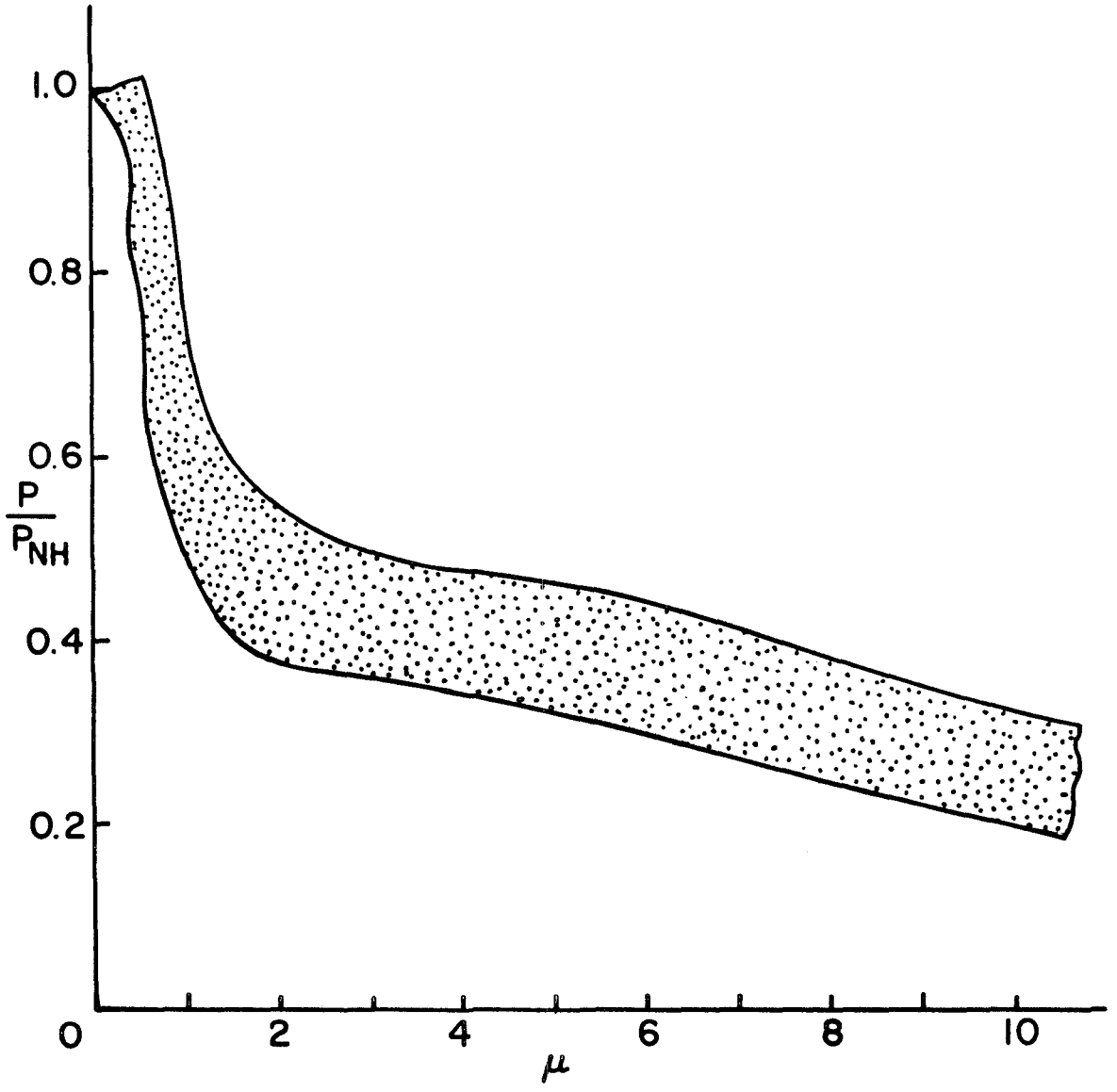

FIG.22 SUMMARY OF BUCKLING LOADS FOR MYLAR SHELLS

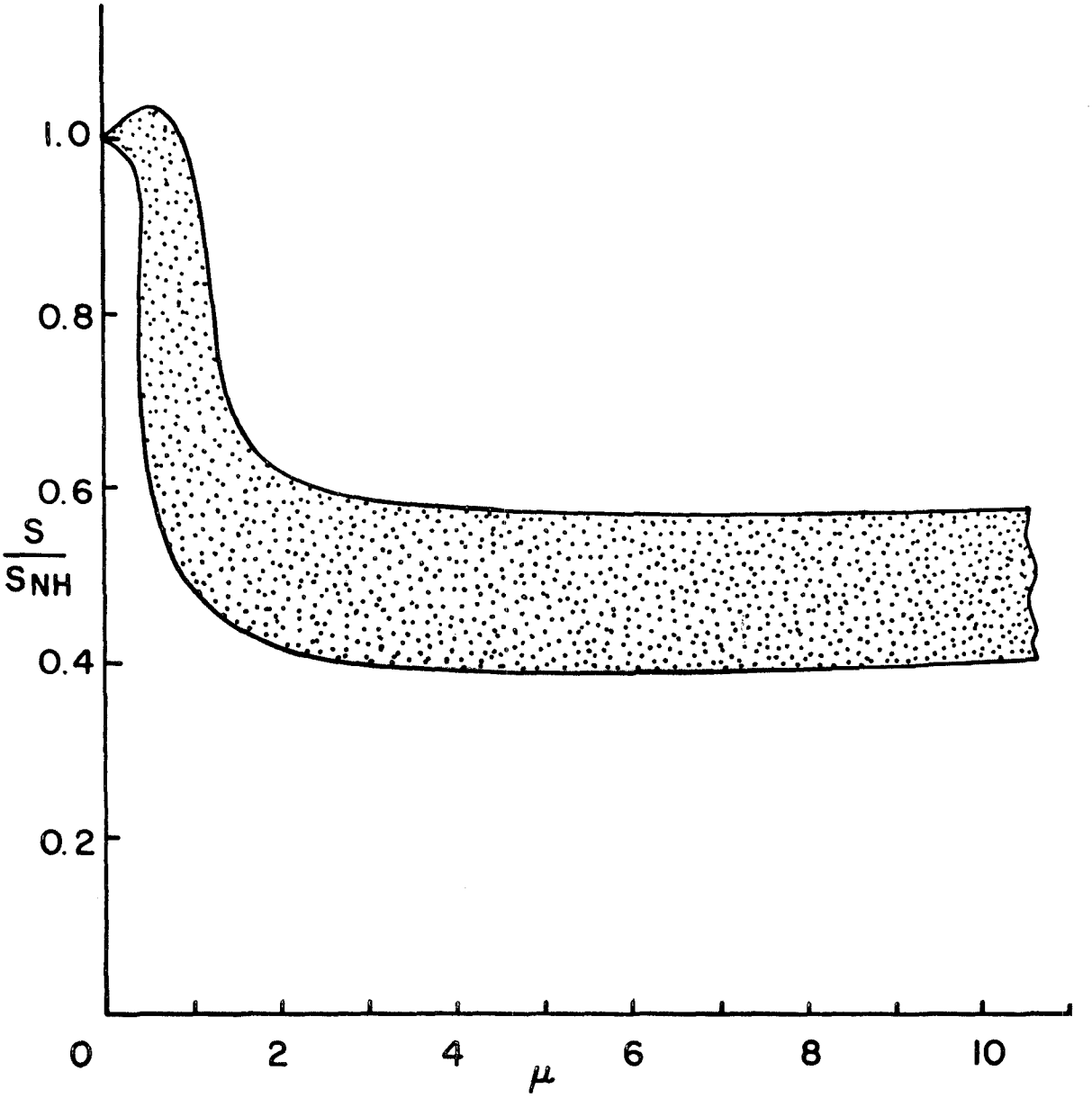

FIG.23 SUMMARY OF BUCKLING STRESSES FOR MYLAR SHELLS

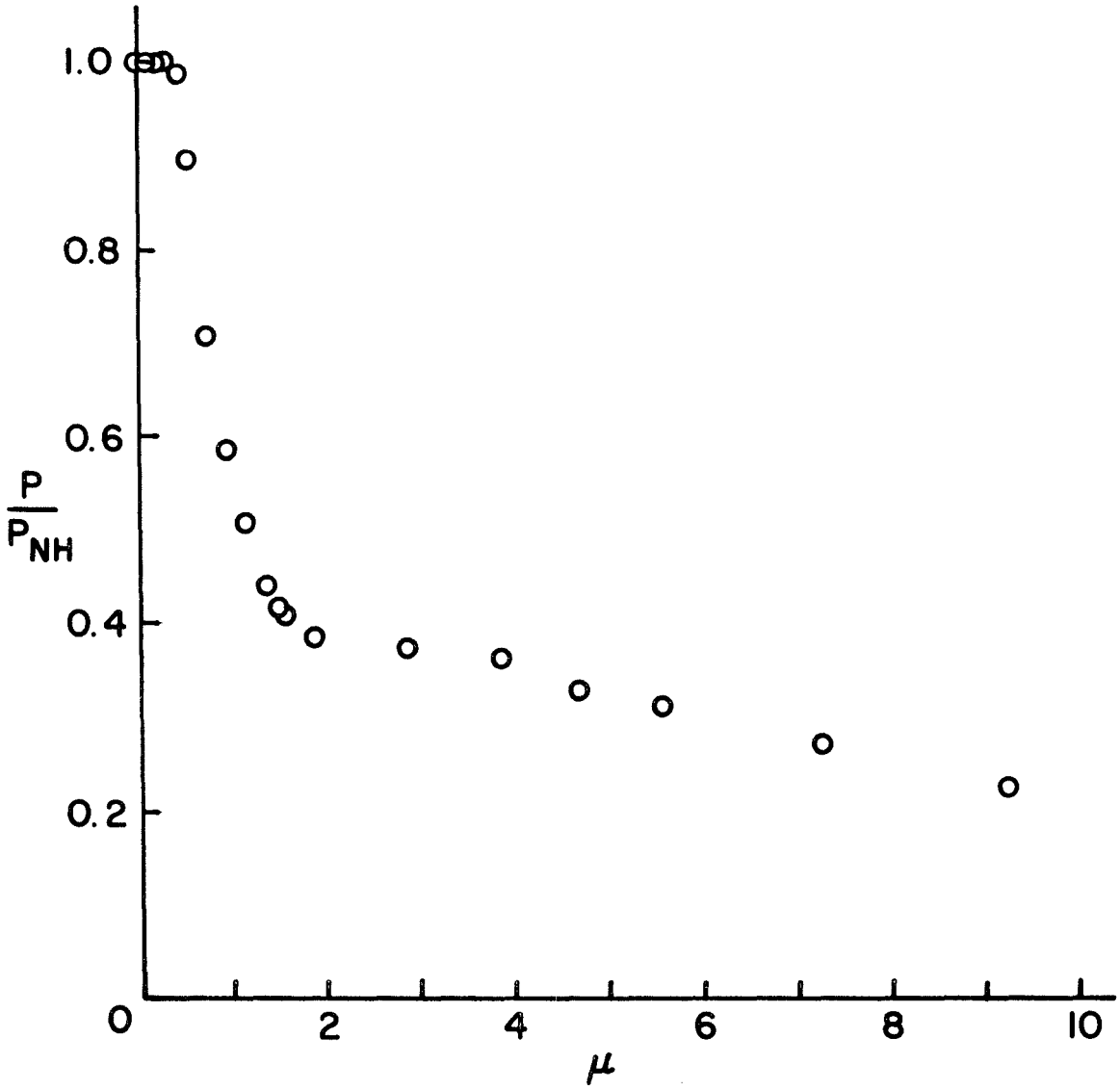

FIG. 24 BUCKLING LOADS OF SHELL 6

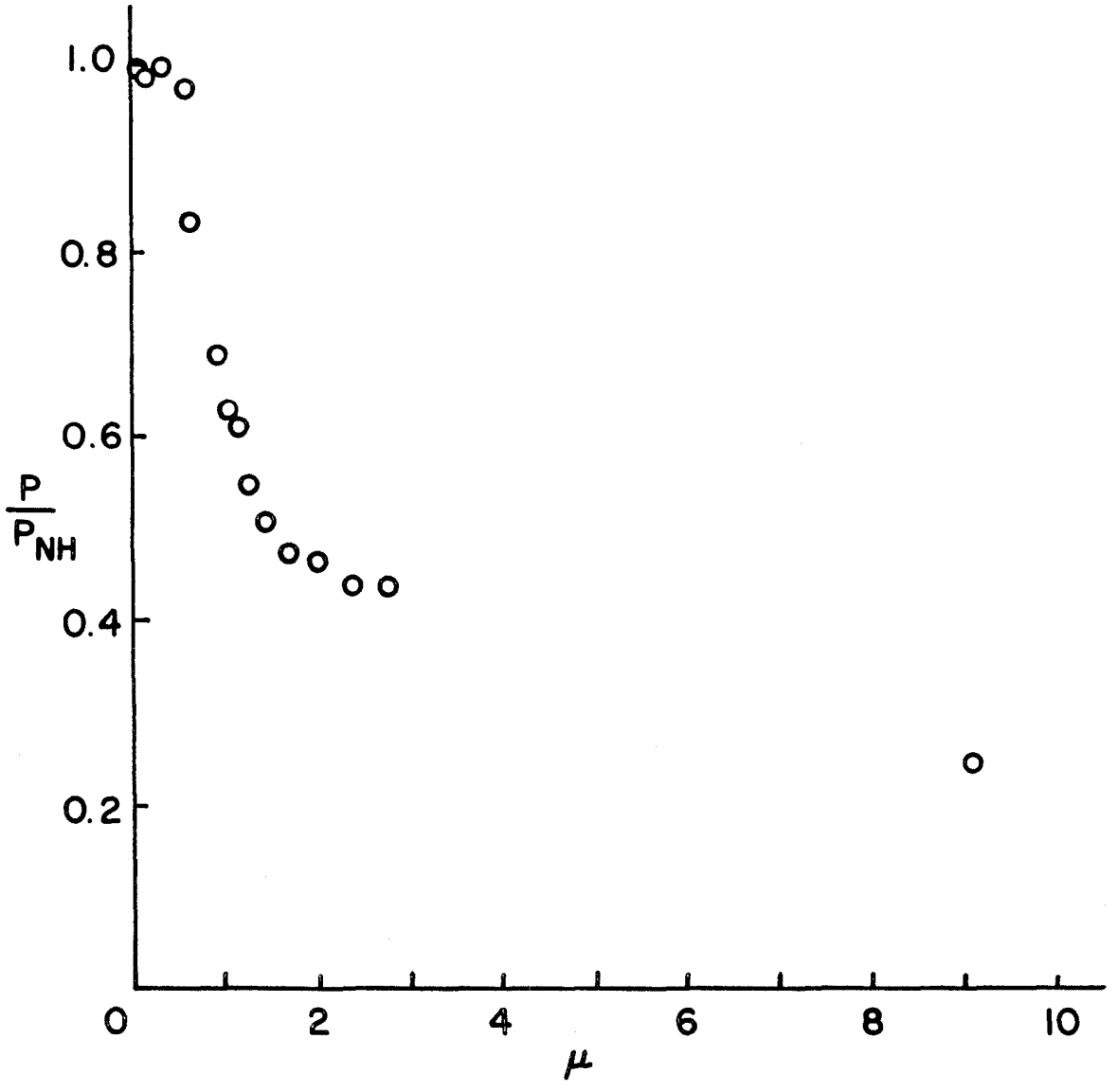

FIG.25 BUCKLING LOADS OF SHELL 14

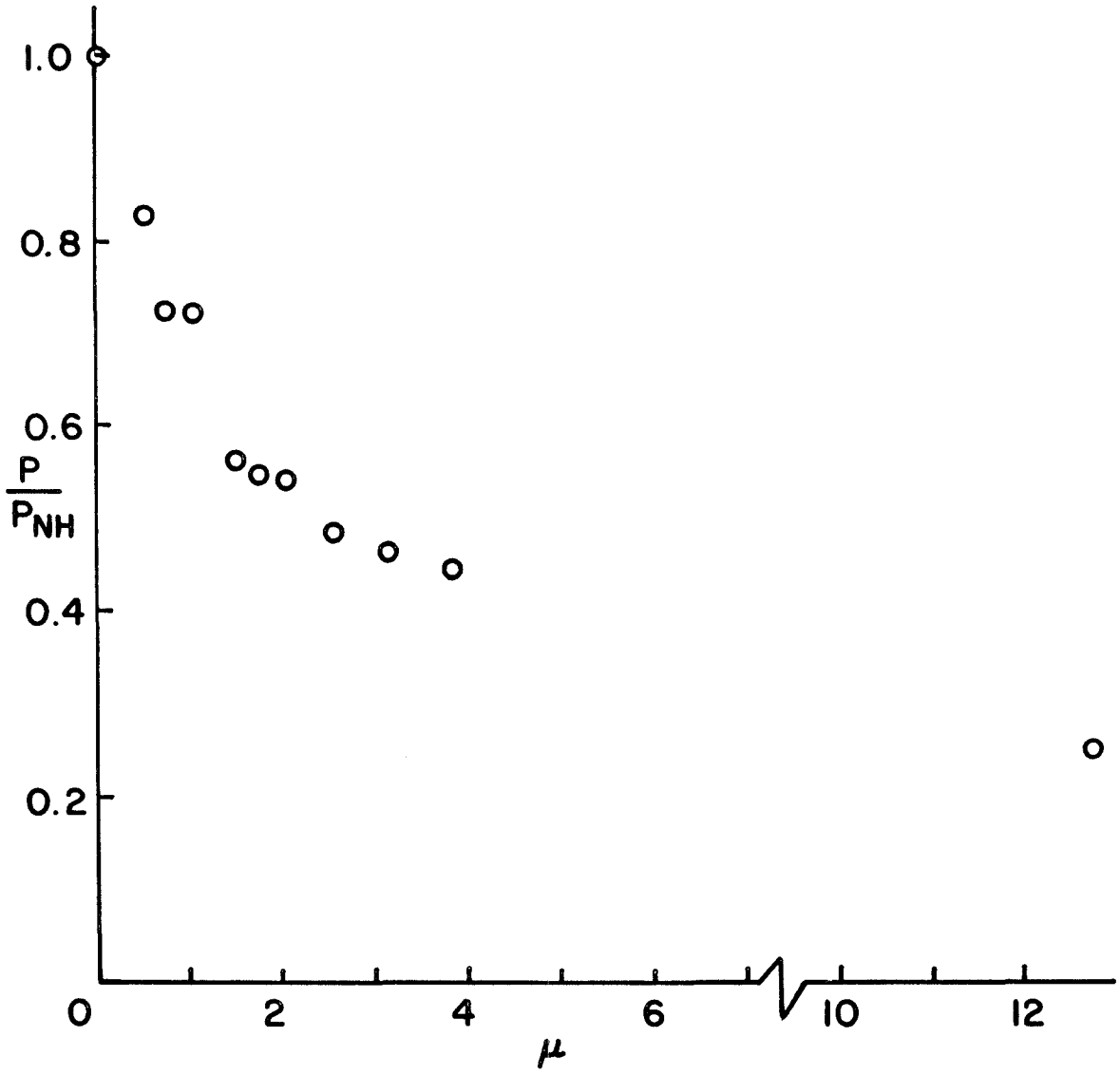

FIG.26 BUCKLING LOADS OF SHELL 20

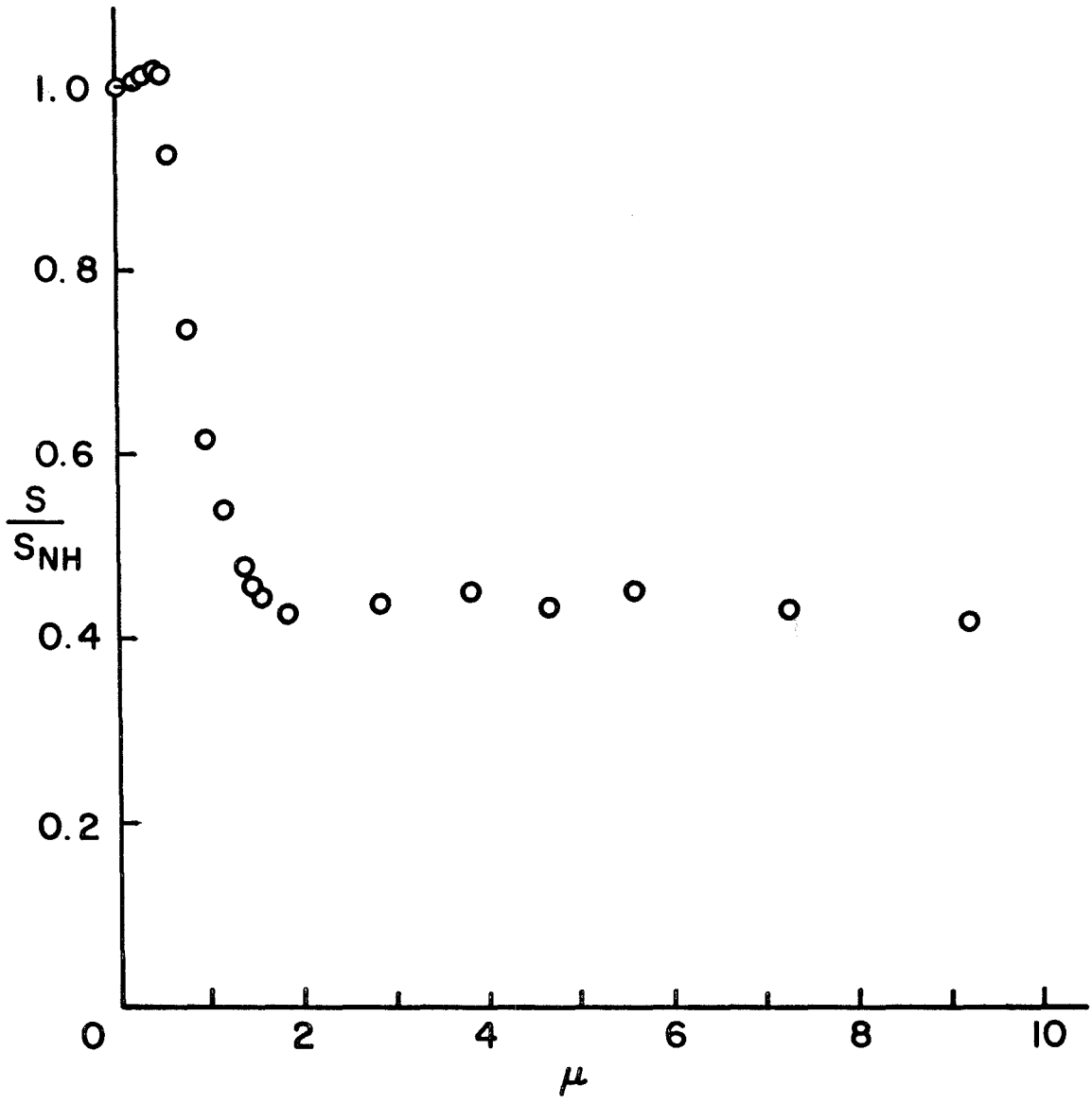

FIG.27 BUCKLING STRESSES OF SHELL 6

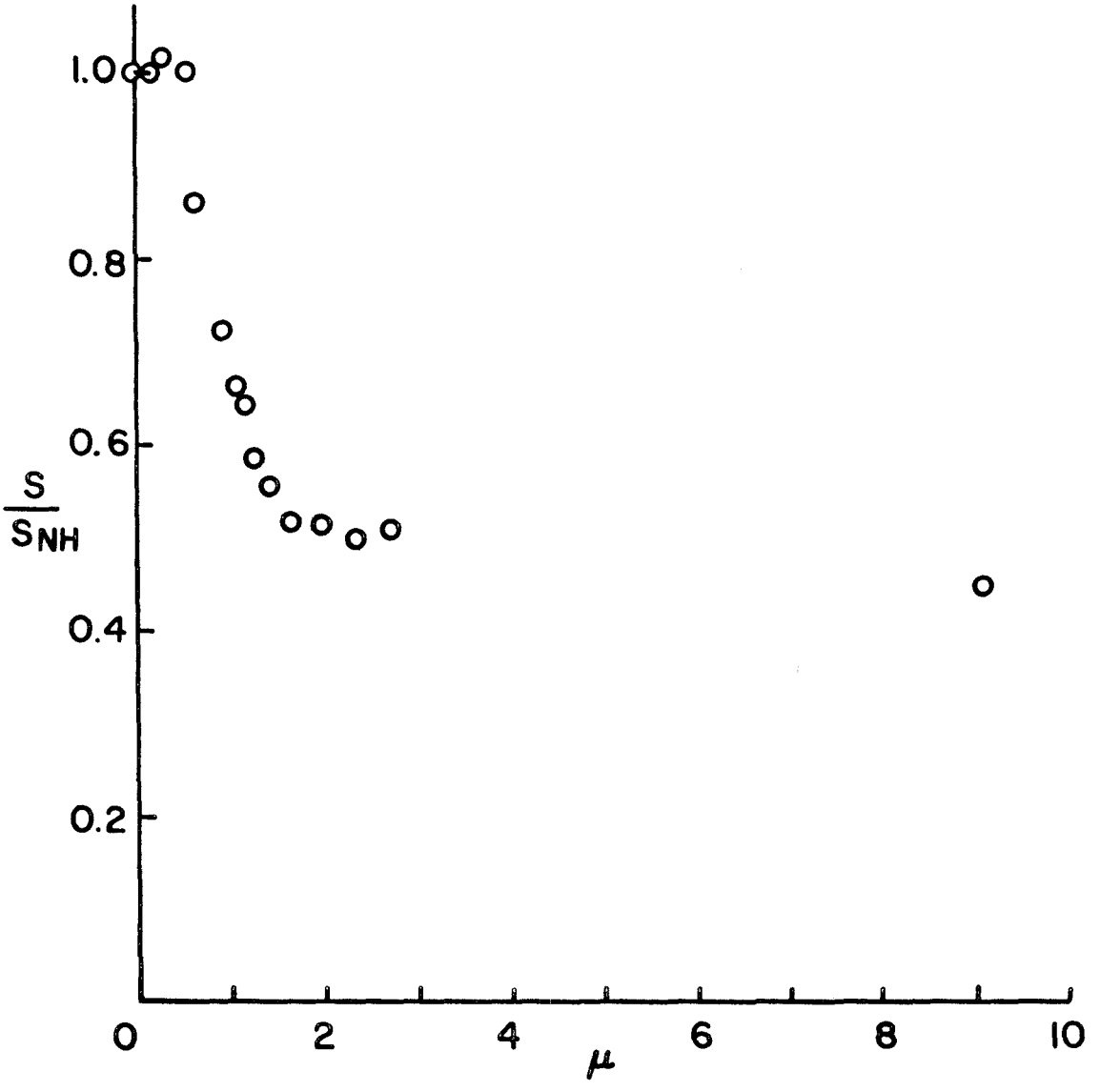

FIG.28 BUCKLING STRESSES OF SHELL 14

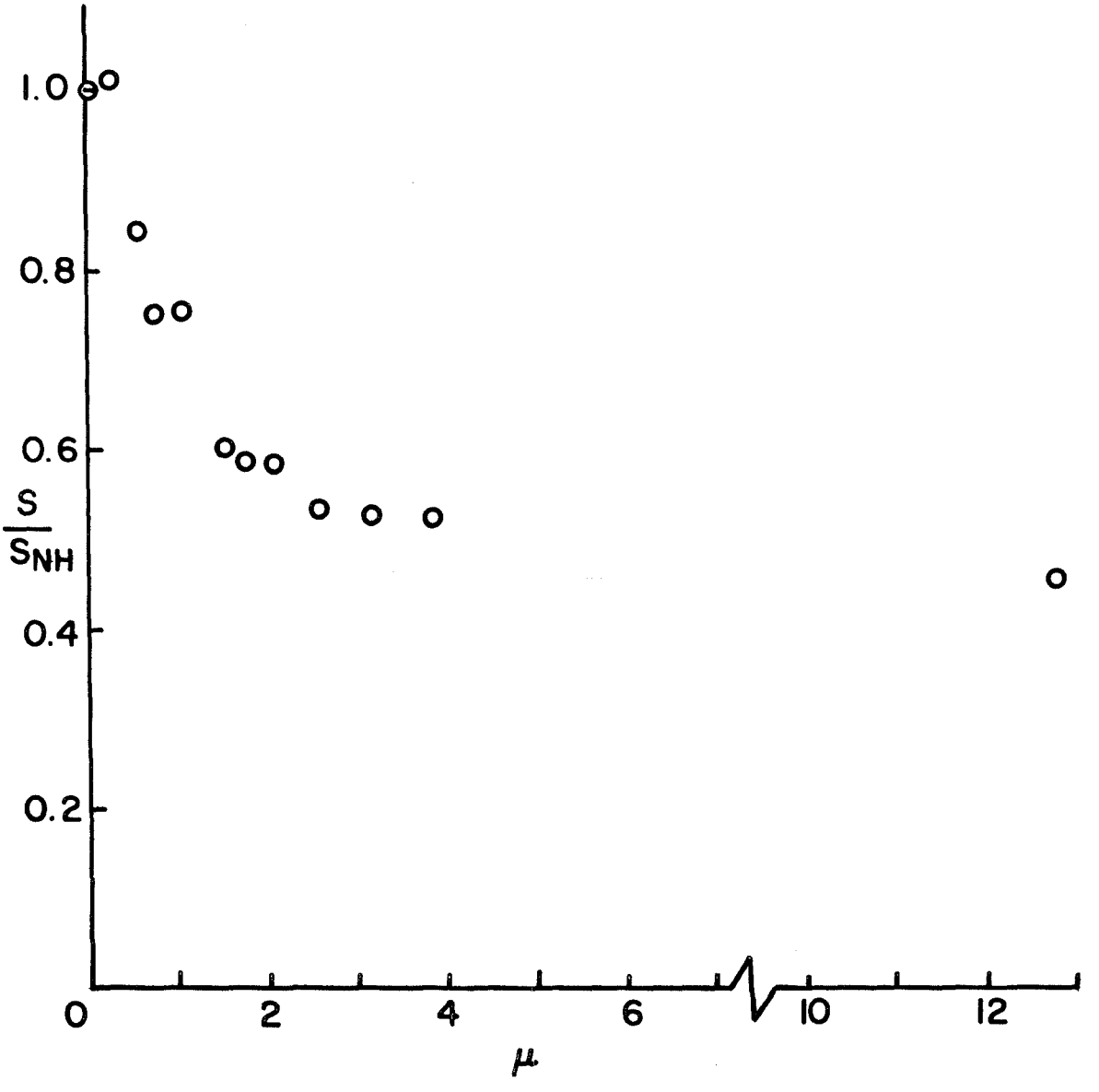

FIG.29 BUCKLING STRESSES OF SHELL 20

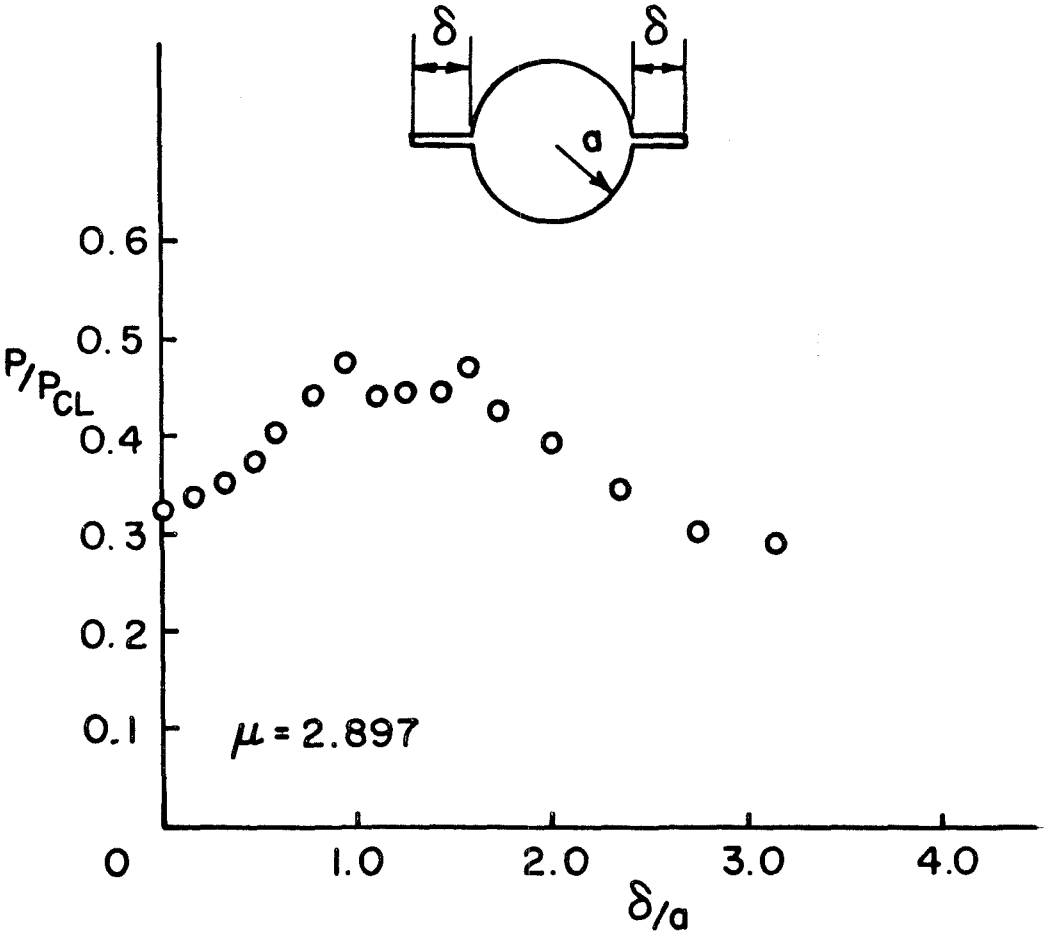

FIG. 30 EFFECT OF SLOTS ON THE BUCKLING LOADS OF SHELL 7

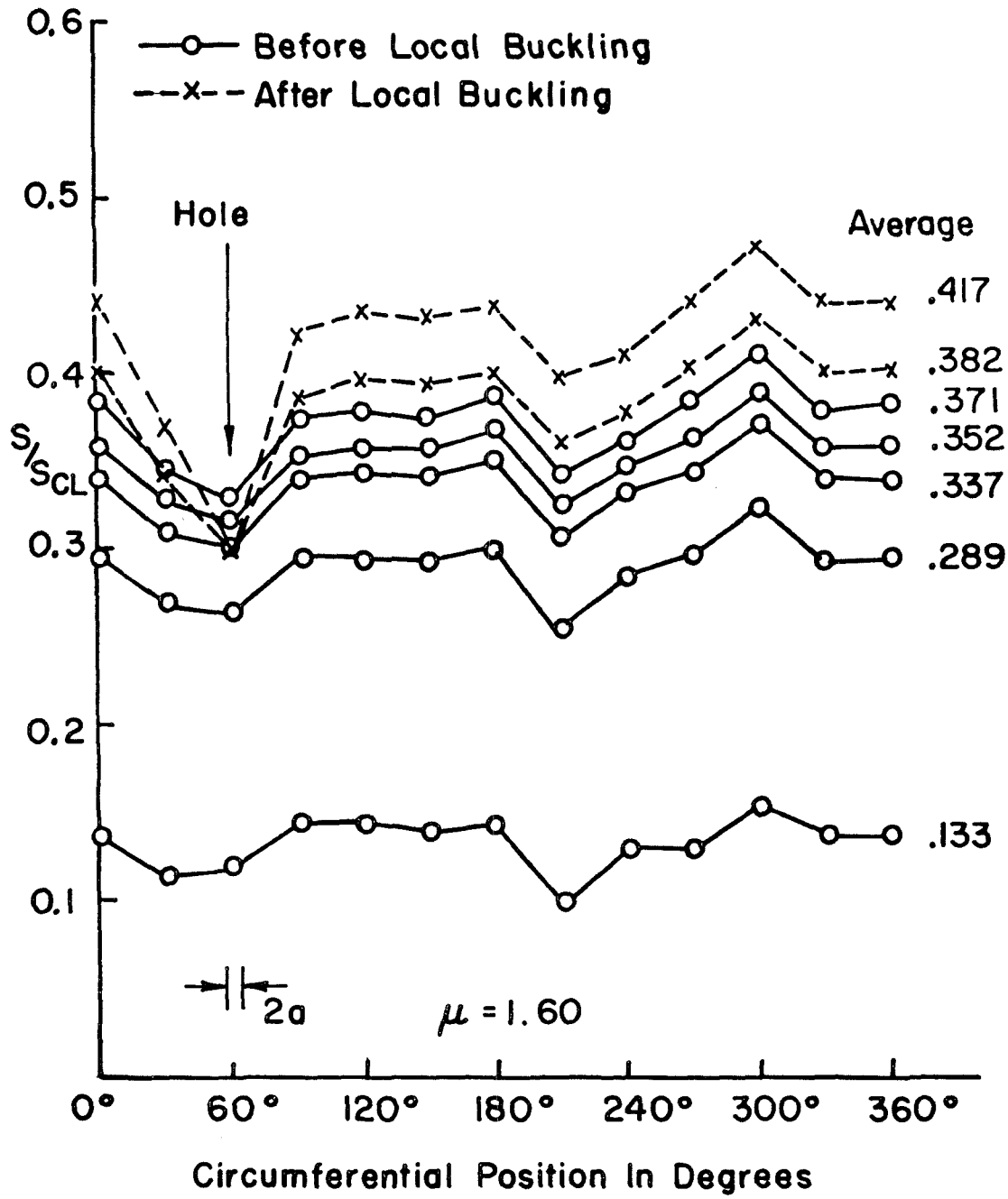

FIG.31 SHELL C3 STRESS DISTRIBUTION

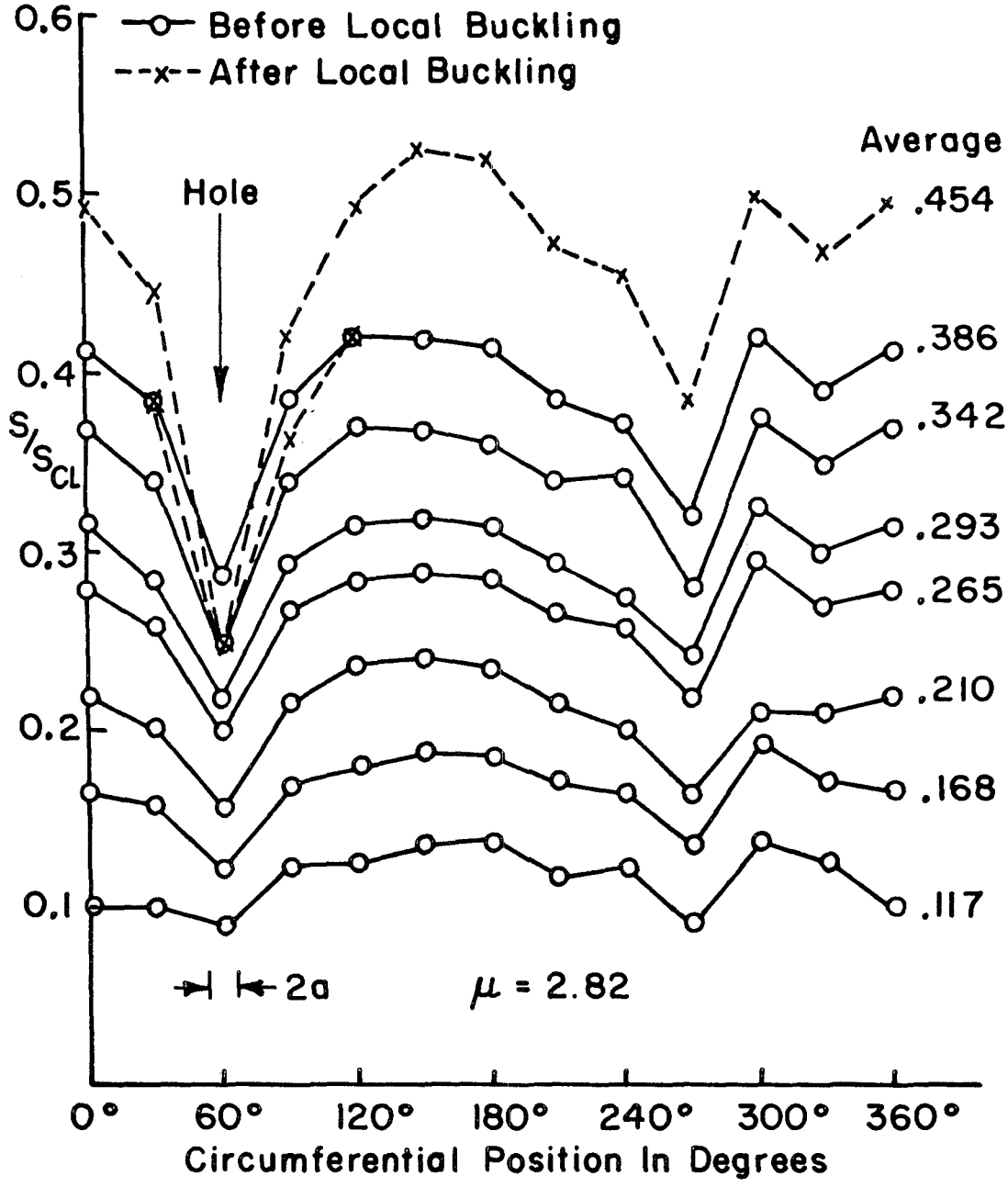

FIG. 32 SHELL C6 STRESS DISTRIBUTION

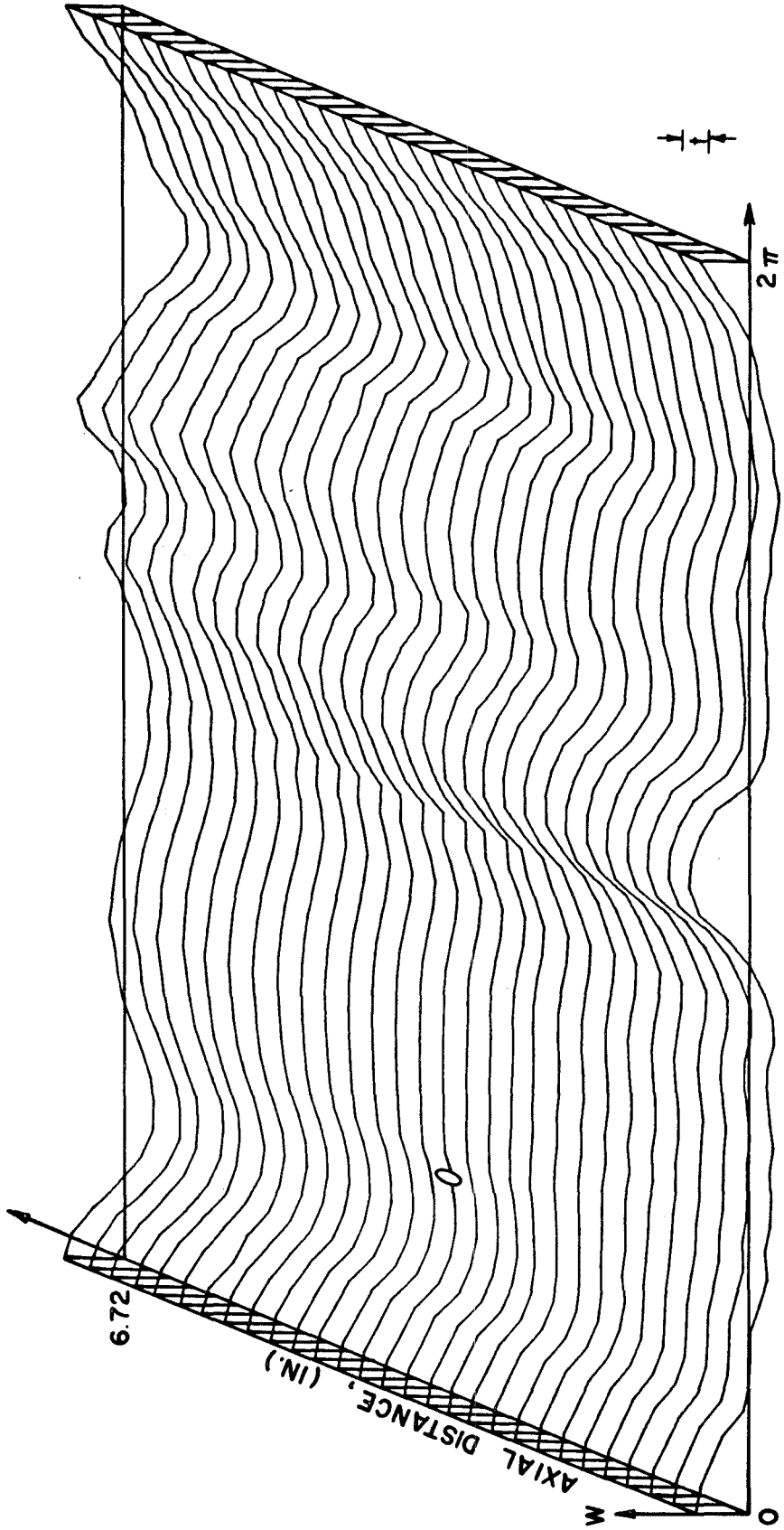

FIG. 33 INITIAL SURFACE OF SHELL C5

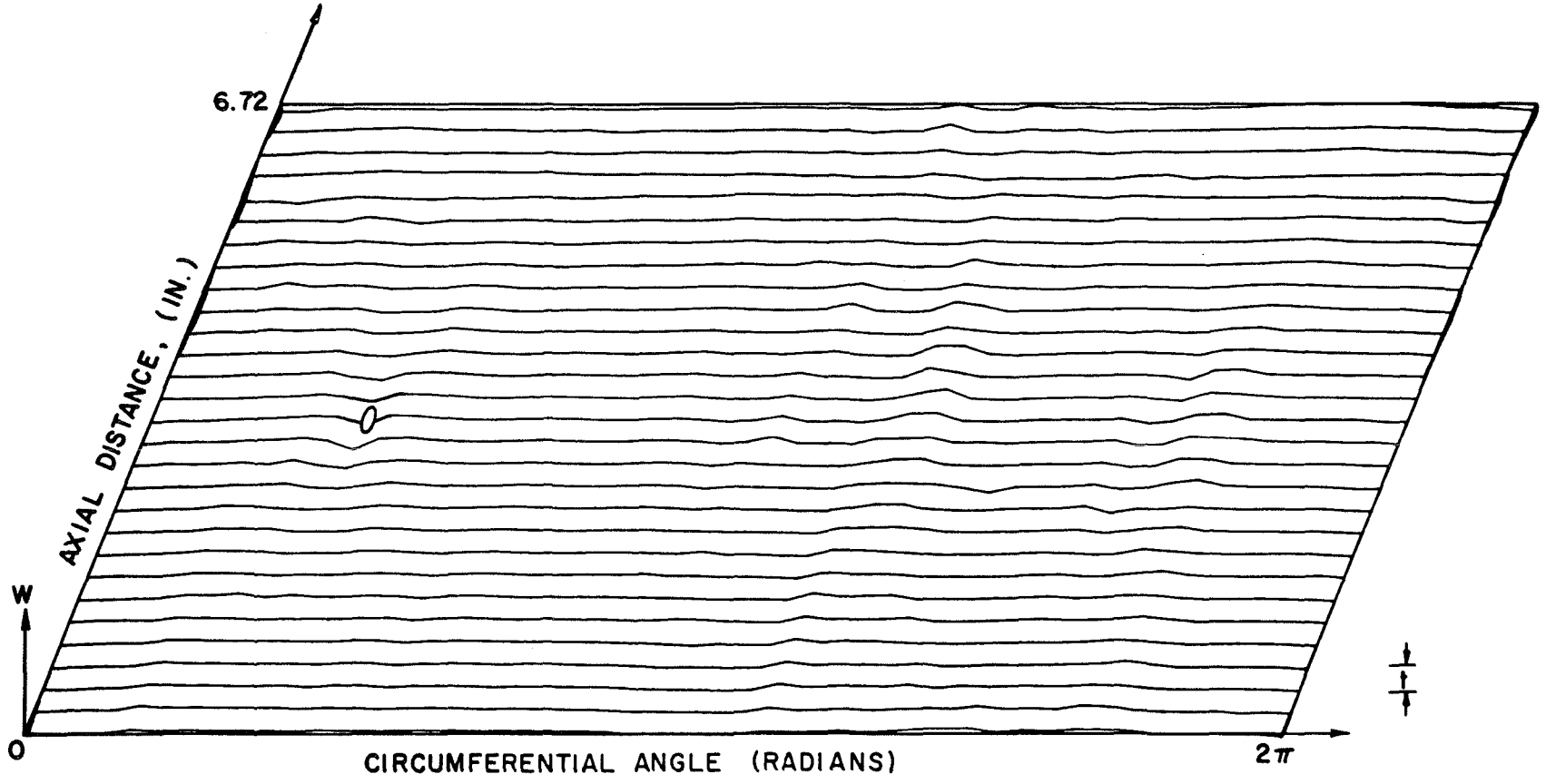

FIG. 34 PREBUCKLING DISPLACEMENT OF SHELL C5 AT $S/S_{CL} = 0.47$

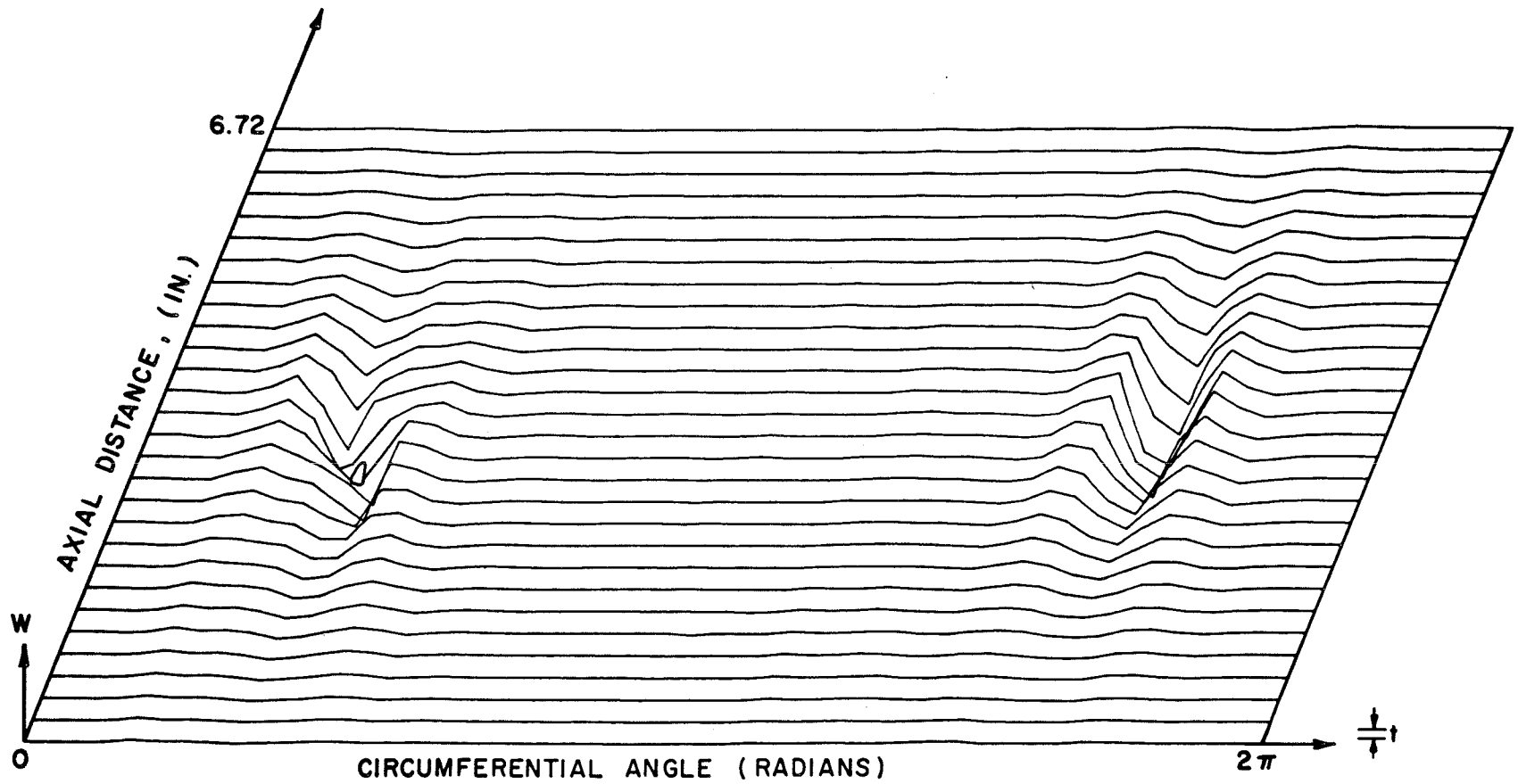

FIG. 35 DISPLACEMENT OF SHELL C5 AFTER LOCAL BUCKLING

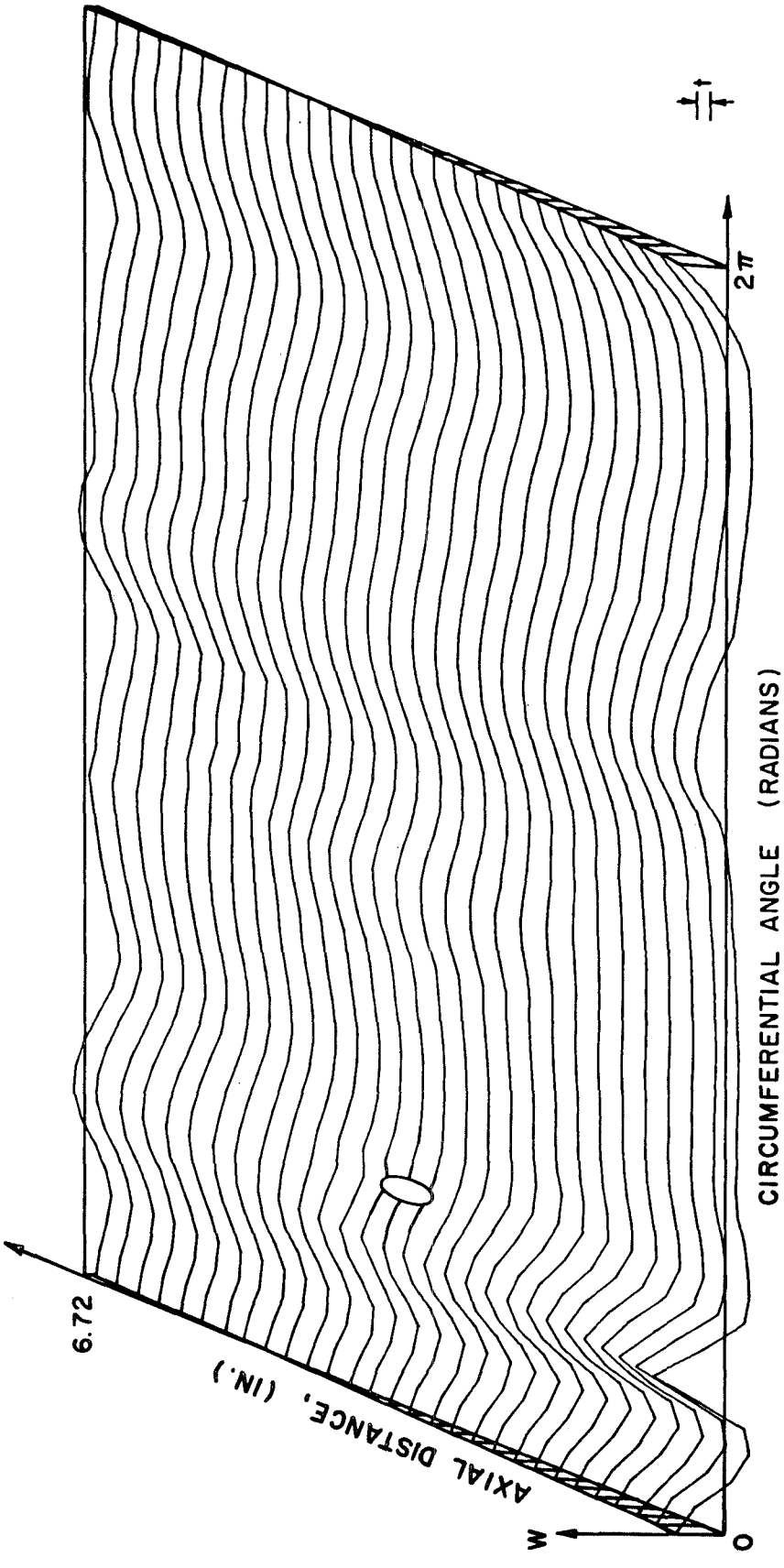

FIG. 36 INITIAL SURFACE OF SHELL C3

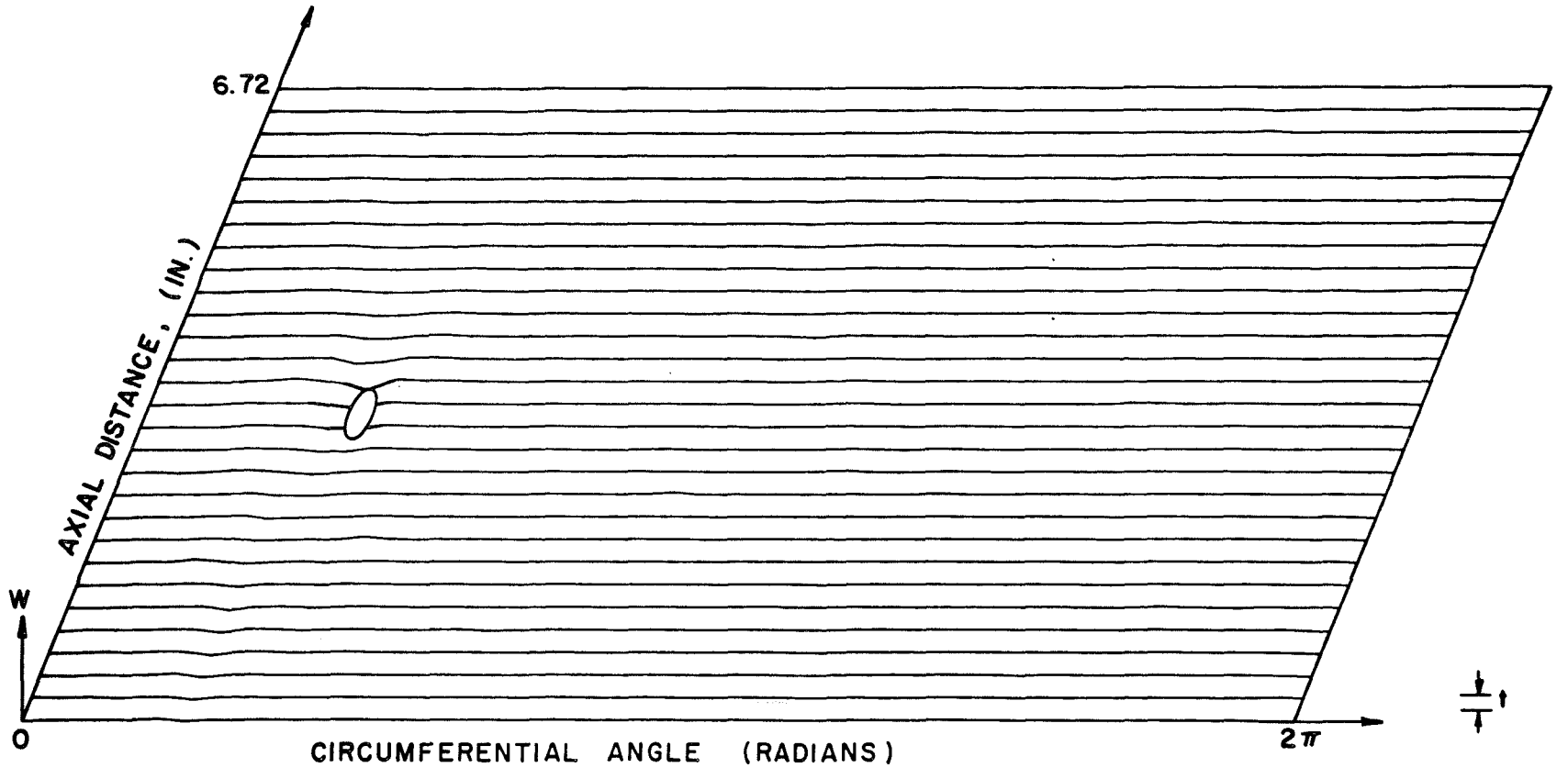

FIG.37 PREBUCKLING DISPLACEMENT OF SHELL C3 AT S/S_{CL} = 0.136

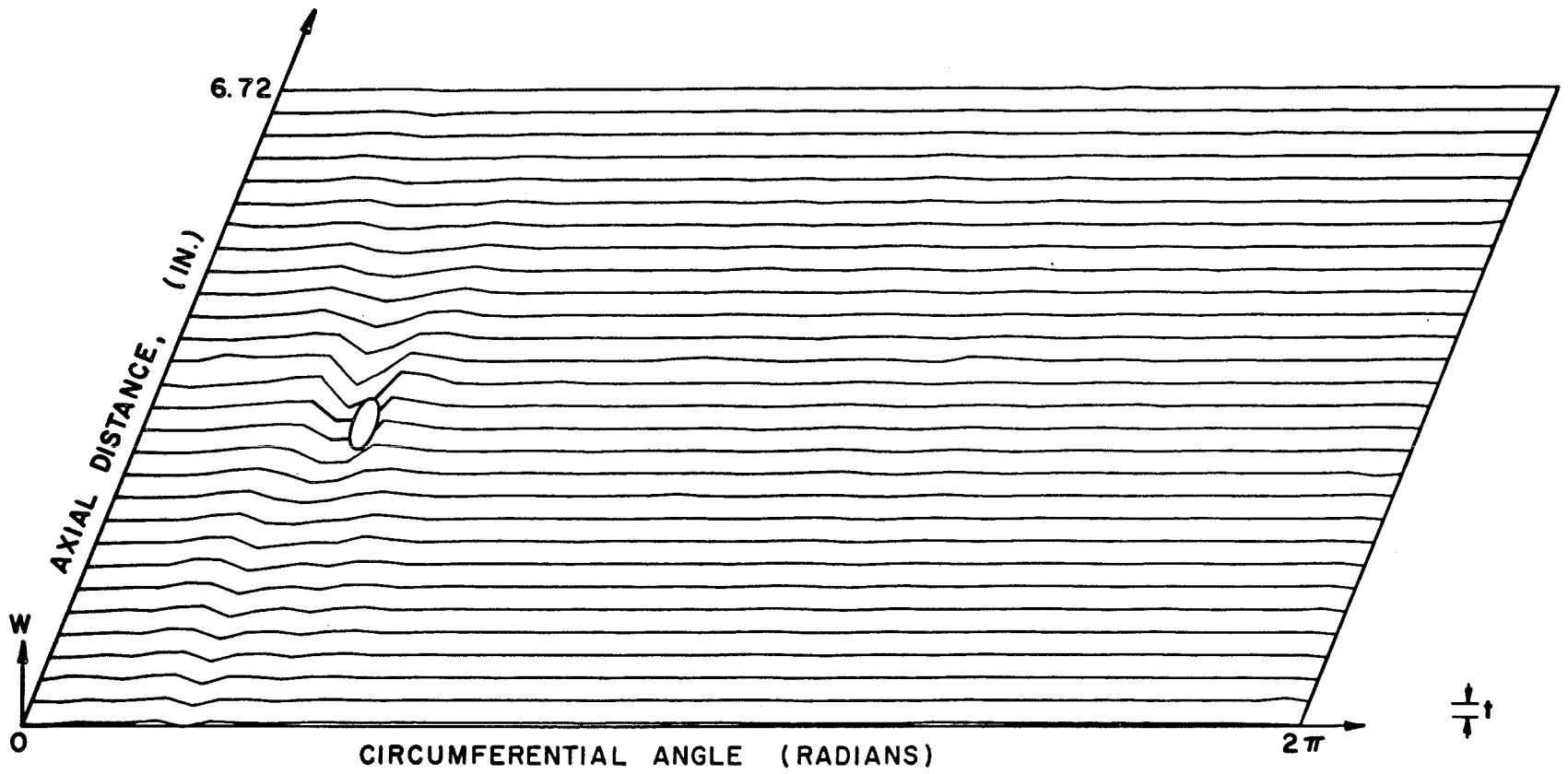

FIG. 38 PREBUCKLING DISPLACEMENT OF SHELL C3 AT $S/S_{CL} = 0.380$

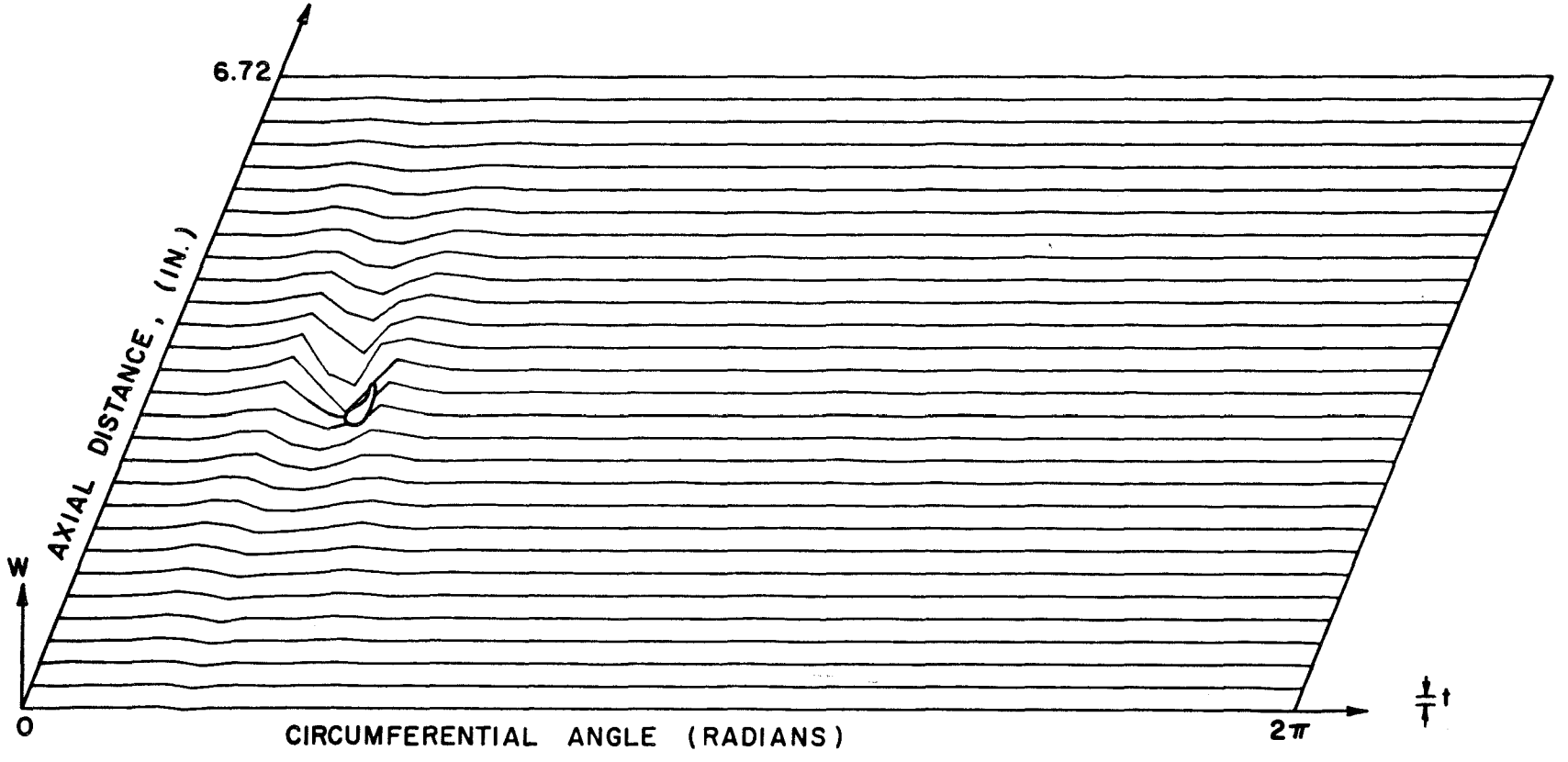

FIG. 39 DISPLACEMENT OF SHELL C3 AFTER LOCAL BUCKLING

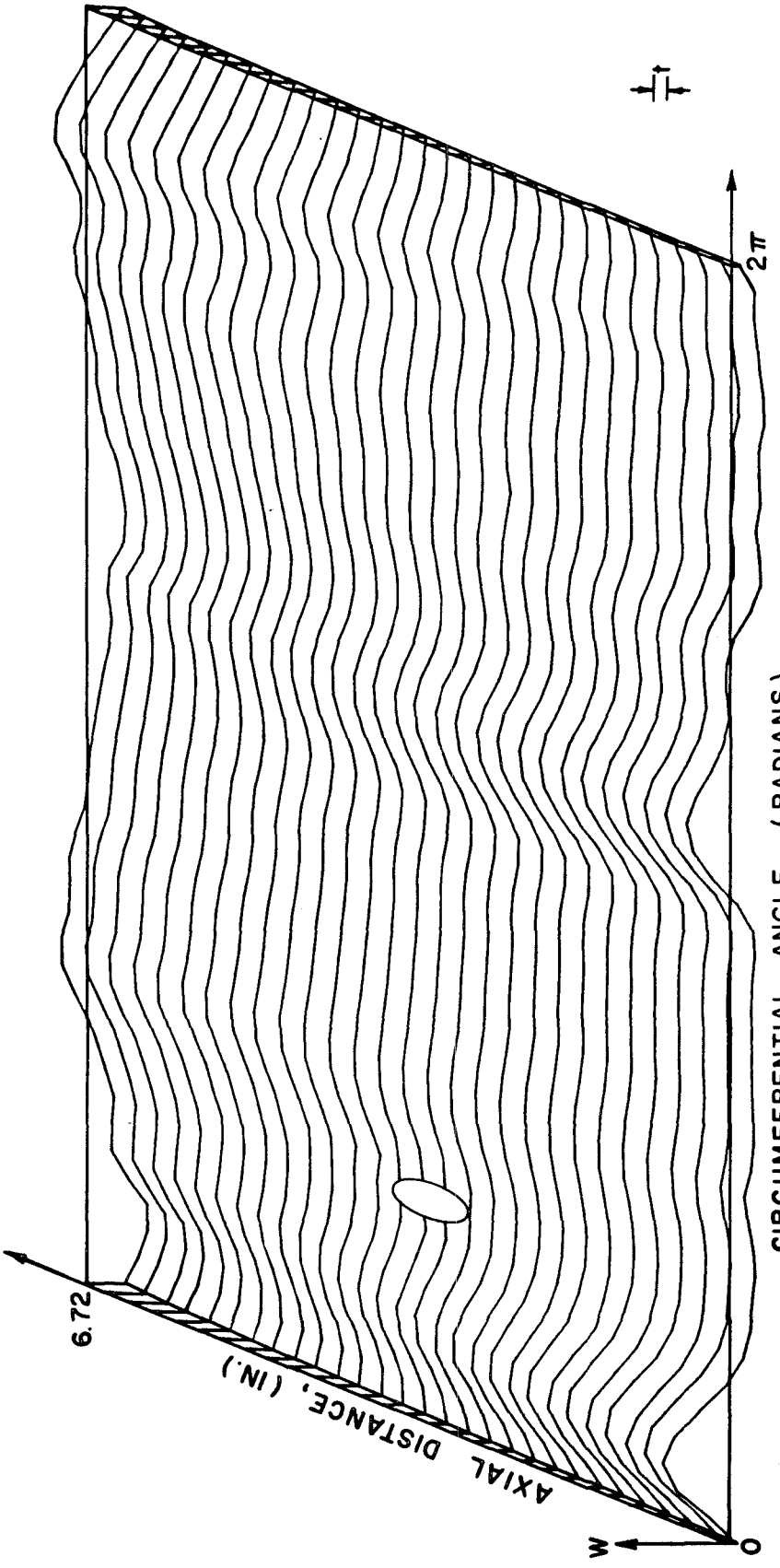

FIG.40 INITIAL SURFACE OF SHELL C6

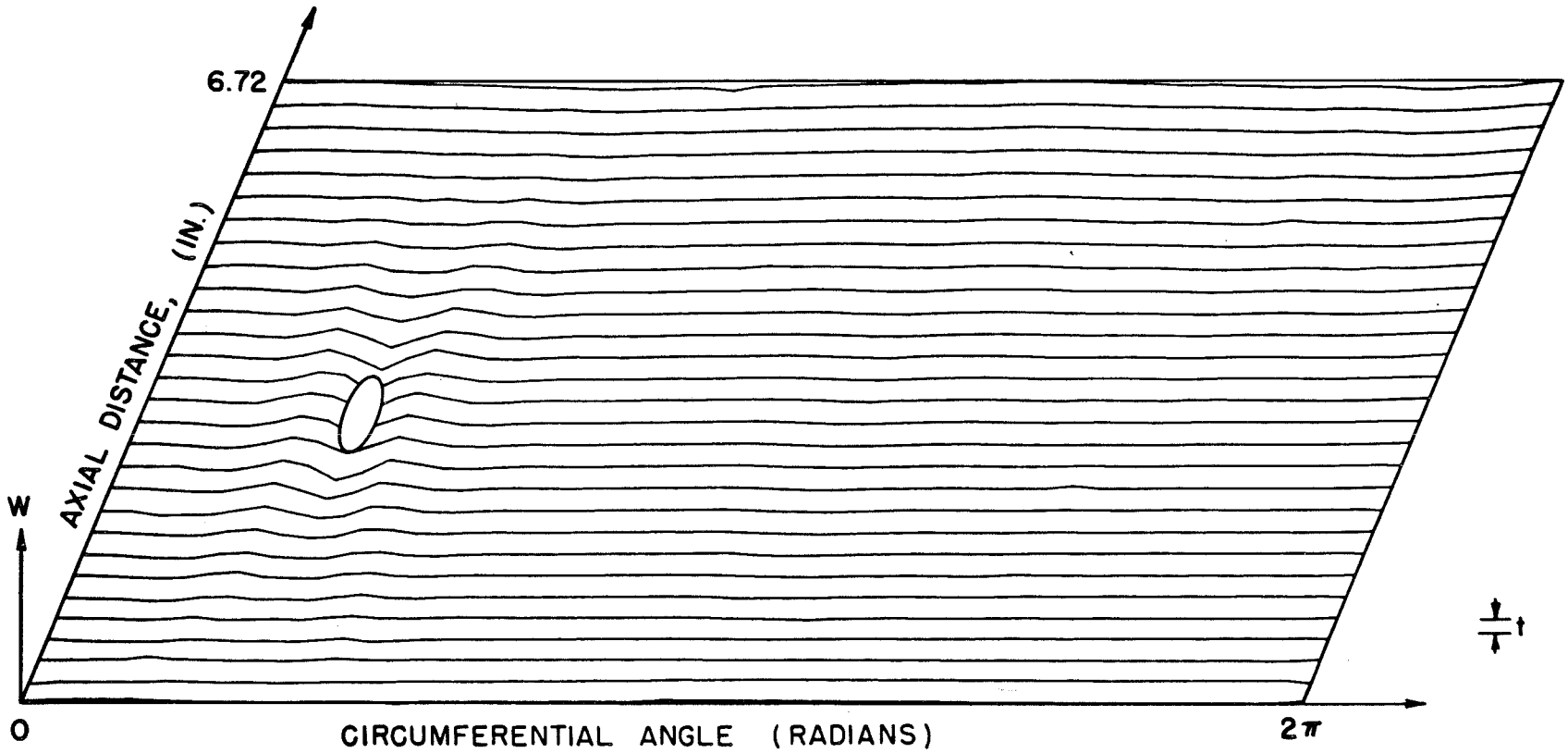

FIG.41 PREBUCKLING DISPLACEMENT OF SHELL C6 AT $S/S_{CL} = 0.174$

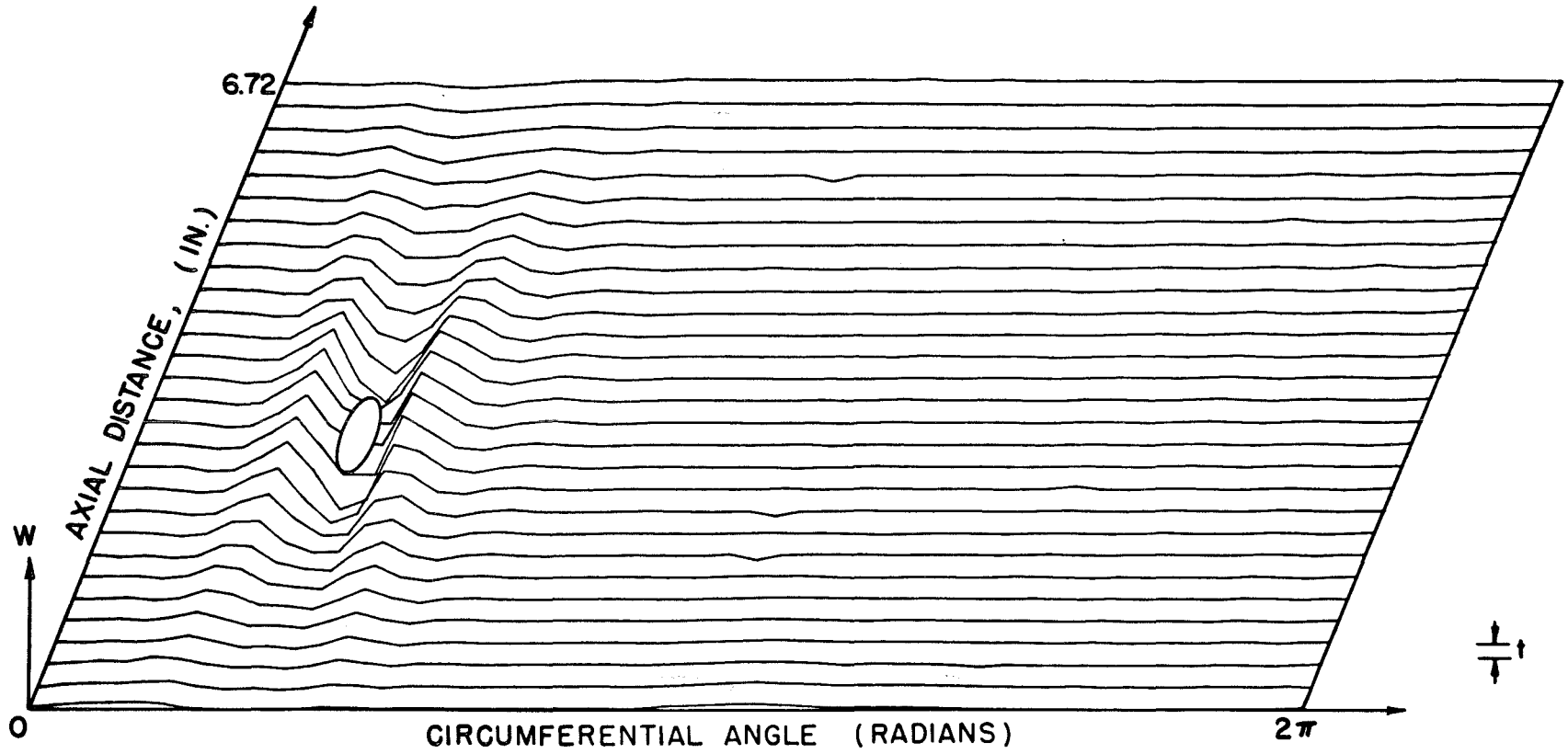

FIG. 42 PREBUCKLING DISPLACEMENT OF SHELL C6 AT $S/S_{CL} = 0.398$

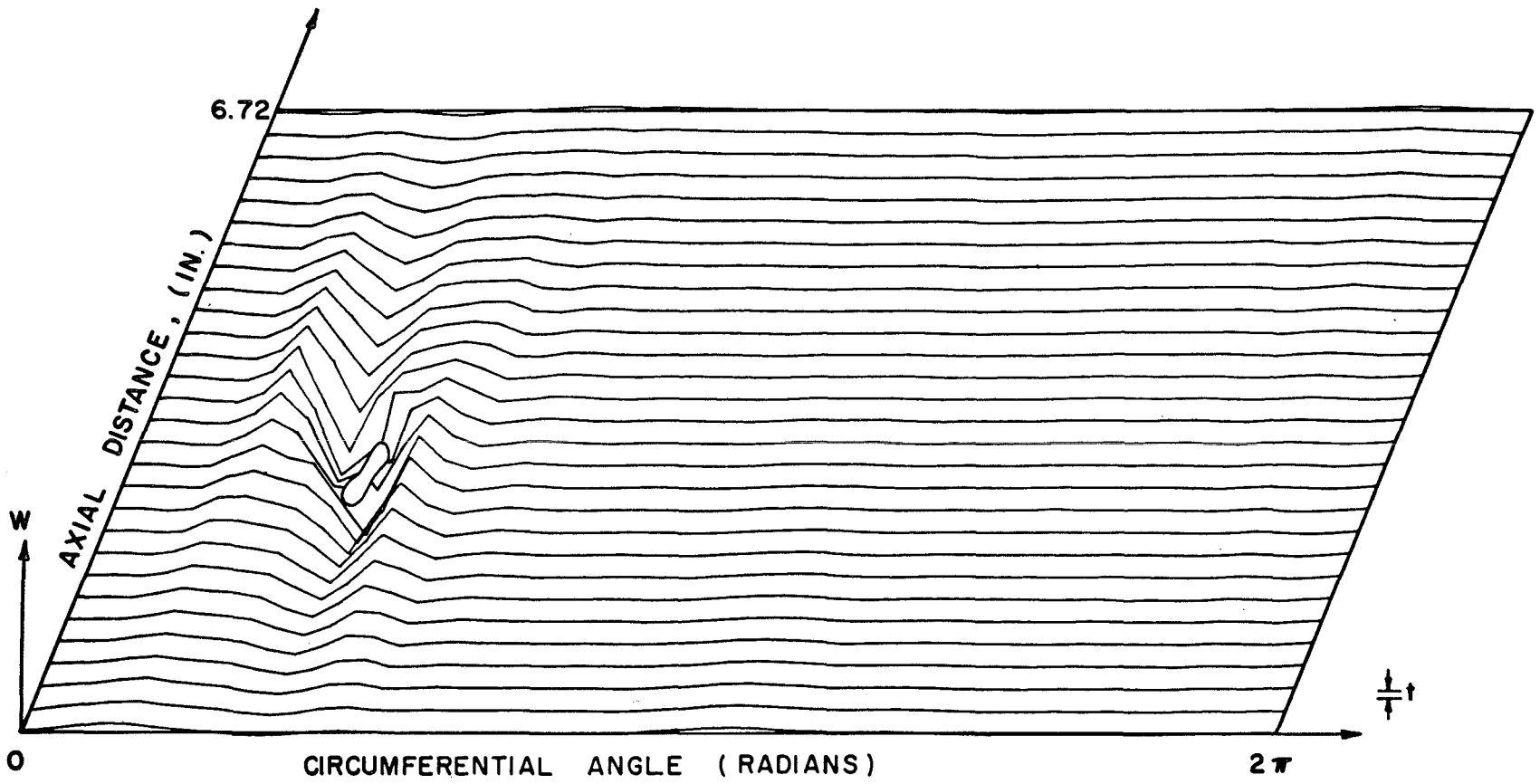

FIG.43 DISPLACEMENT OF SHELL C6 AFTER LOCAL BUCKLING

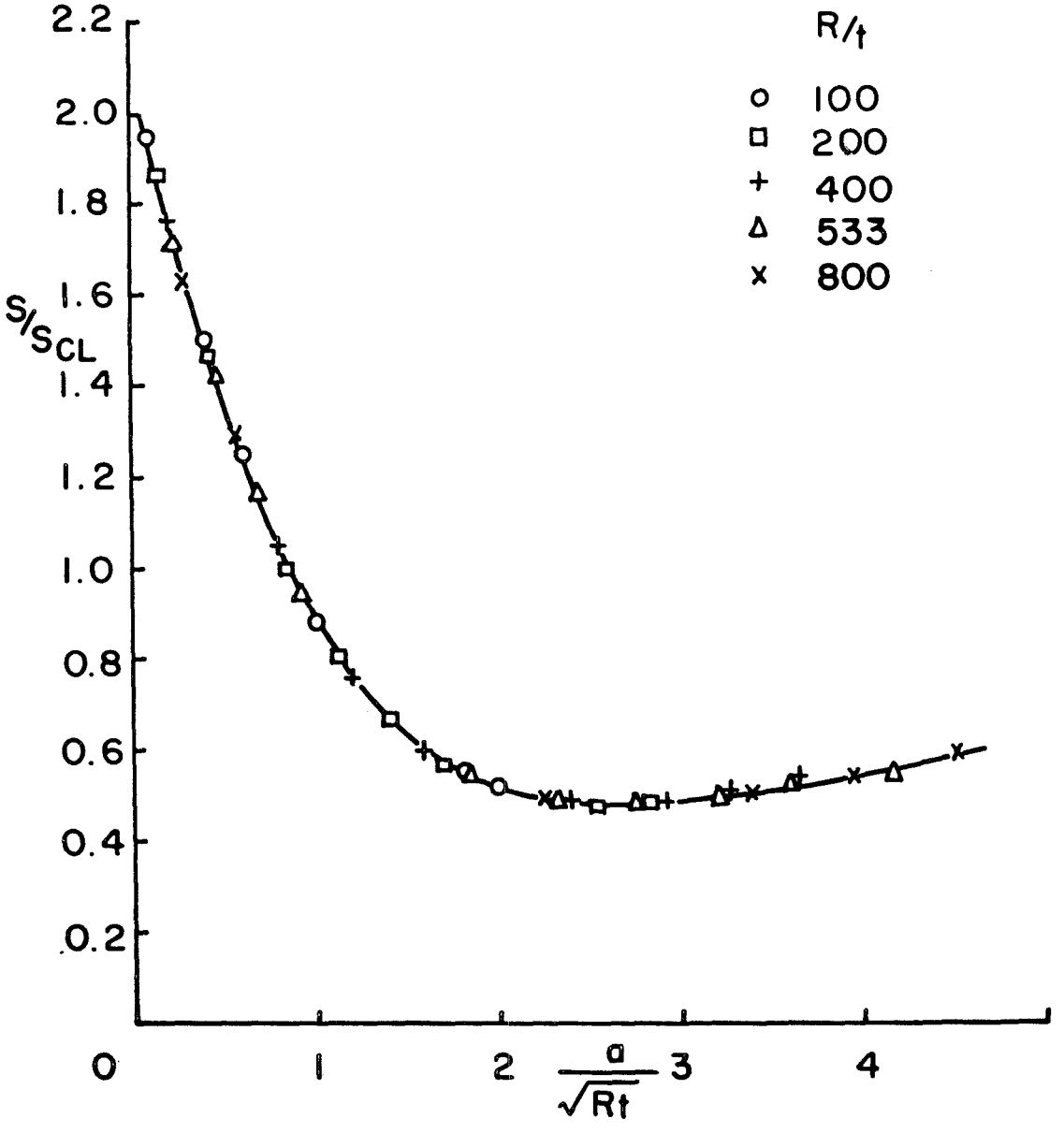

FIG. 44 RESULTS OF ANALYSIS